Electronic Supplementary Material (ESI) for Dalton Transactions.

Supporting Information for:

F-element metalated dipyrrins: Synthesis and characterization of a family of uranyl bis(dipyrrinate) complexes

*Duer Bolotaulo, Alejandro J. Metta-Magaña, and Skye Fortier**

Dept. of Chemistry, University of Texas at El Paso, El Paso, TX 79968

*To whom correspondence should be addressed. Email: asfortier@utep.edu

TABLE OF CONTENTS TABLE OF CONTENTS

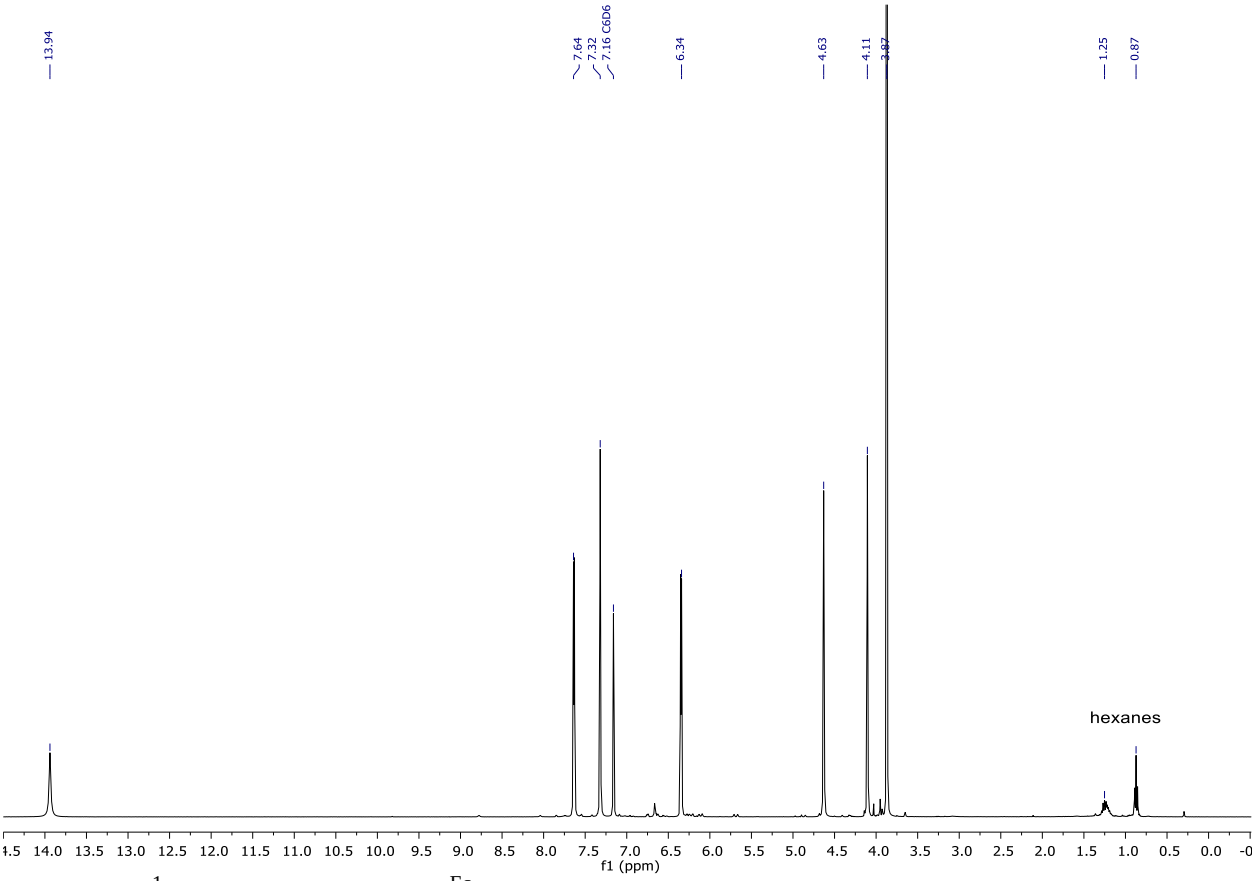

Figure S1. ^{1}H NMR spectrum of 2^{Fc} in C_6D_6.

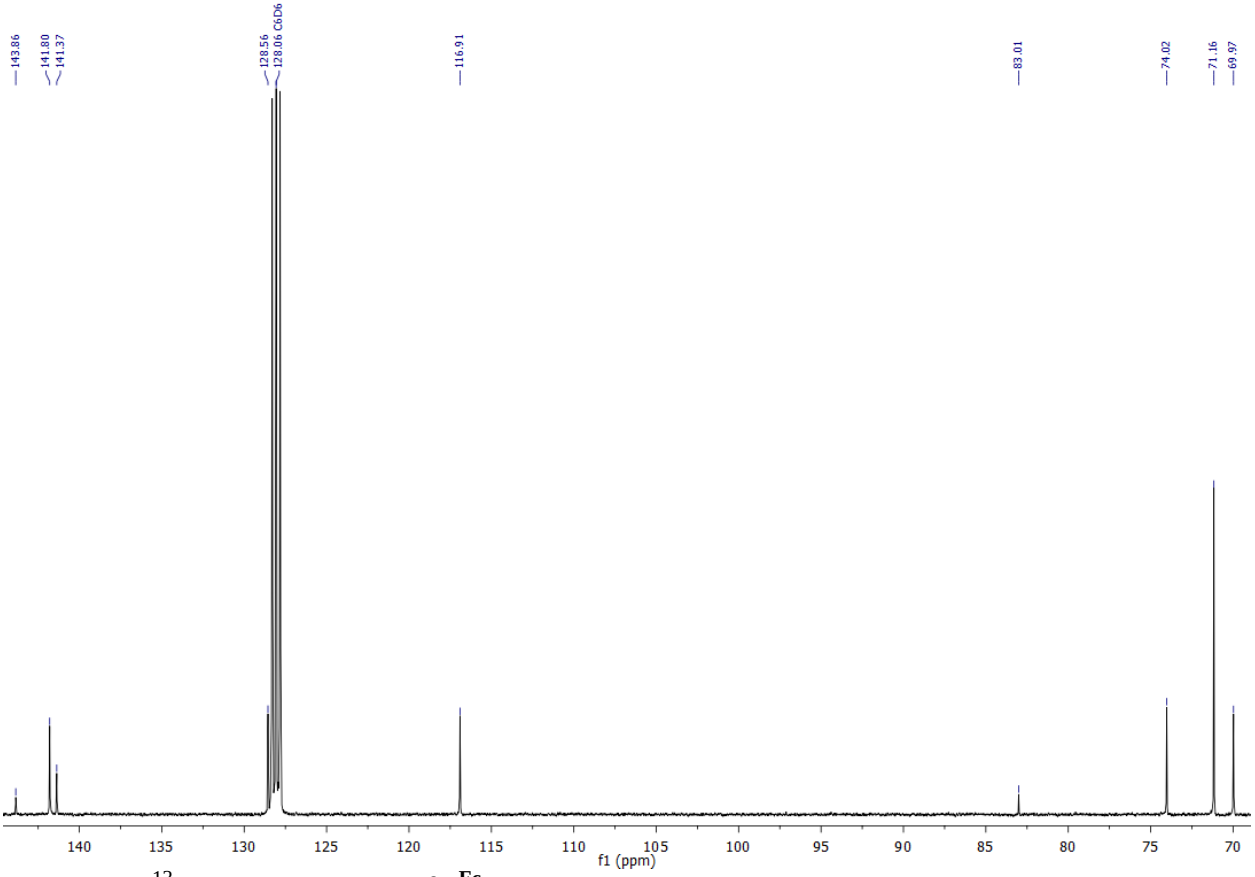

Figure S2. ^{13}C NMR spectrum of $\mathbf{2^{Fc}}$ in C_6D_6.

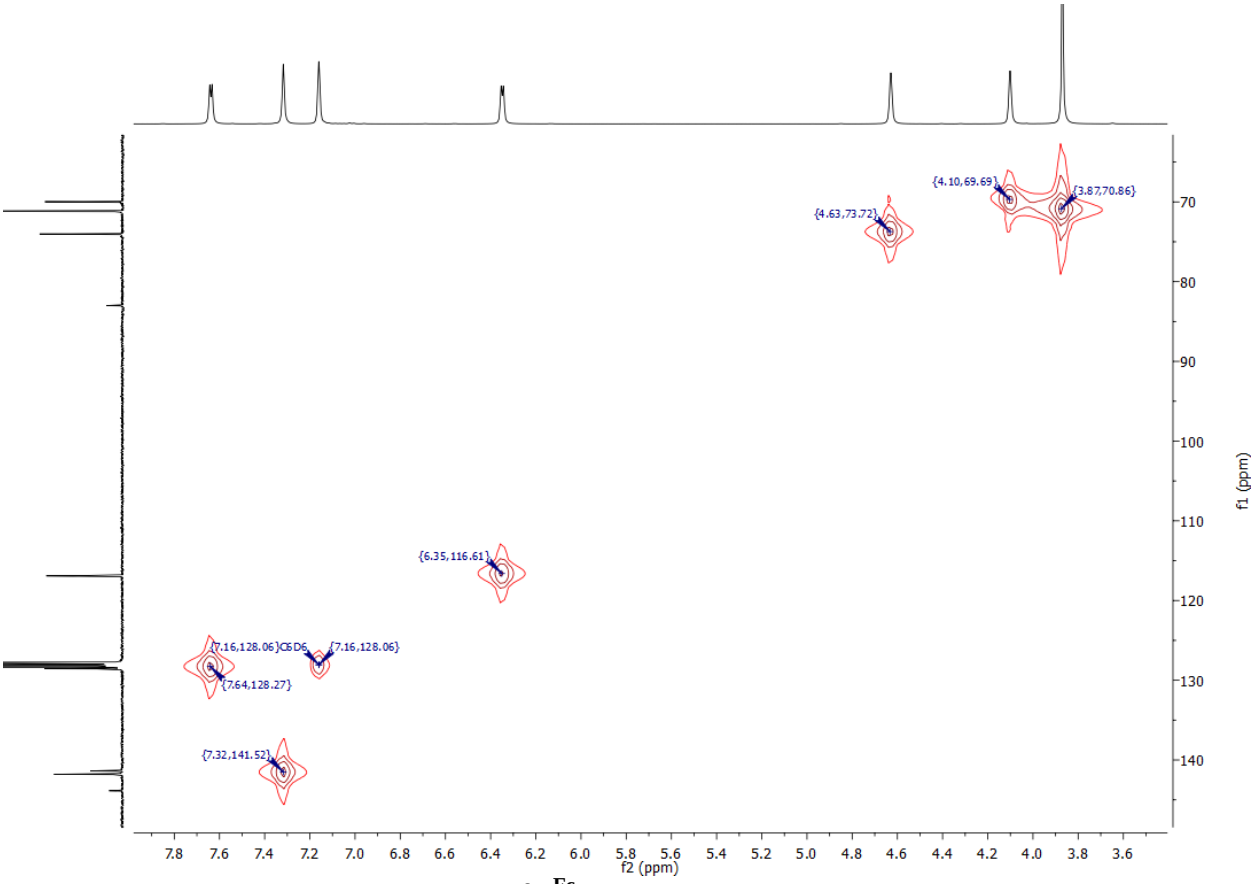

Figure S3. HMQCGP NMR spectrum of $\mathbf{2^{Fc}}$ in C_6D_6.

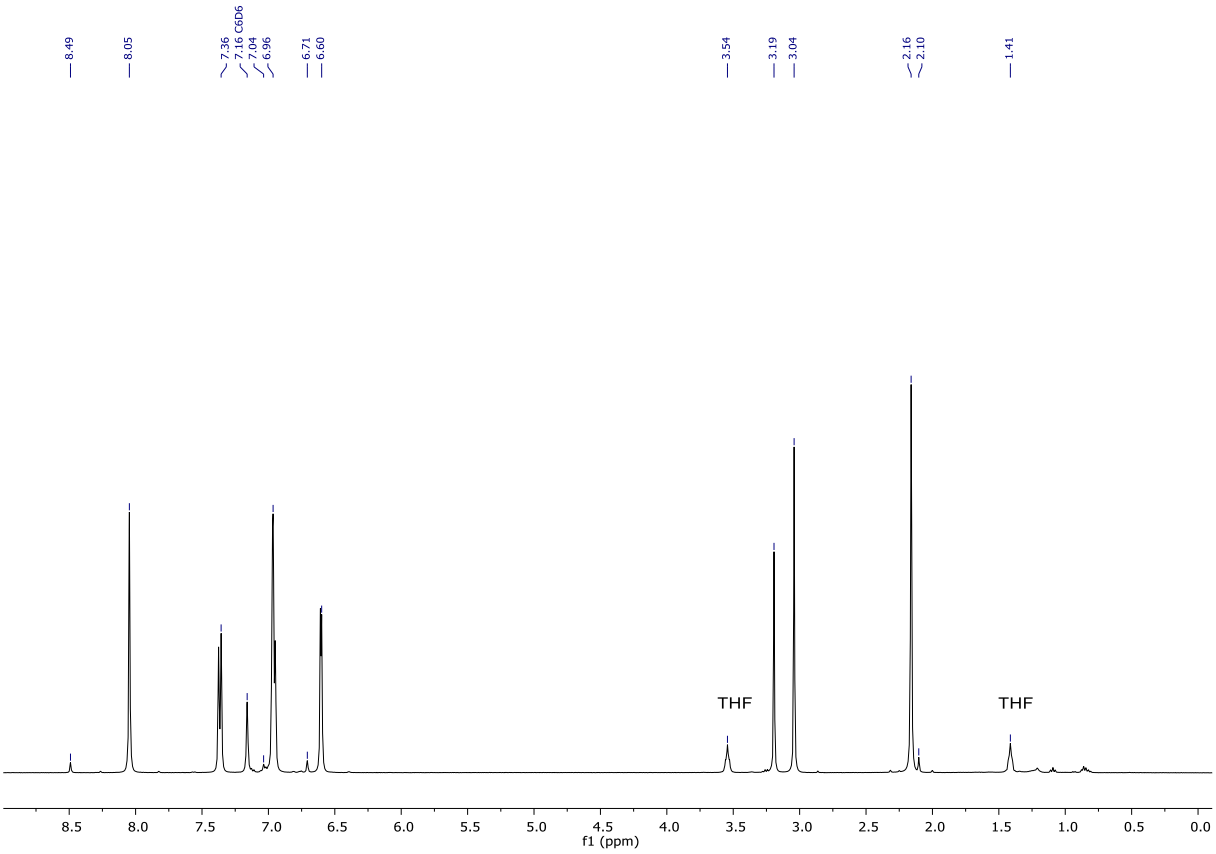

Figure S4. ^{1}H NMR spectrum of **3**$^{\mathbf{tol}}$ in C_6D_6/py-d_5.

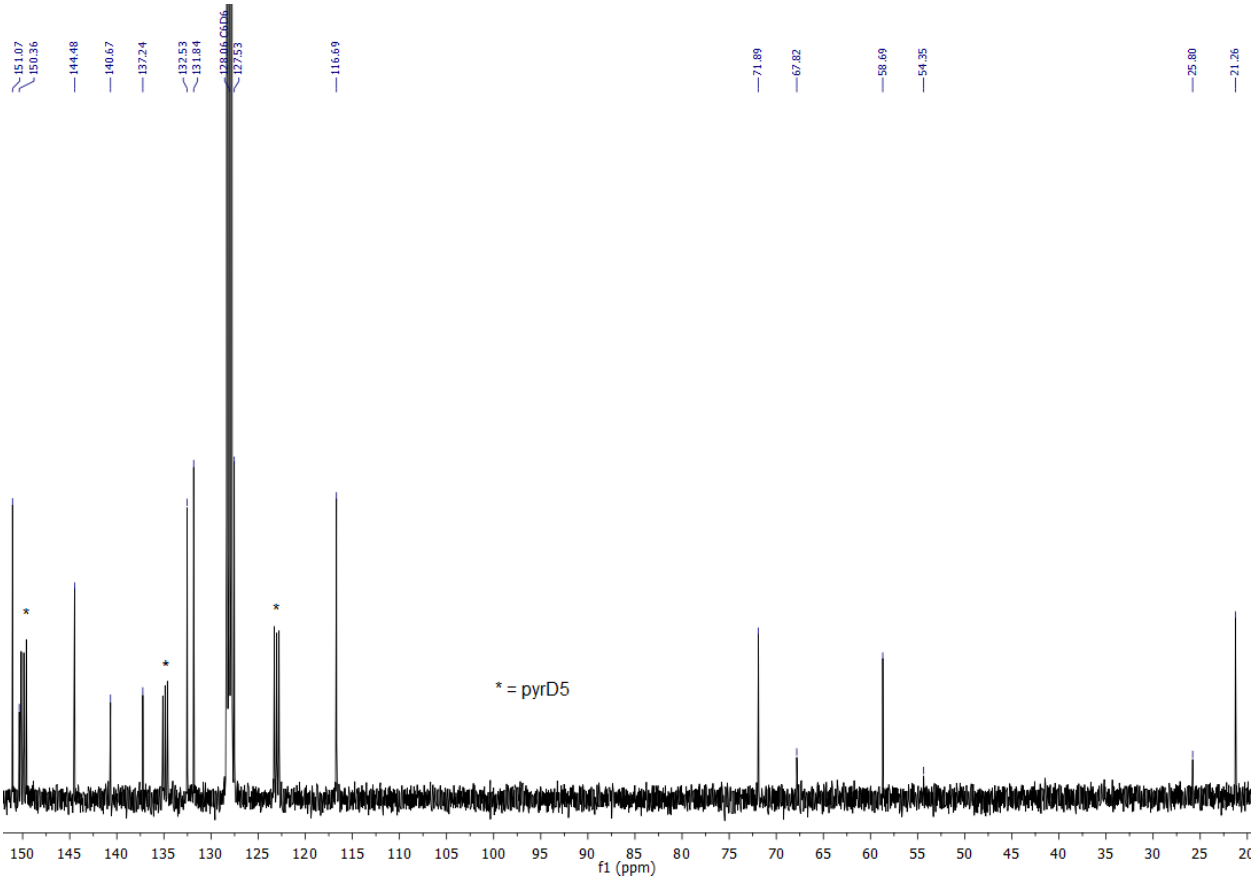

Figure S5. ^{13}C NMR spectrum of **3**$^{\mathbf{tol}}$ in C_6D_6/py-d_5.

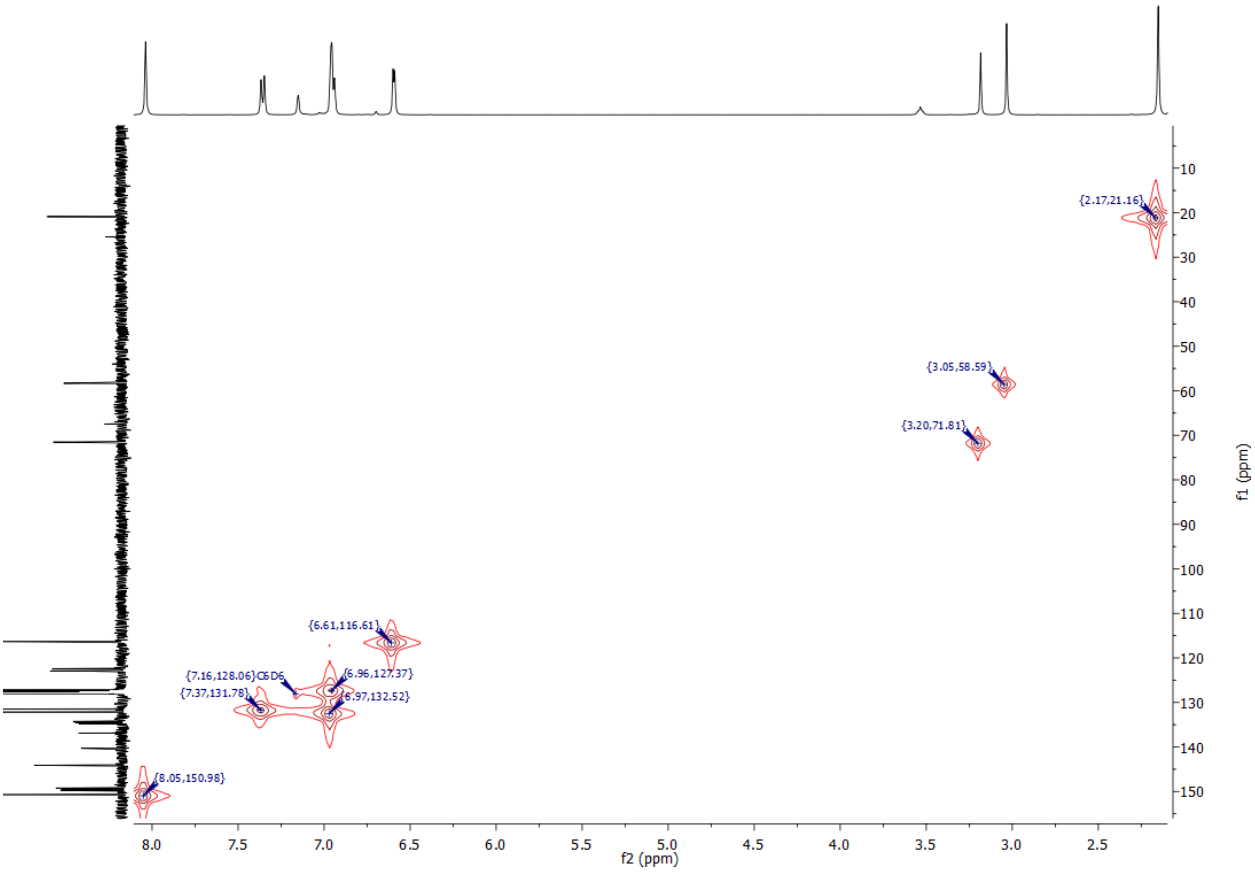

Figure S6. HMQCGP NMR spectrum of $\mathbf{3}^{\mathbf{tol}}$ in C_6D_6/py-d_5.

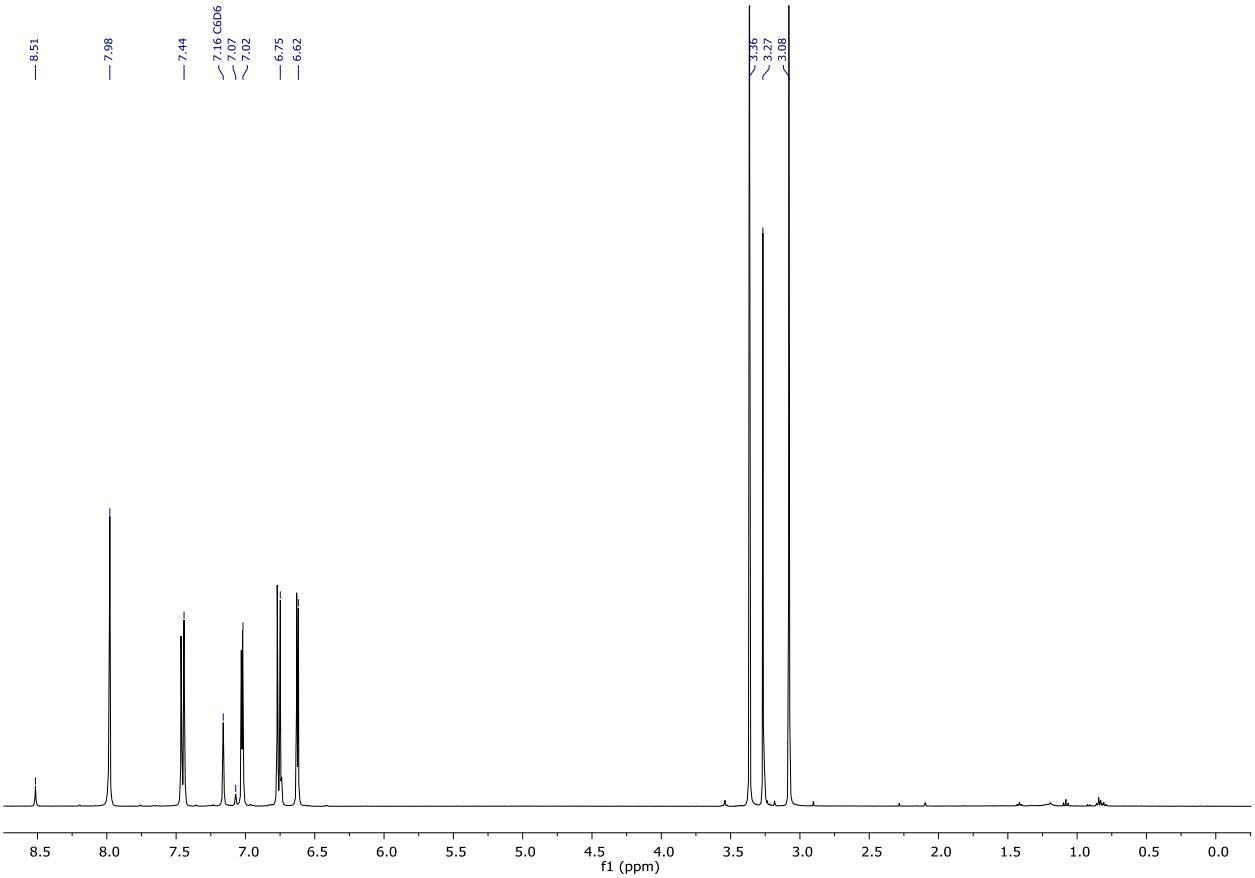

Figure S7. ^{1}H NMR spectrum of **3**$^{\mathbf{anis}}$ in C_6D_6/py-d_5.

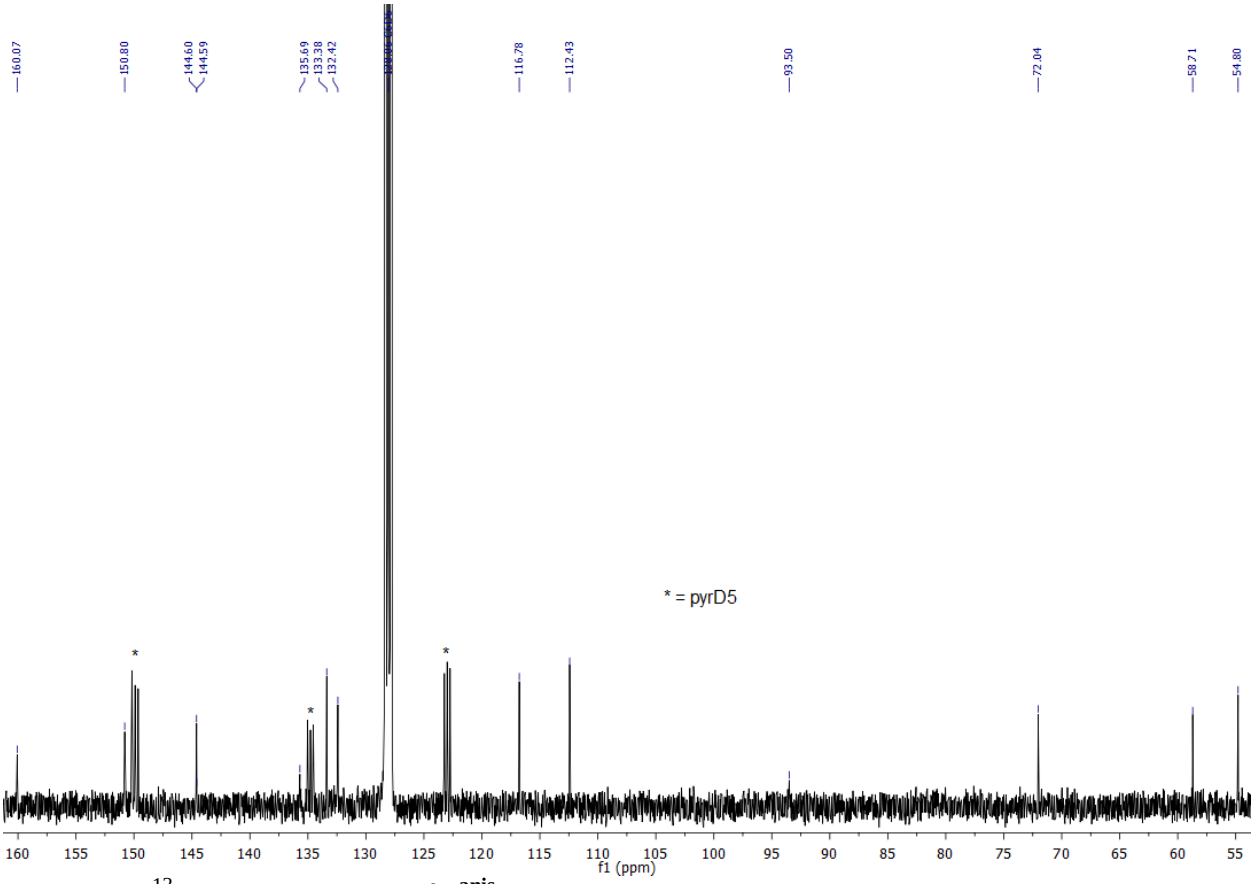

Figure S8. ^{13}C NMR spectrum of **3**$^{\mathbf{anis}}$ in C_6D_6/py-d_5.

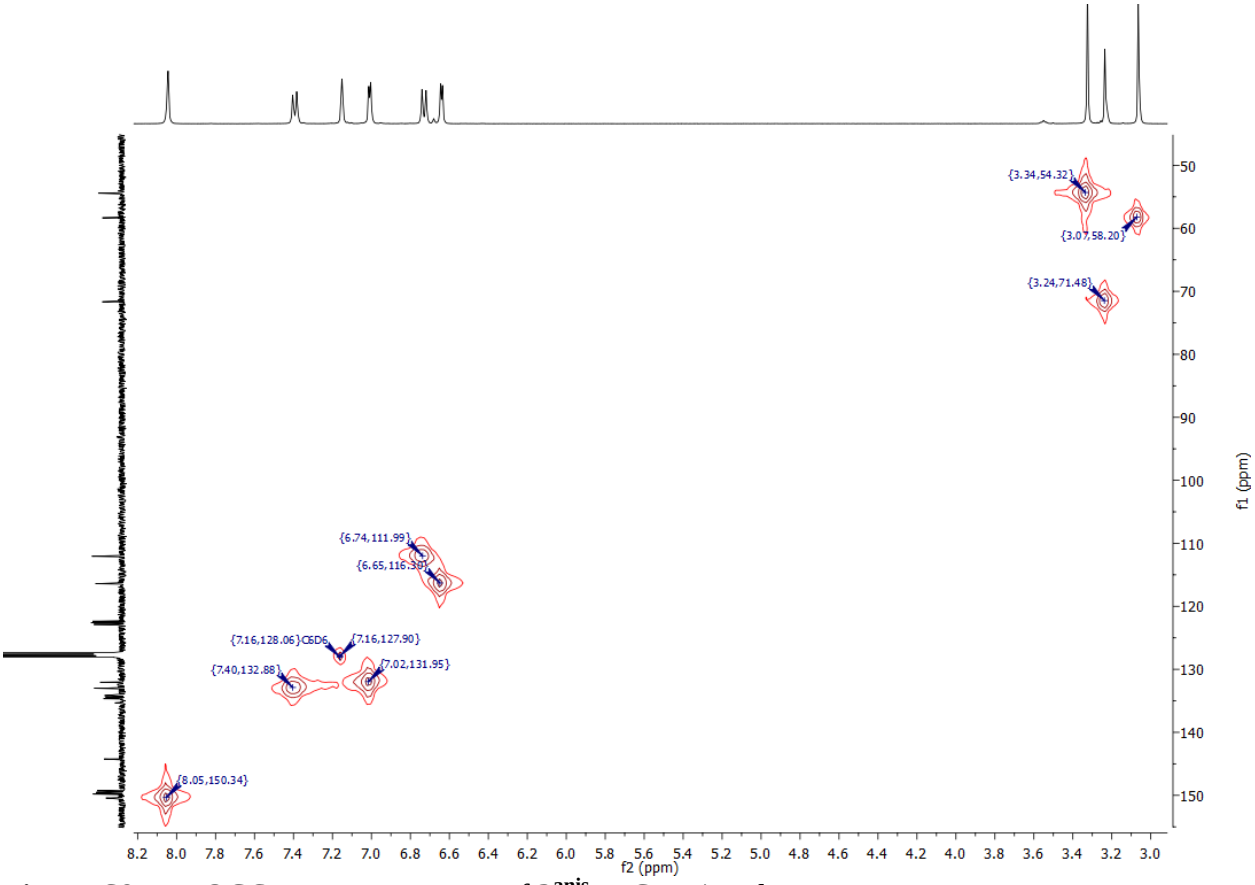

Figure S9. HMQCGP NMR spectrum of $\mathbf{3}^{\mathbf{anis}}$ in C_6D_6/py-d_5.

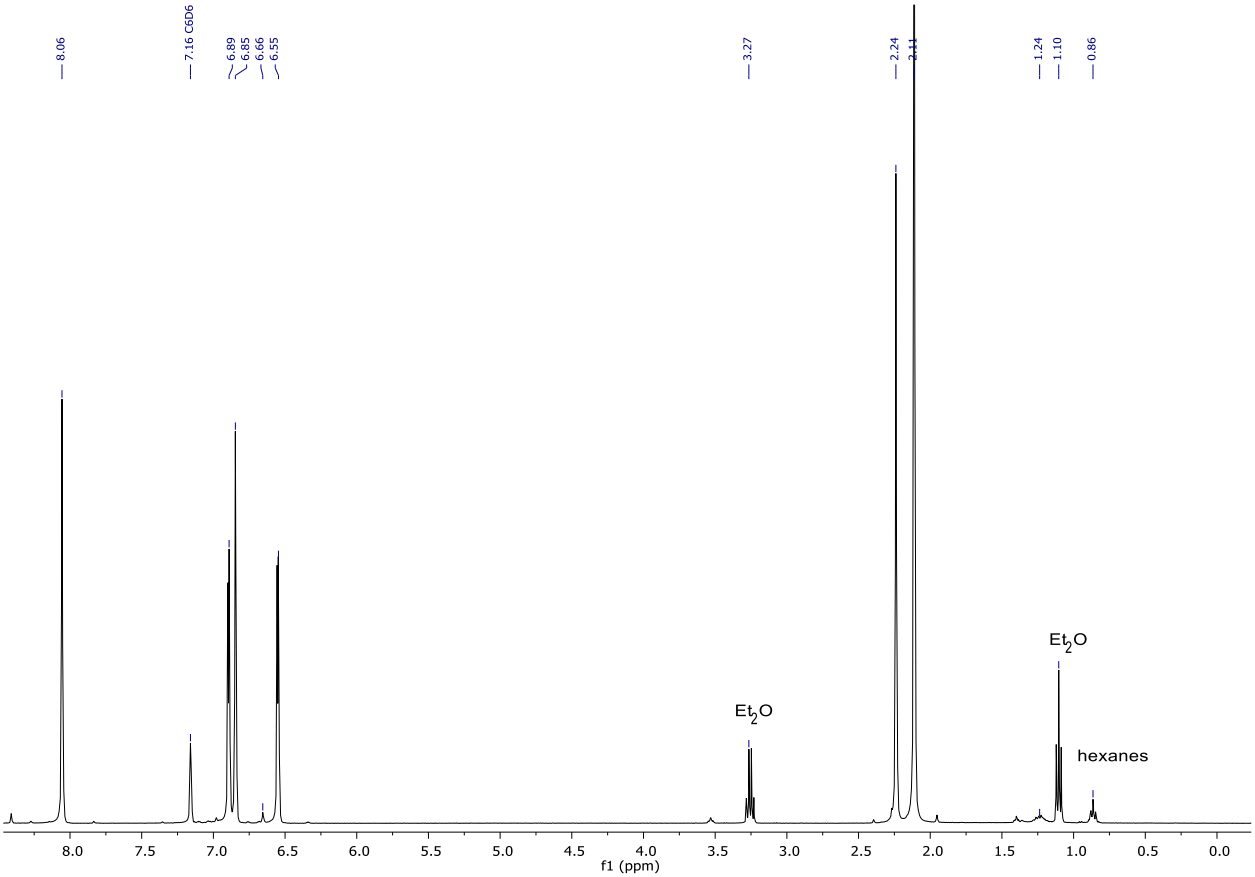

Figure S10. ^{1}H NMR spectrum of **3**$^{\mathbf{mes}}$ in C_6D_6/py-d_5.

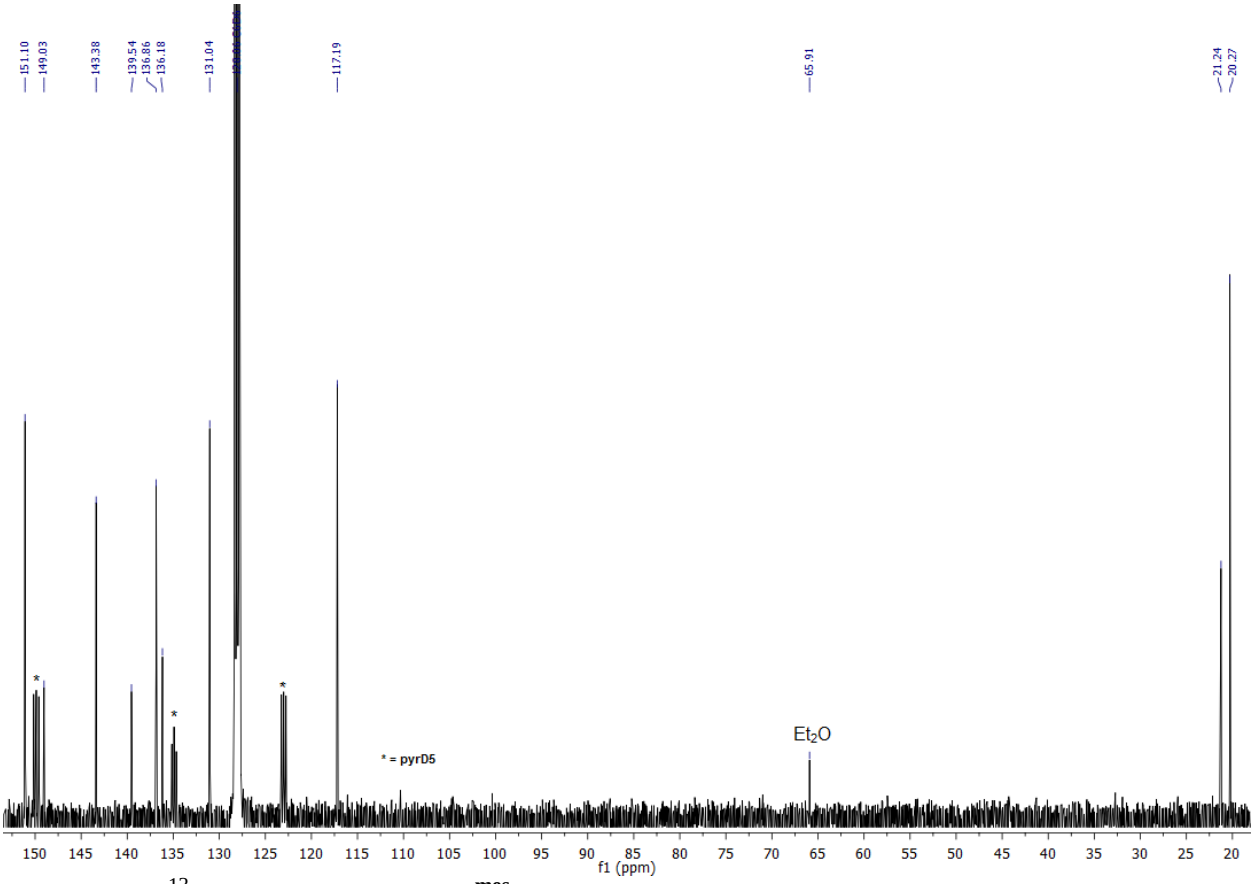

Figure S11. ^{13}C NMR spectrum of **3**$^{\mathbf{mes}}$ in C_6D_6/py-d_5.

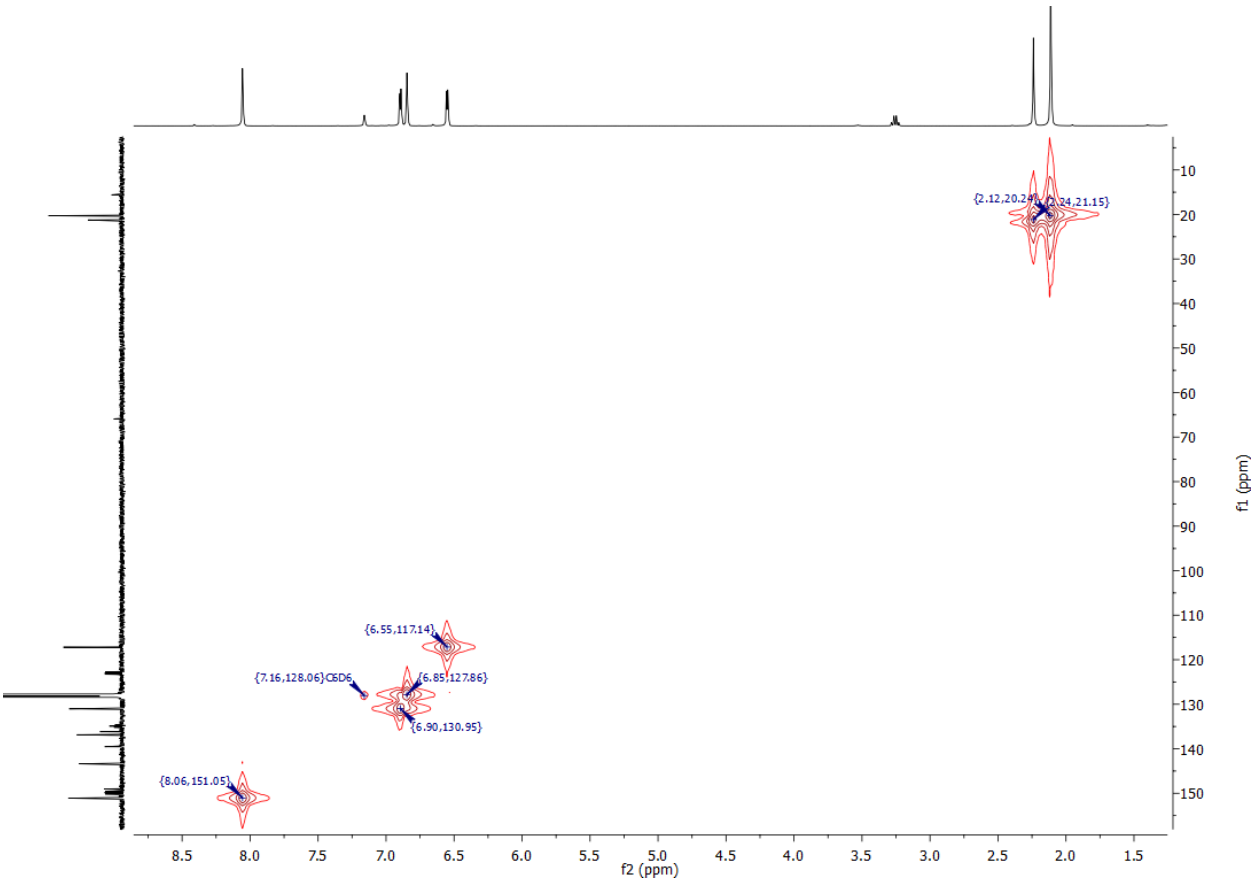

Figure S12. HMQCGP NMR spectrum of $\mathbf{3}^{\mathbf{mes}}$ in C_6D_6/py-d_5.

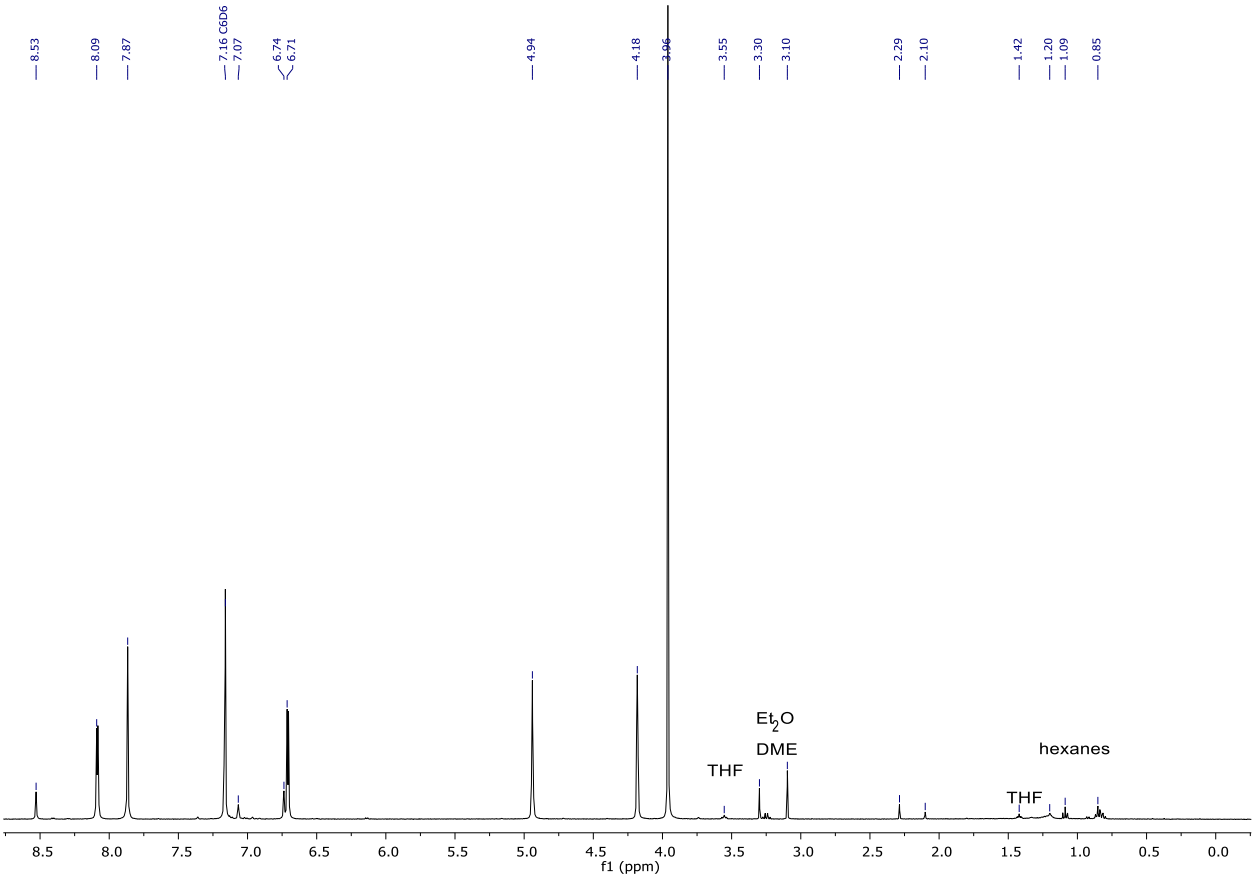

Figure S13. ^{1}H NMR spectrum of $\mathbf{3^{Fc}}$ in C_6D_6/py-d_5.

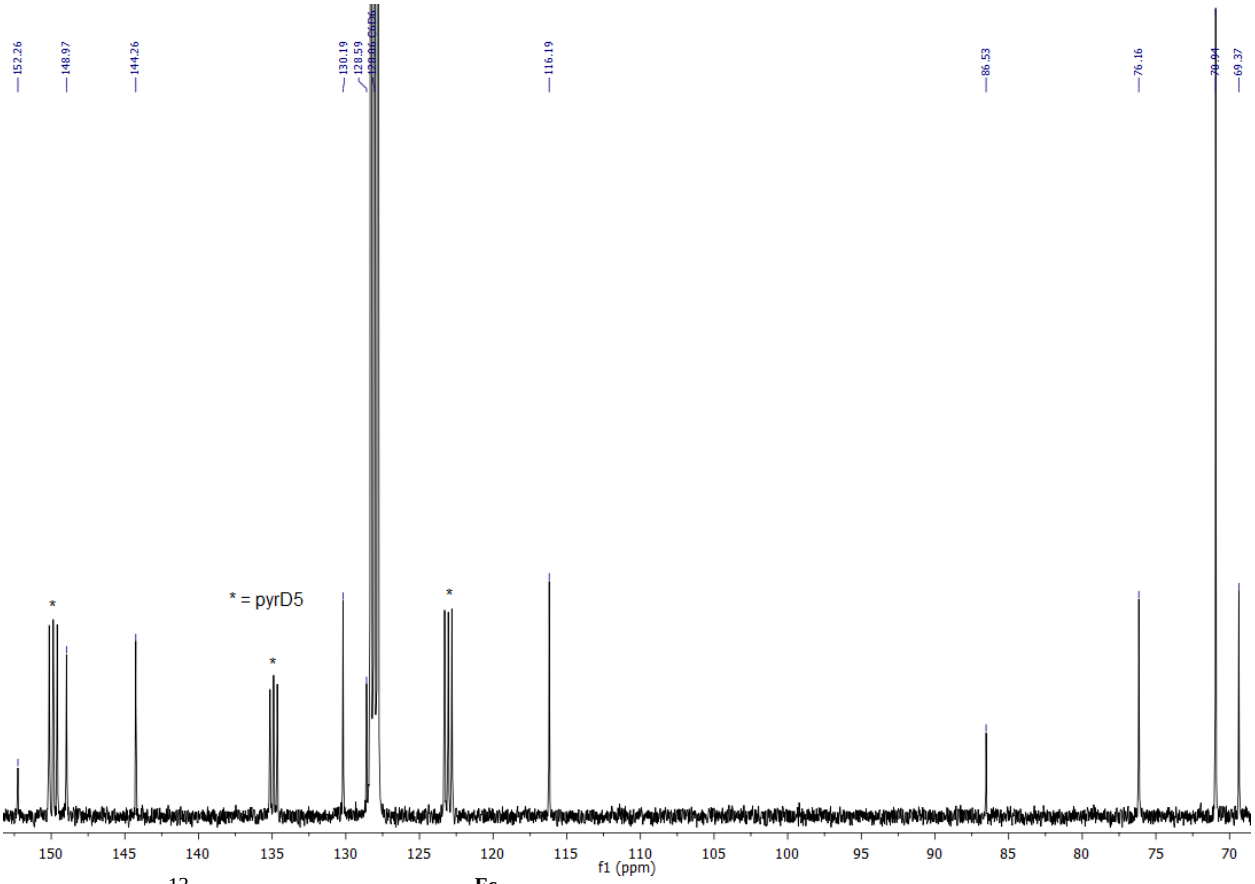

Figure S14. ^{13}C NMR spectrum of $\mathbf{3^{Fc}}$ in C_6D_6/py-d_5.

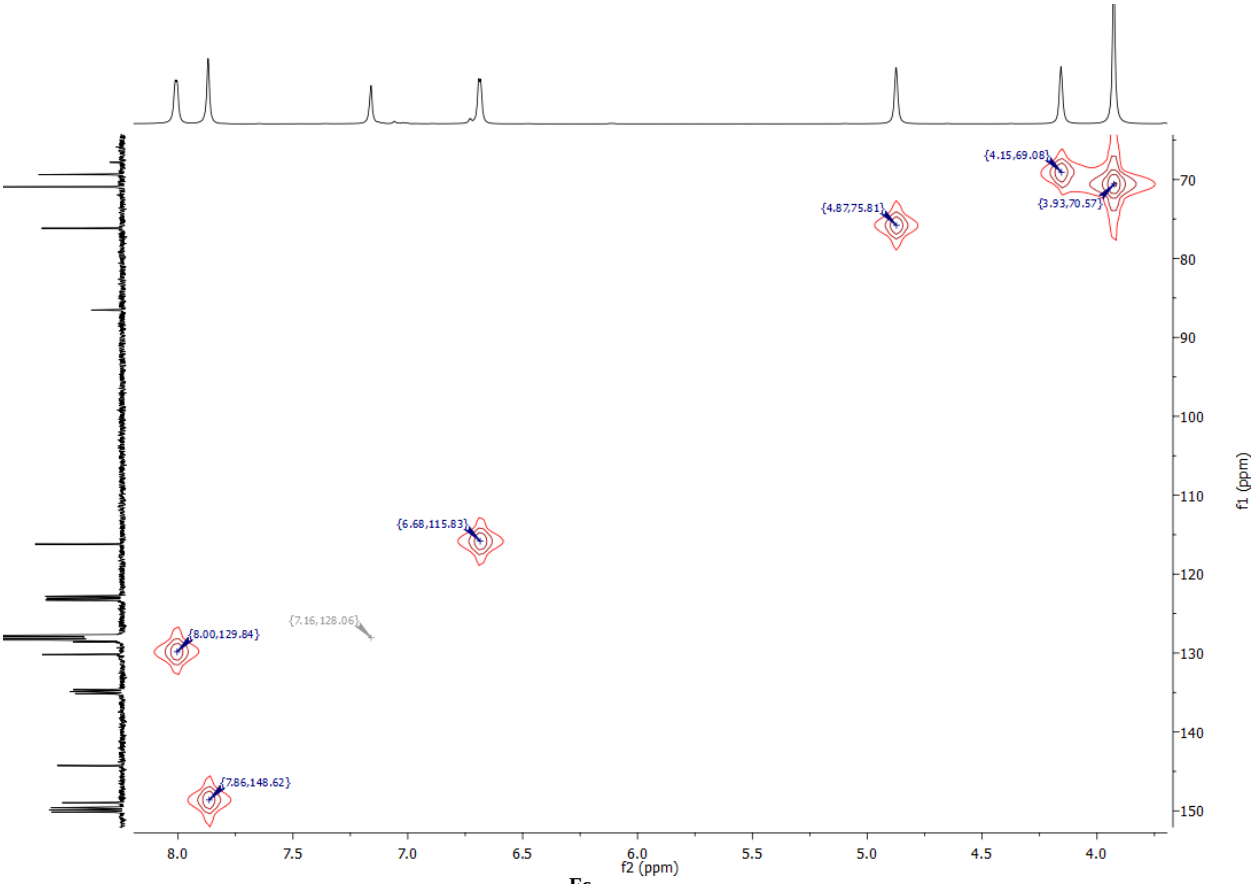

Figure S15. HMQCGP NMR spectrum of $\mathbf{3^{Fc}}$ in C_6D_6/py-d_5.

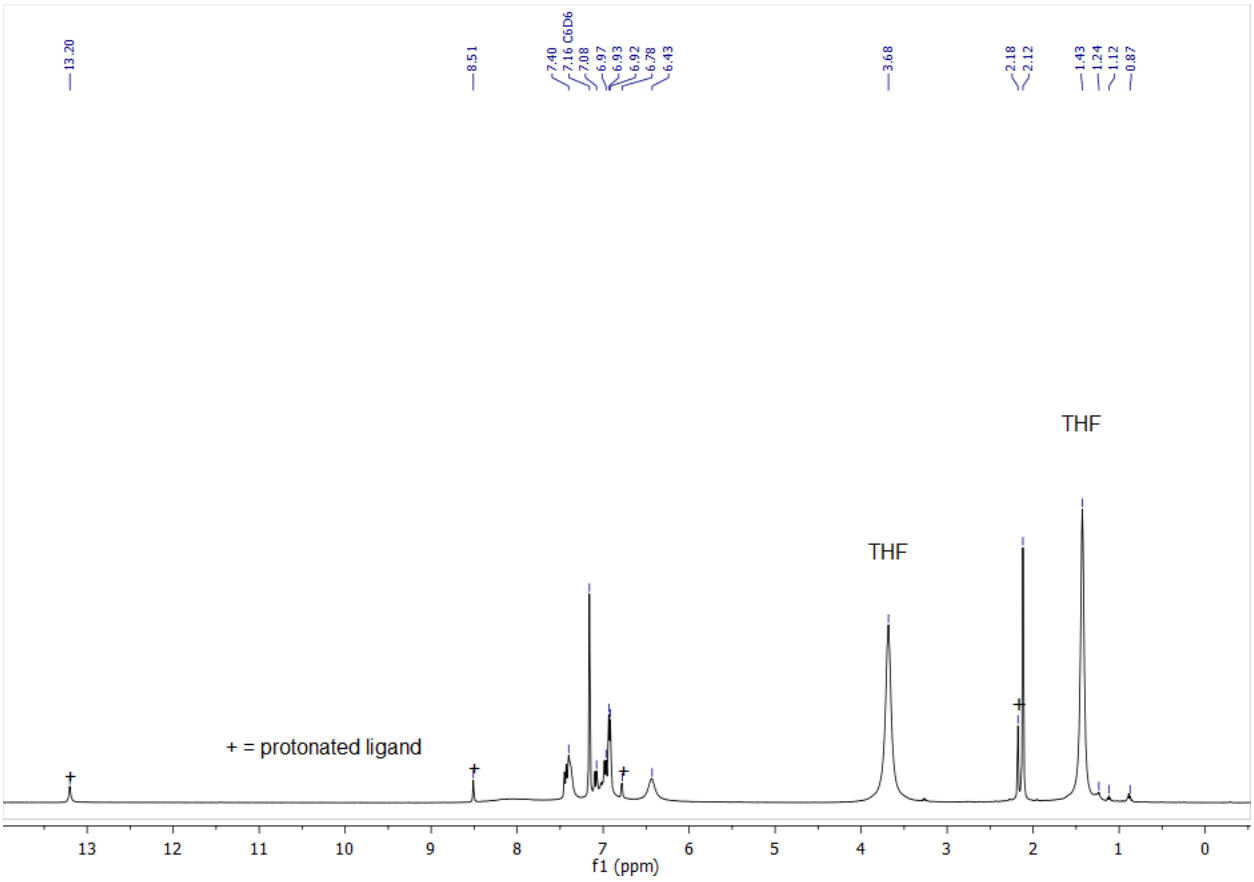

Figure S16. ^{1}H NMR spectrum of **4**$^{\mathbf{tol}}$-THF in C_6D_6/py-d_5.

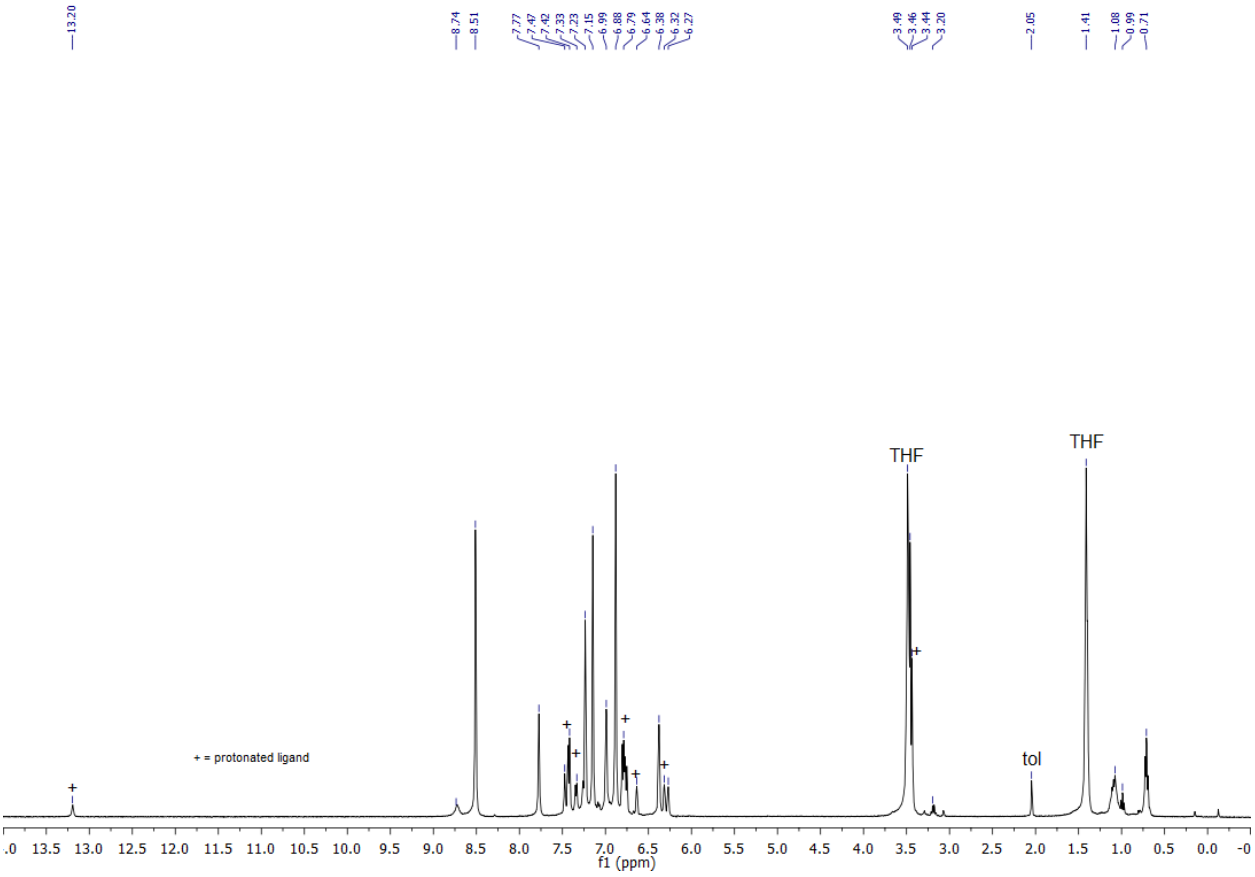

Figure S17. ^{1}H NMR spectrum of **4**$^{\mathbf{anis}}$-THF in py-d_5.

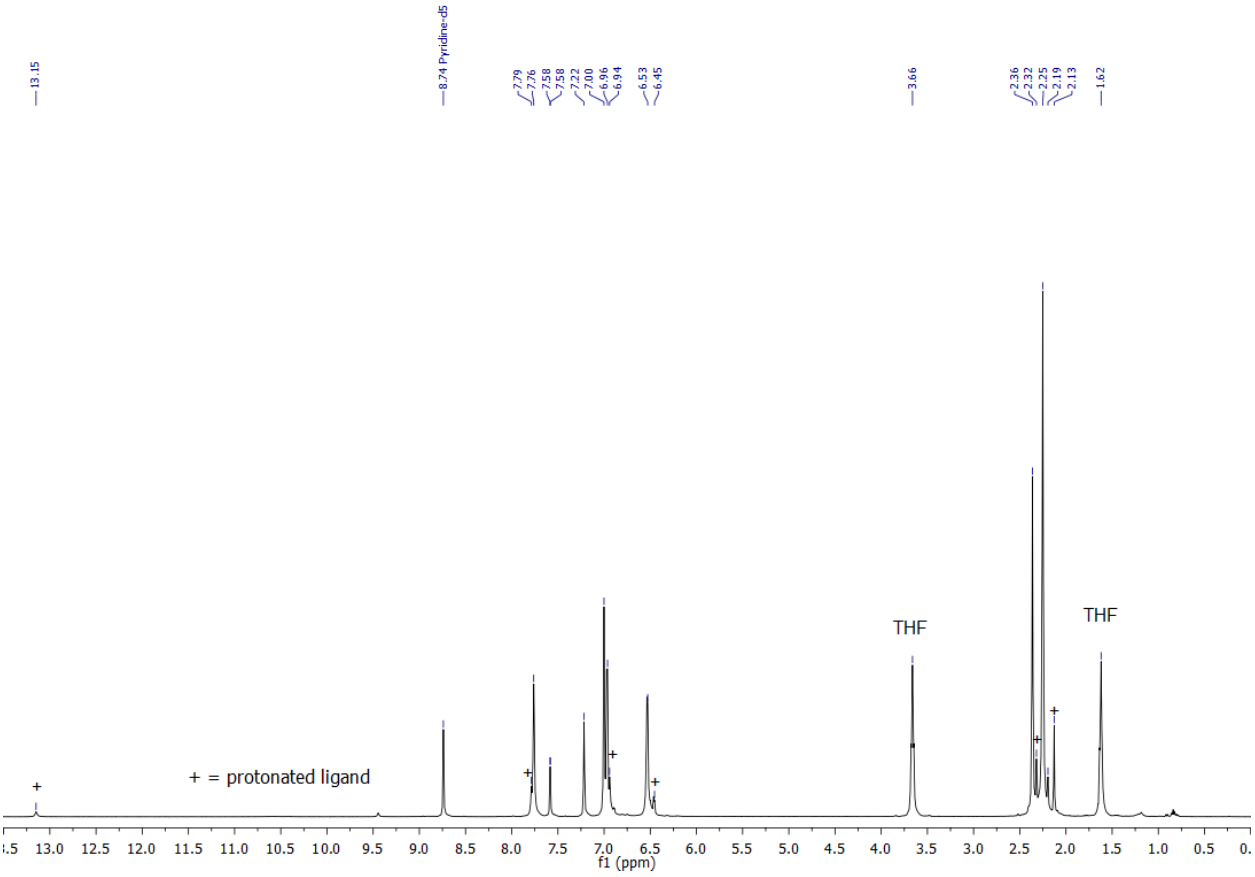

Figure S18. ^{1}H NMR spectrum of **4**$^{\mathbf{mes}}$-THF in py-d_5.

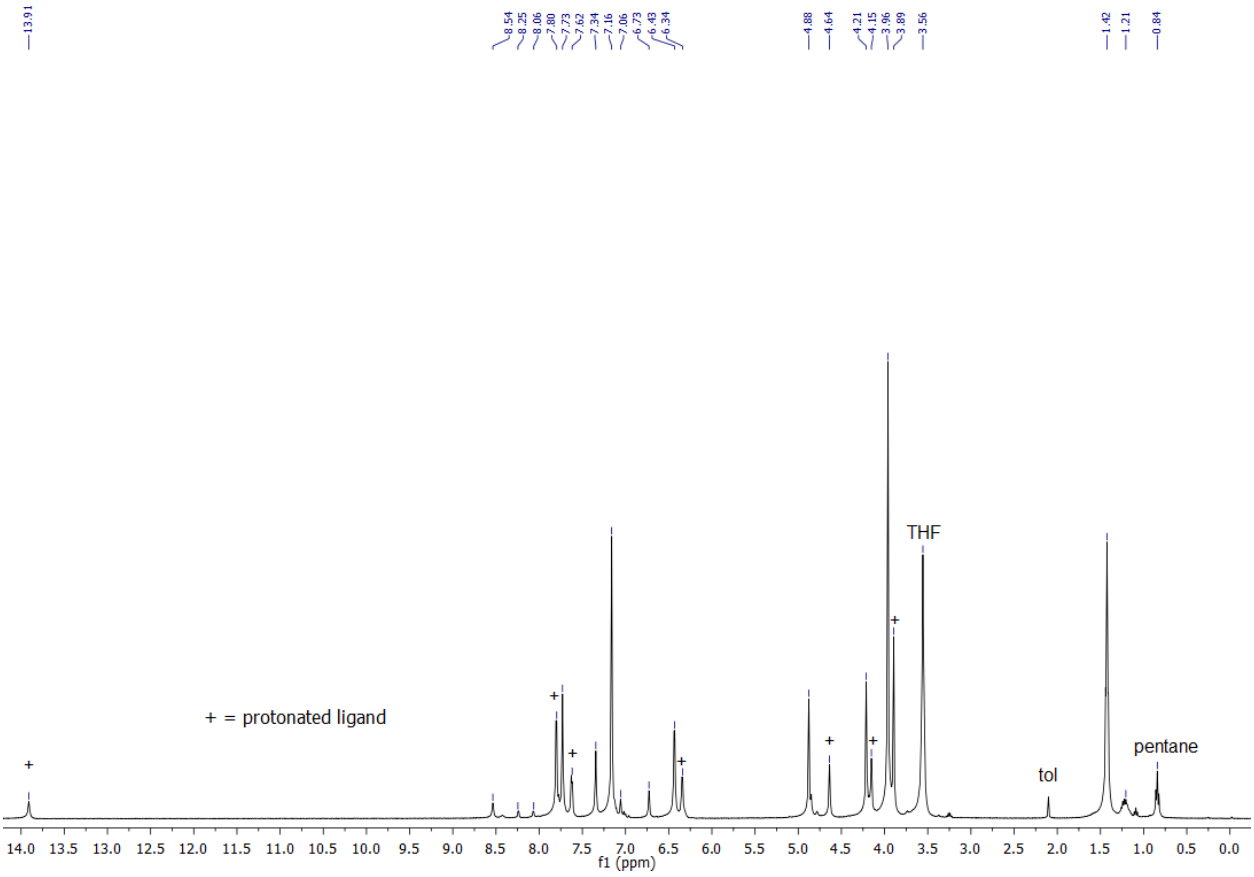

Figure S19. ^{1}H NMR spectrum of $\mathbf{4}^{\mathbf{Fc}}$-THF in C_6D_6/py-d_5.

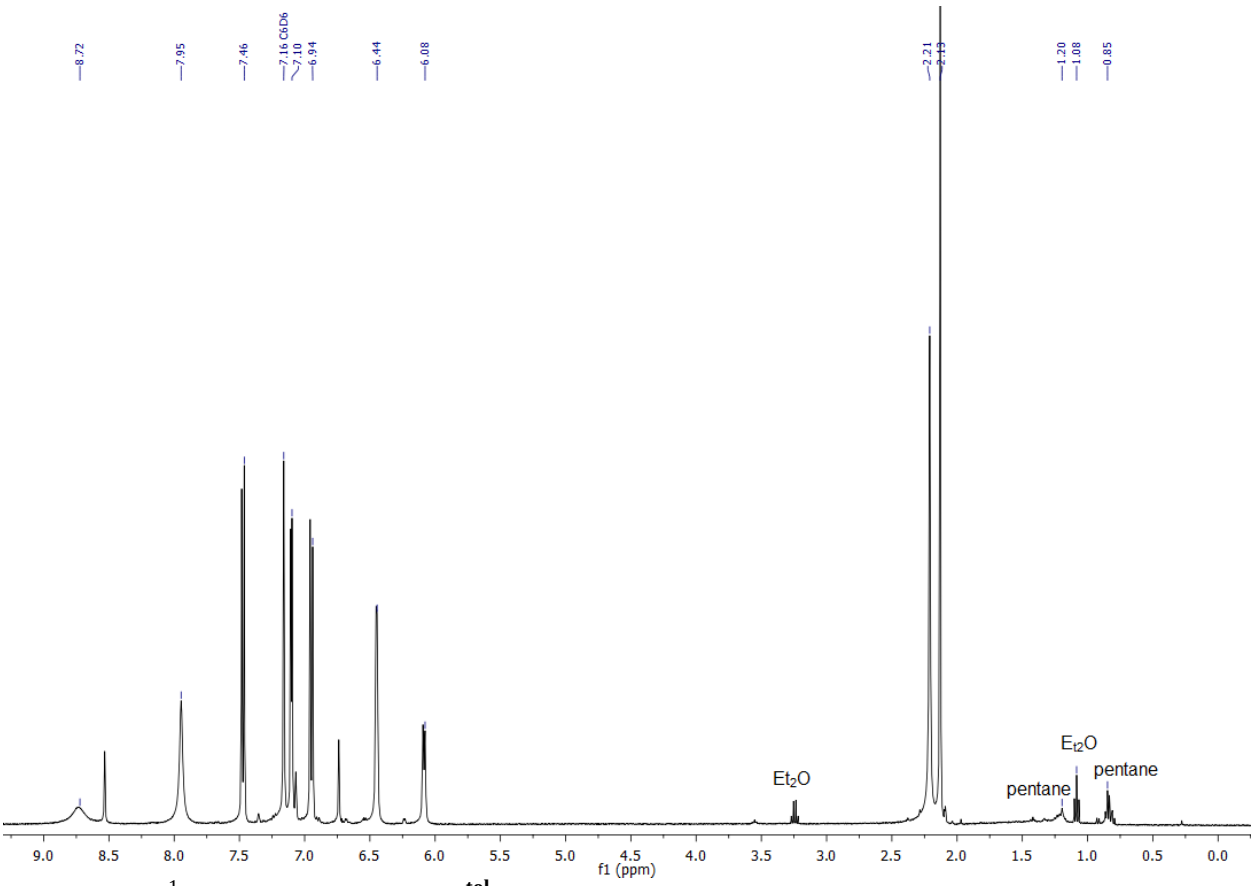

Figure S20. ^{1}H NMR spectrum of **4**$^{\mathbf{tol}}$-DMAP in C_6D_6/py-d_5.

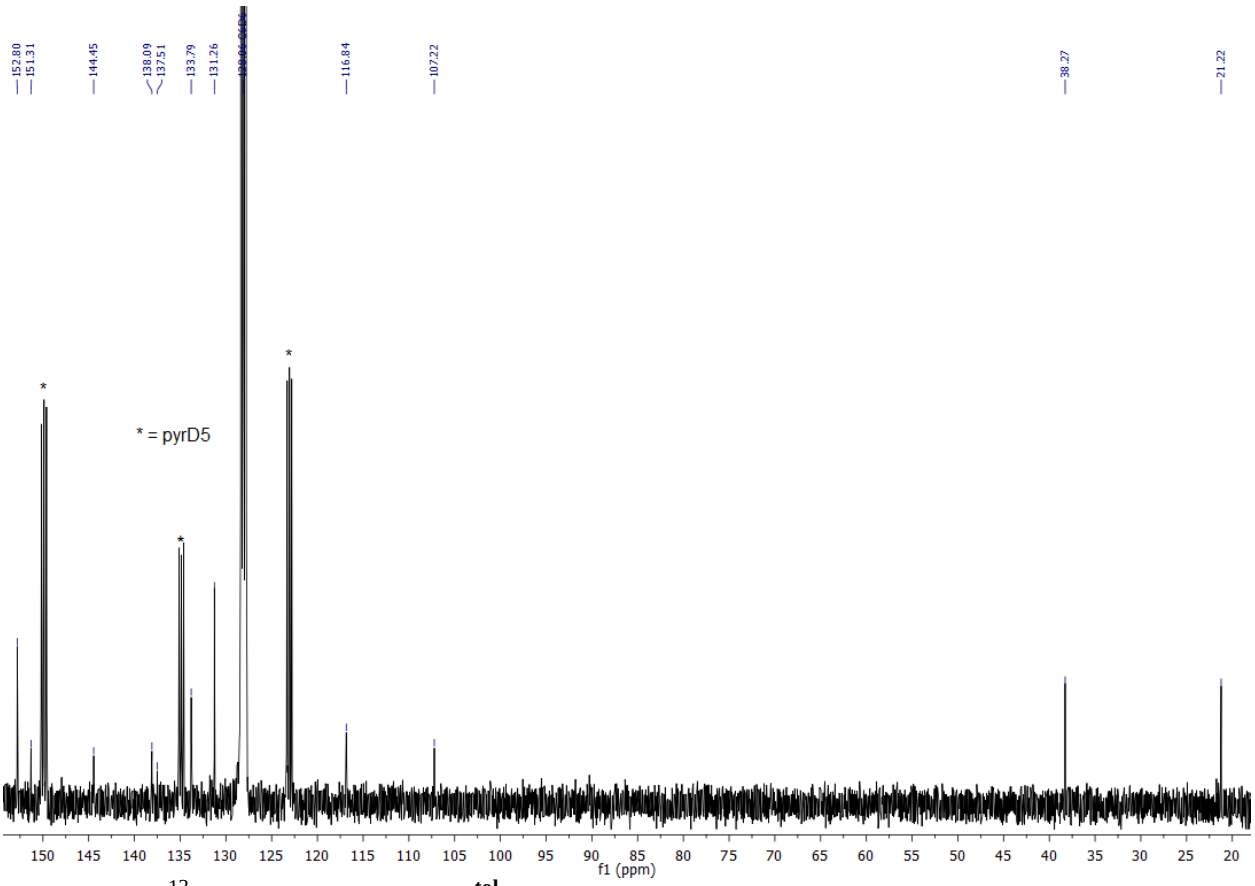

Figure S21. ^{13}C NMR spectrum of **4^{tol}**-DMAP in C_6D_6/py-d_5.

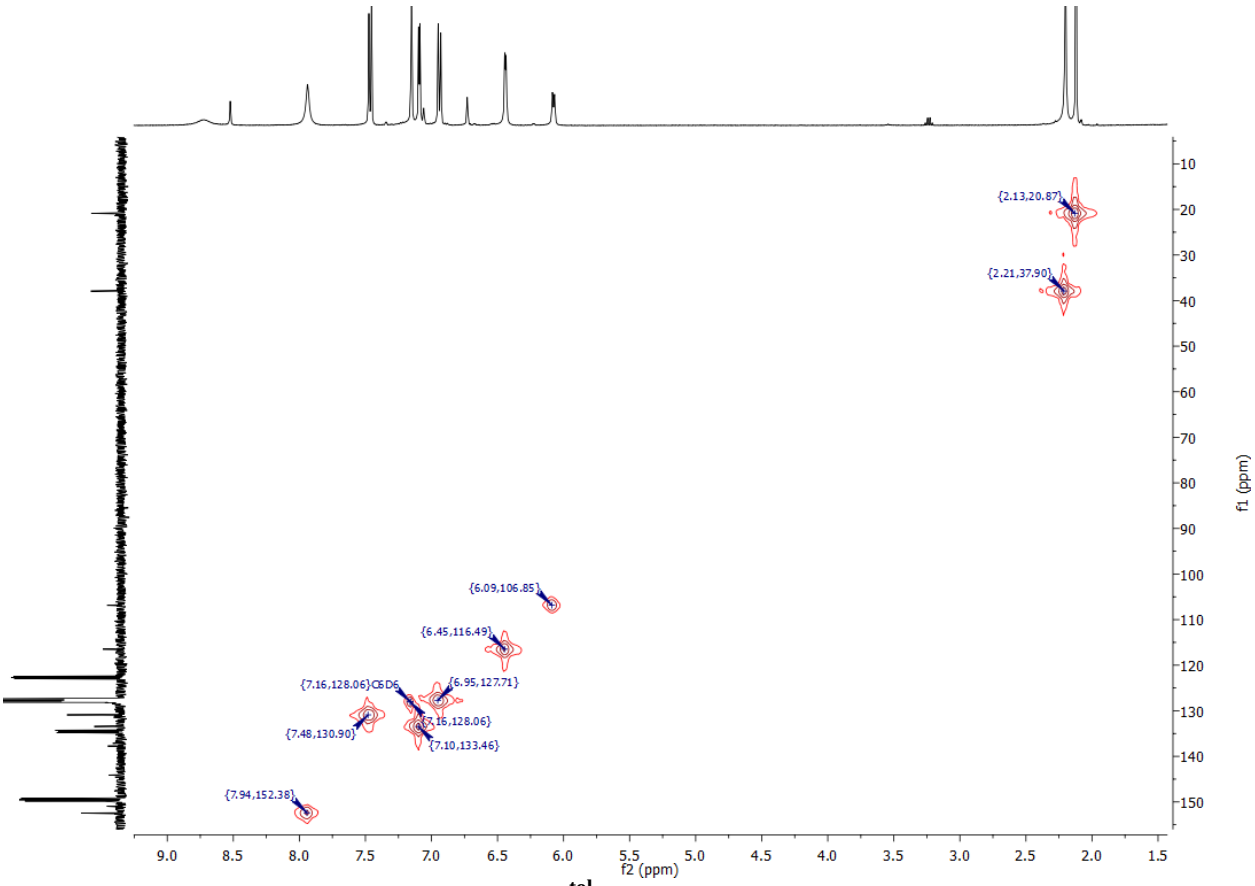

Figure S22. HMQCGP NMR spectrum of **4**$^{\mathbf{tol}}$-DMAP in C_6D_6/py-d_5.

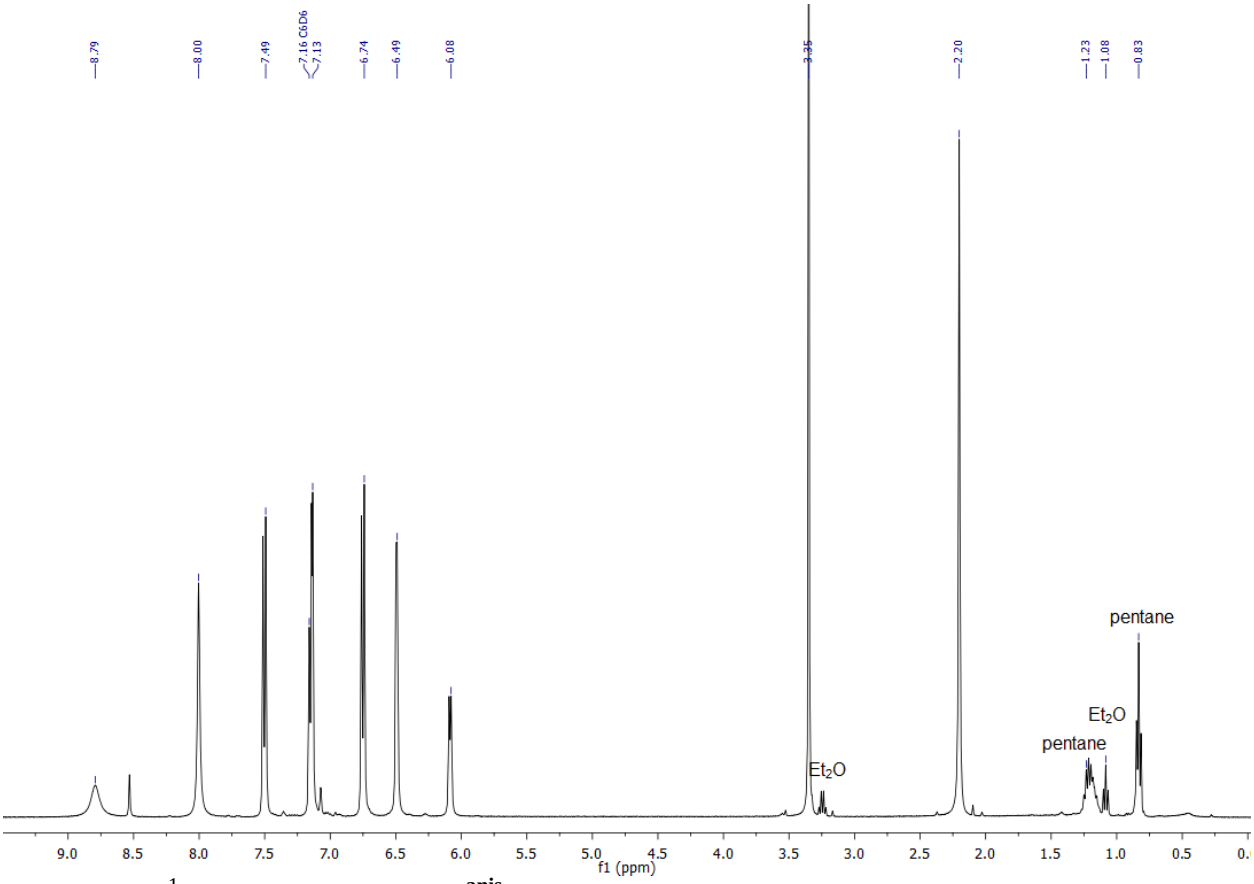

Figure S23. ^{1}H NMR spectrum of **4**$^{\mathbf{anis}}$-DMAP in C_6D_6/py-d_5.

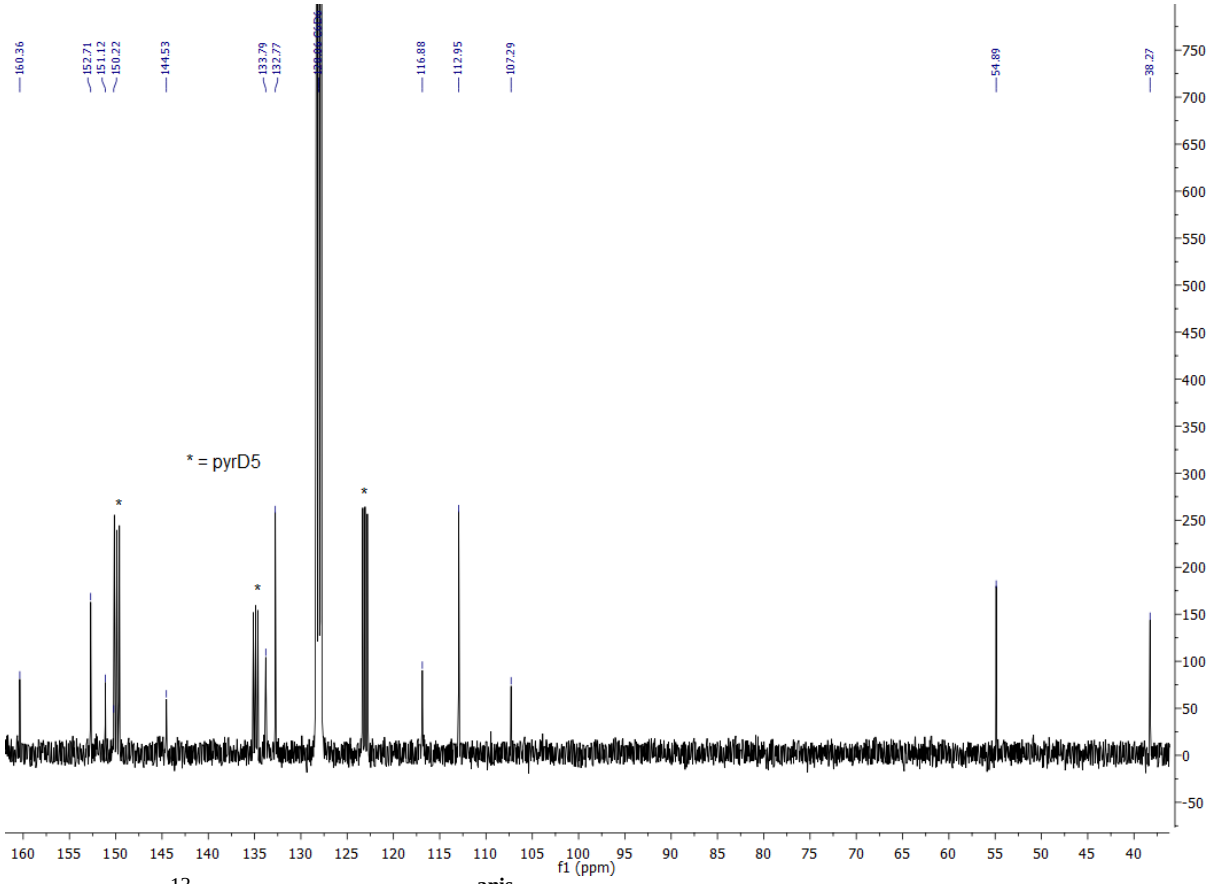

Figure S24. ^{13}C NMR spectrum of **4**$^{\mathbf{anis}}$-DMAP in C_6D_6/py-d_5.

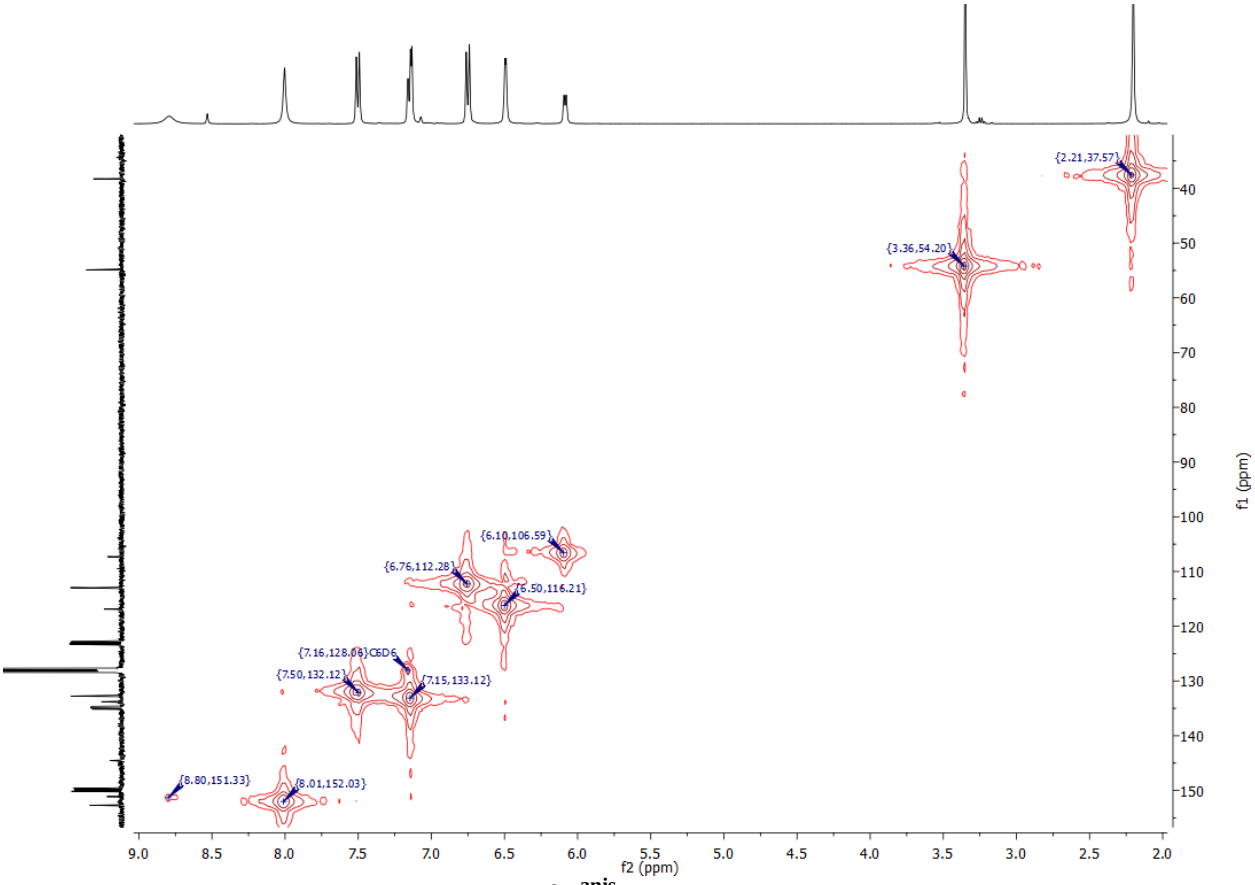

Figure S25. **HMQCGP** NMR spectrum of **4^{anis}DMAP** in C_6D_6/ py-d5.

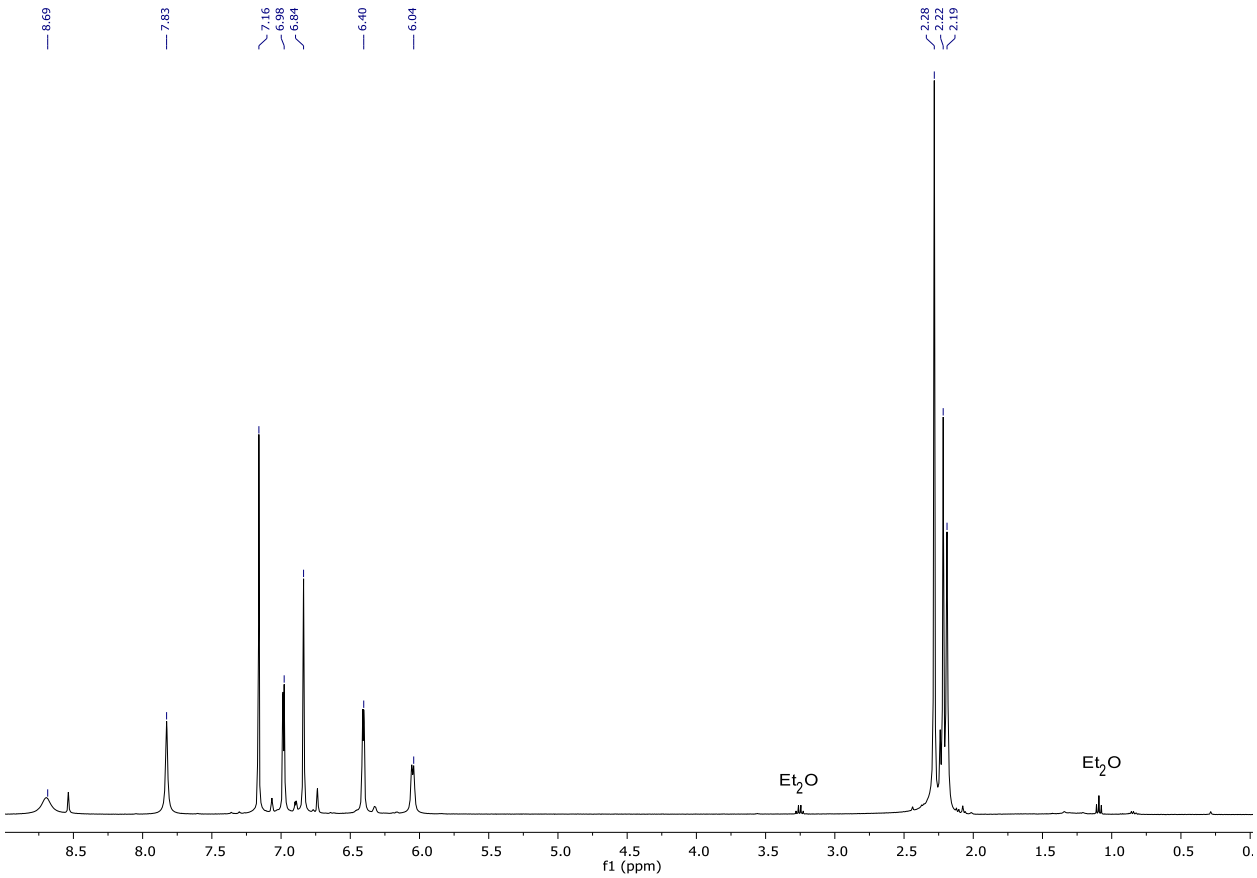

Figure S26. ^{1}H NMR spectrum of **4**$^{\mathbf{mes}}$-DMAP in C_6D_6/py-d_5.

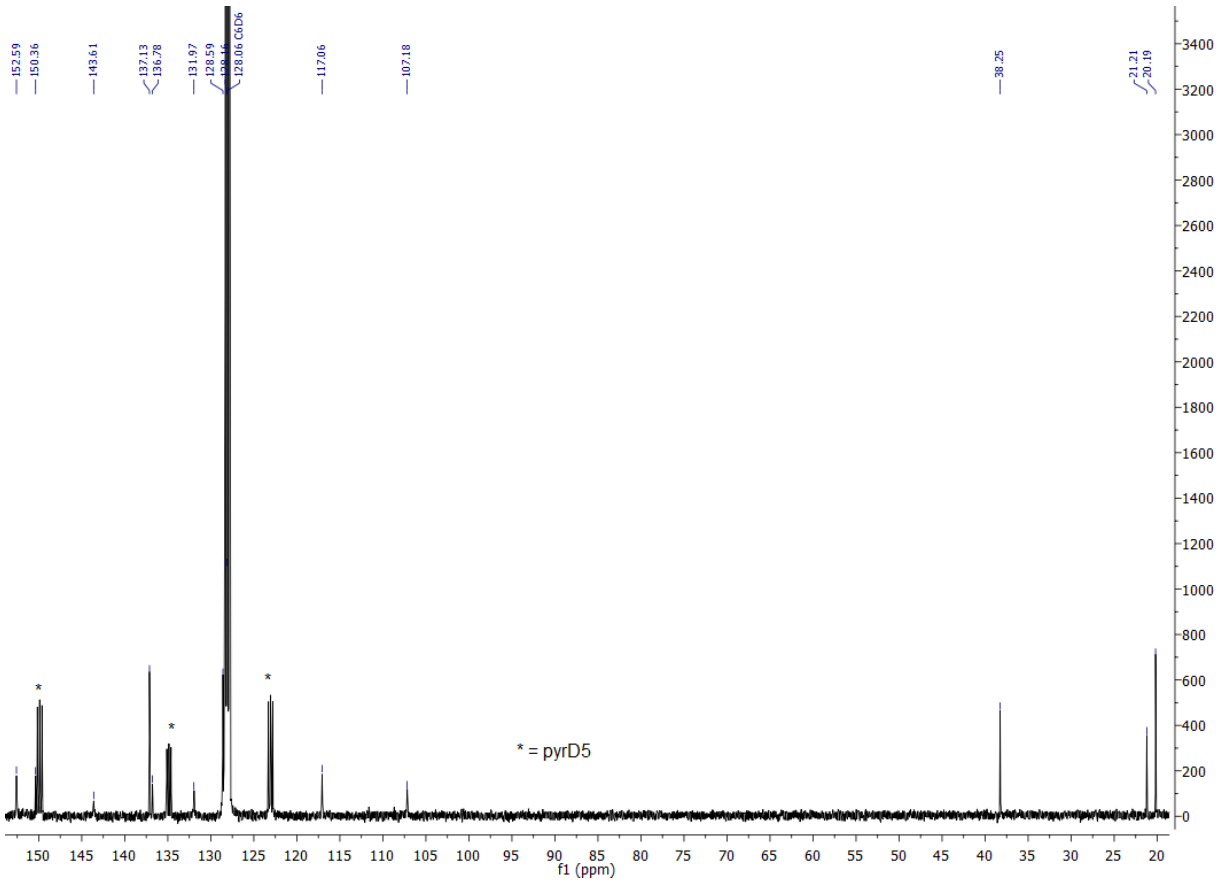

Figure S27. ^{13}C NMR spectrum of **4**$^{\mathbf{mes}}$-DMAP in C_6D_6/py-d_5.

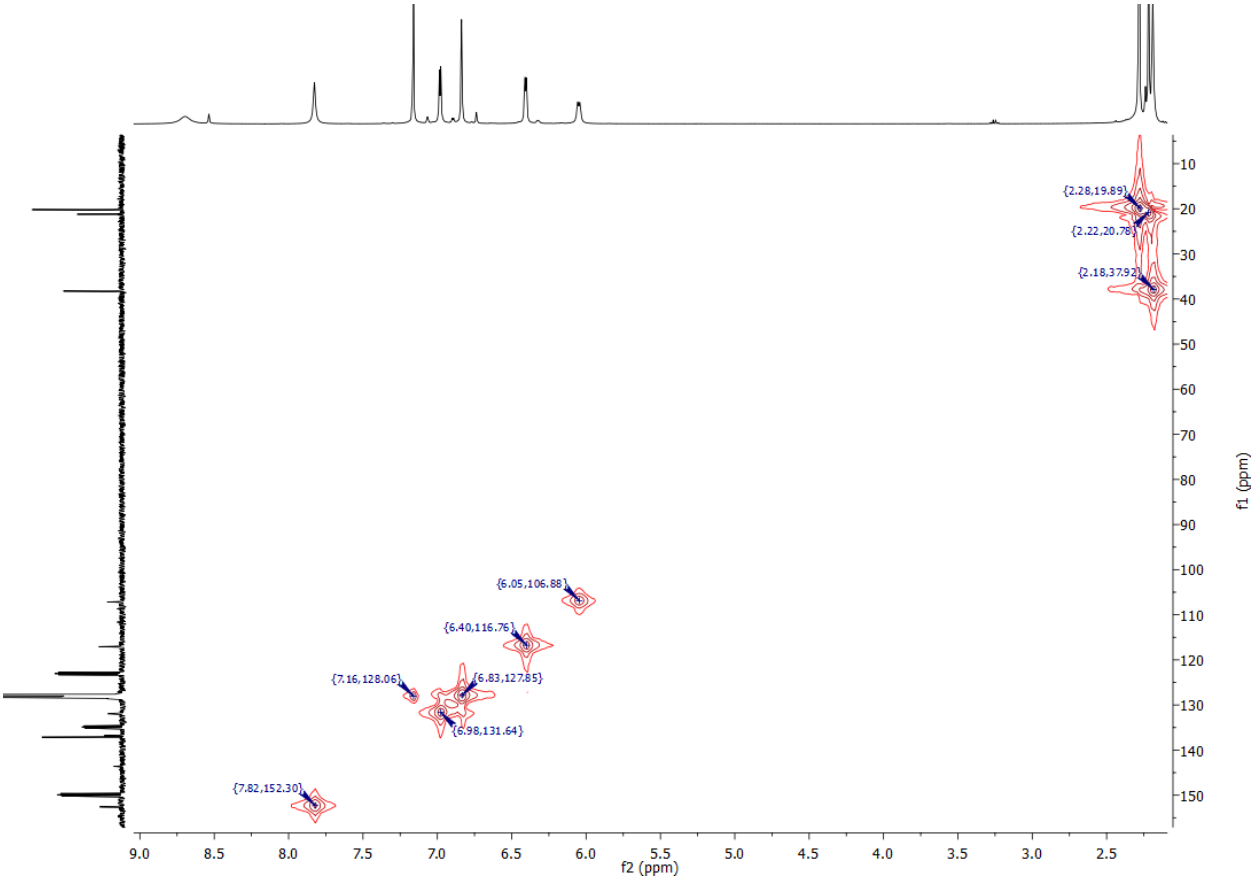

Figure S28. HMQCGP NMR spectrum of **4**$^{\mathbf{mes}}$-DMAP in C_6D_6/py-d_5.

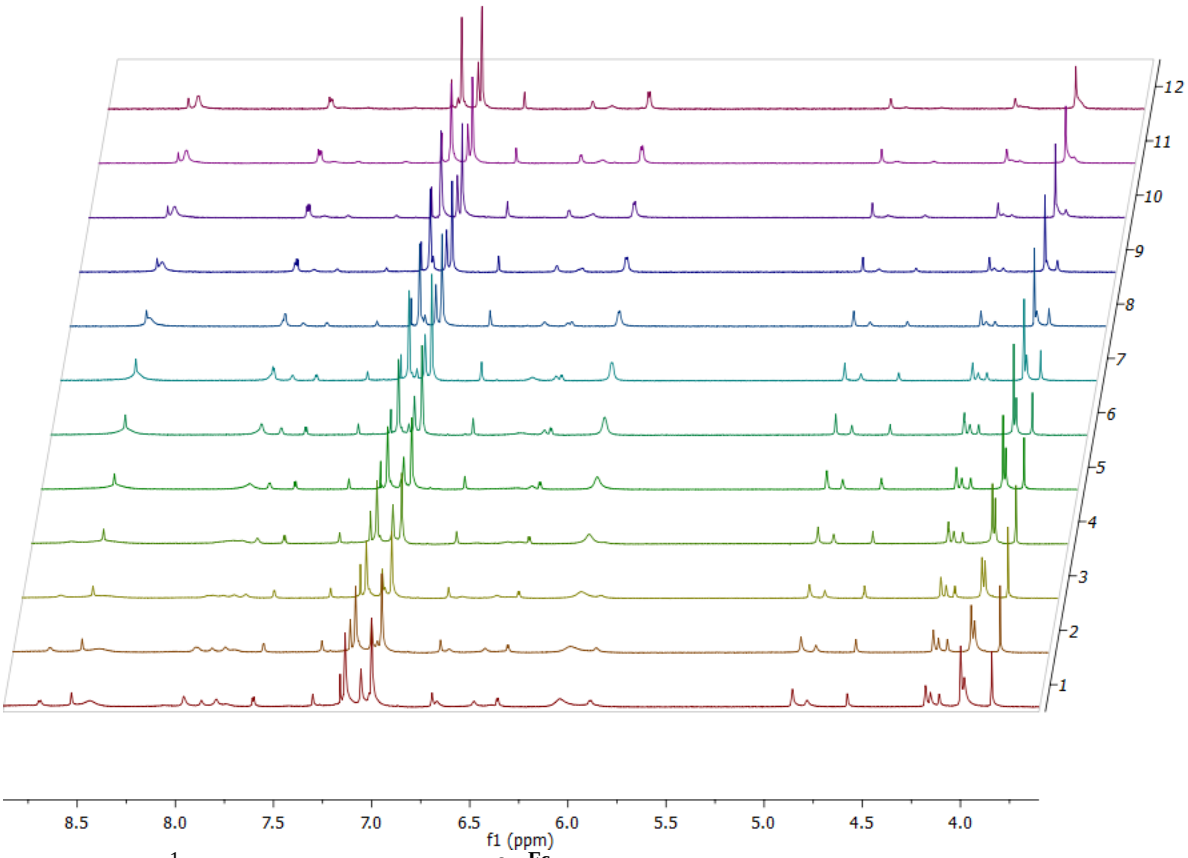

Figure S29. ^{1}H NMR spectral array of **4**$^{\mathbf{Fc}}$-DMAP in C_7D_8/py-d_5. Spectrum 1 corresponds to -30 °C, and the subsequent numbers correspond to increasing temperatures in increments of 10 °C.

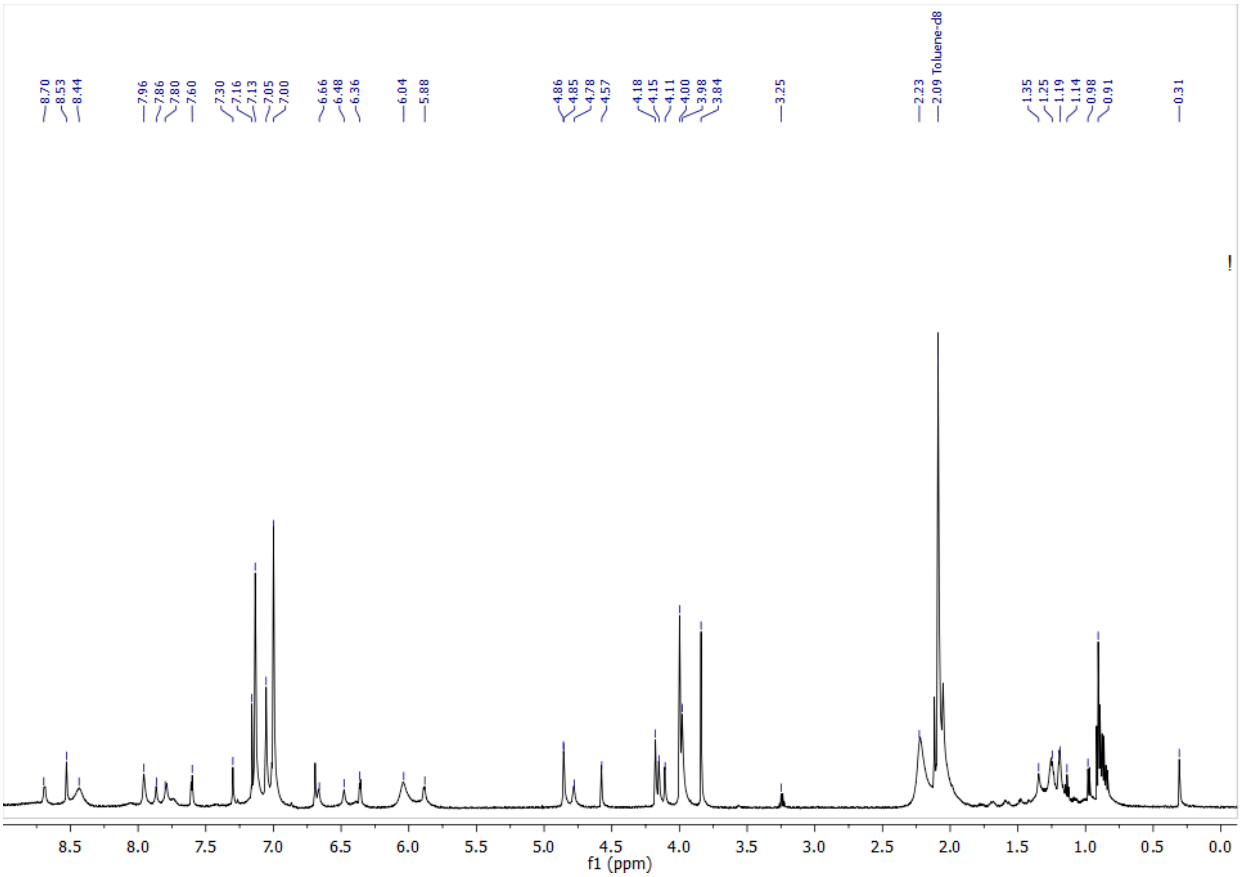

Figure S30. ^{1}H NMR spectrum of **4**$^{\mathbf{Fc}}$-DMAP in C_7D_8/py-d_5 at -30 °C.

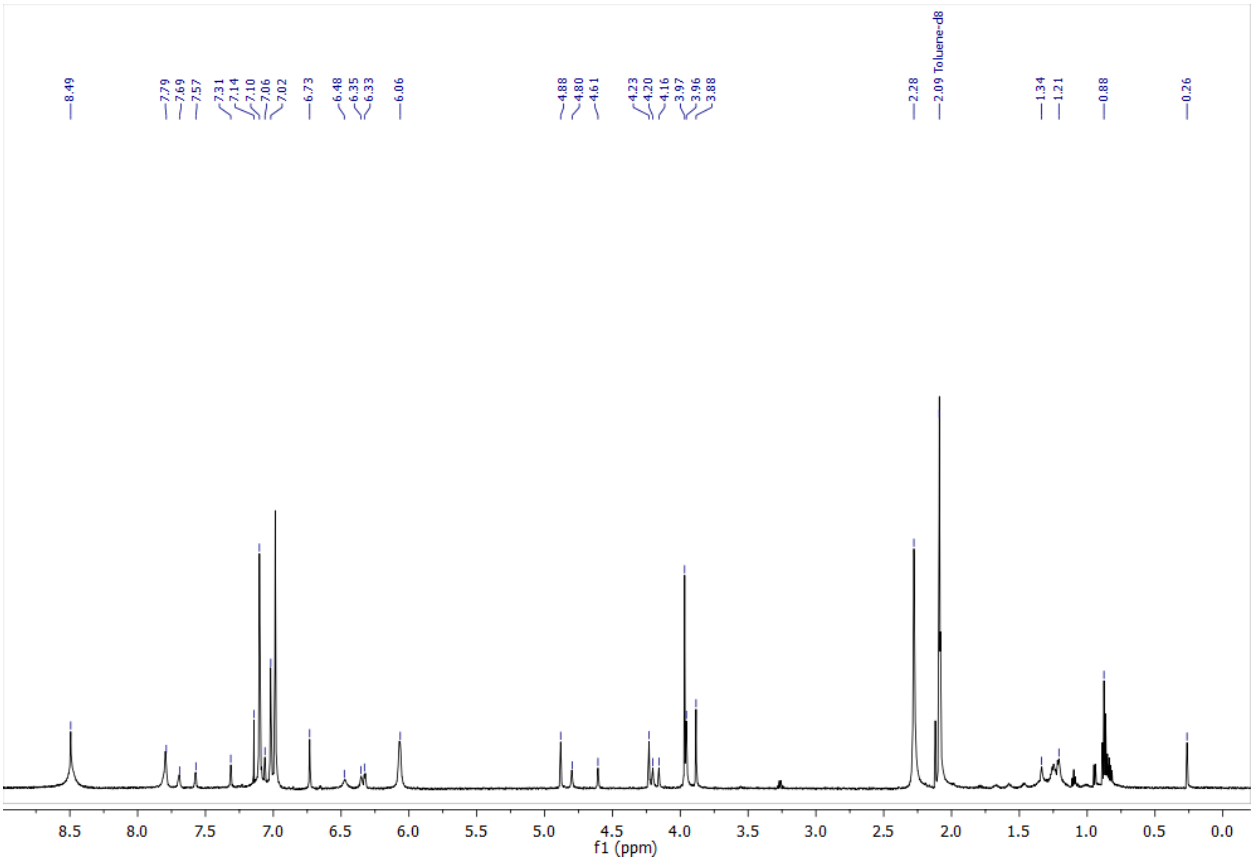

Figure S31. ^{1}H NMR spectrum of **4**$^{\mathbf{Fc}}$-DMAP in C_7D_8/py-d_5 at 30 °C.

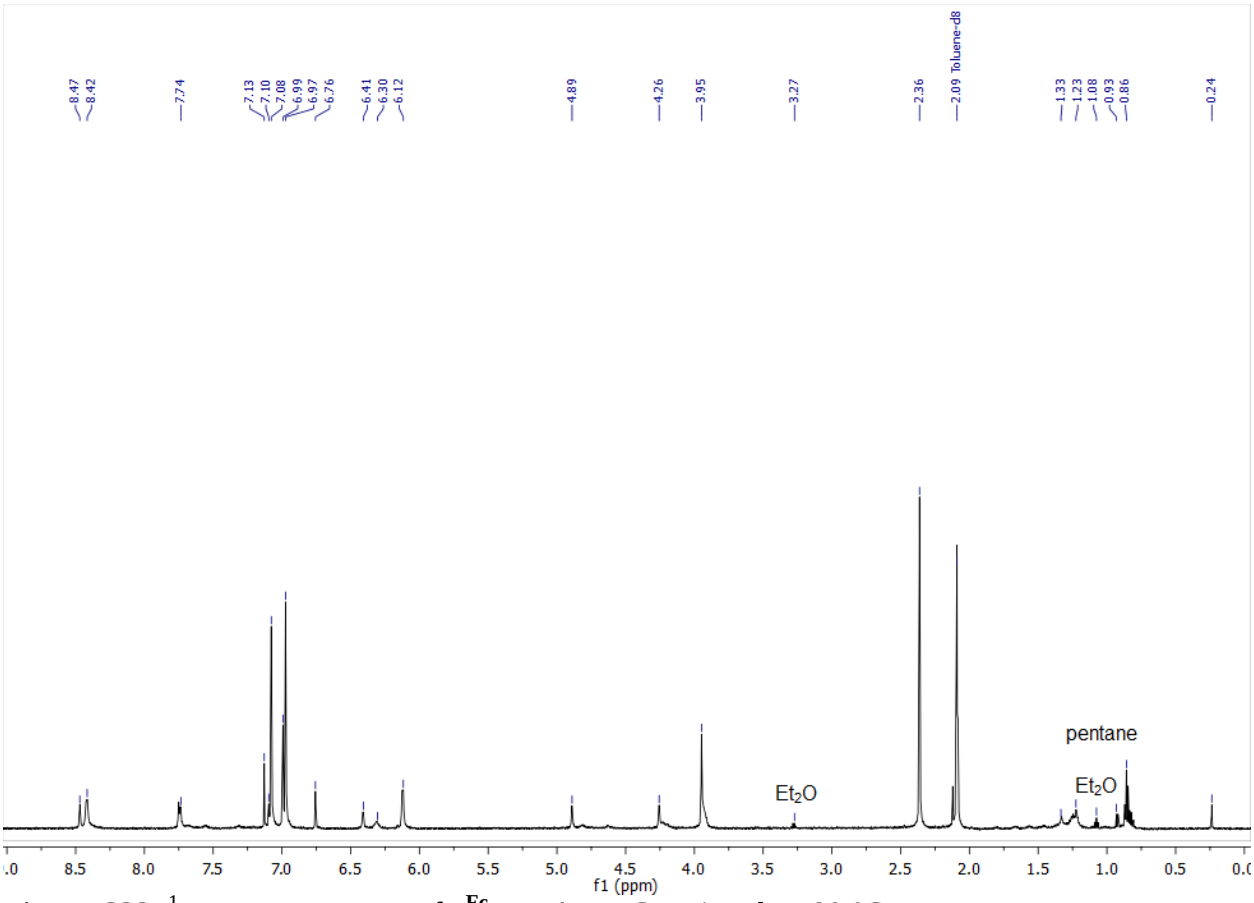

Figure S32. ^{1}H NMR spectrum of **4**$^{\mathbf{Fc}}$-DMAP in C_7D_8/py-d_5 at 80 °C.

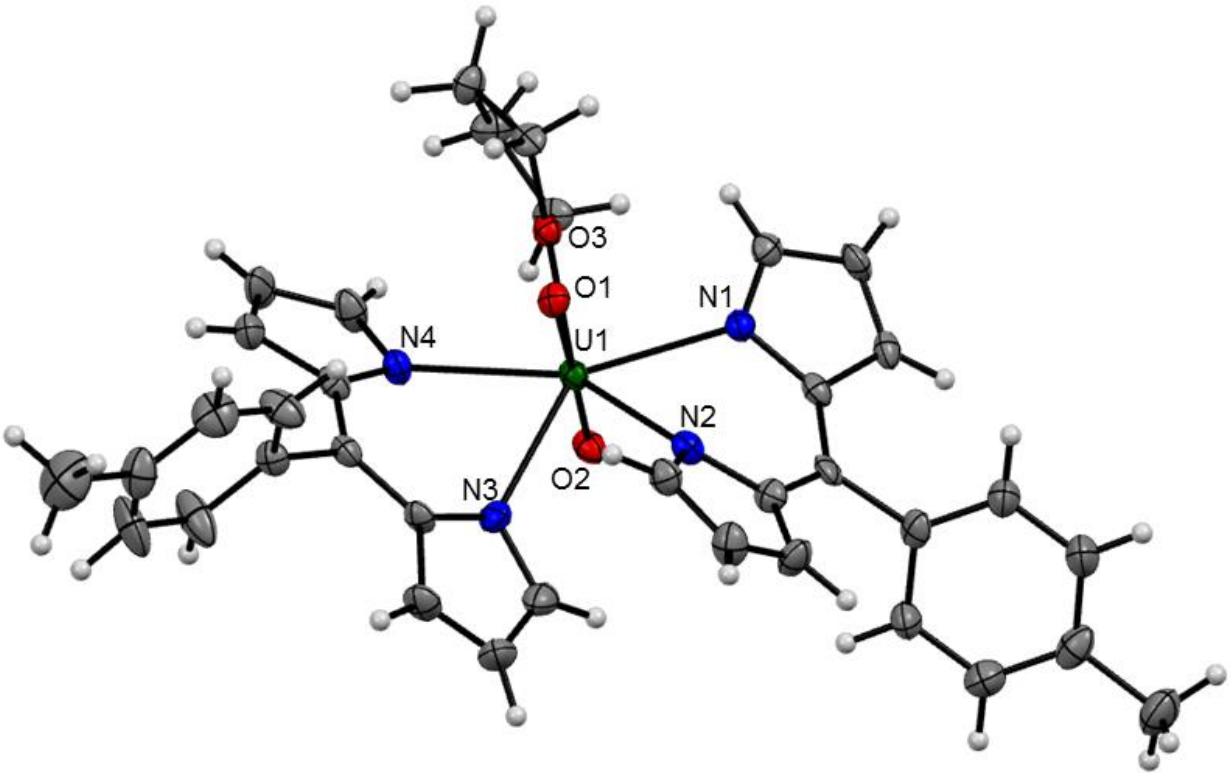

Figure S33. Solid-state molecular structure of **4**$^{\mathbf{tol}}$-THF·3THF with 50% probability ellipsoids. Co-crystallized THF and second molecule of **4**$^{\mathbf{tol}}$-THF omitted for clarity. Selected bond lengths (Å) and bond angles (°): U1-O1 = 1.765(5); U1-O2 =1.768(5); U1-O3 = 2.445(5); U1-N1 = 2.464(6); U1-N2 = 2.532(6); U1-N3 = 2.482(6); U1-N4 = 2.546(6); O1-U1-O2 = 177.3(2); N2-N1-C1 = 163.9(5); N1-N2-C2 = 160.1(5); N4-N3-C3 = 161.8(5); C4-N4-N3 = 165.7(5); N4-U1-O1 = 84.4(2); O3-U1-O1 = 84.2(2); N1-U1-O1 = 99.2(2); N2-U1-O1 = 82.3(2); N3-U1-O1 = 97.0(2); N4-U1-O1 = 84.4(2). Dihedral angle of the planes between pyrrole 4 (containing N4) and pyrrole 3 (containing N3) = 27.31°. Dihedral angle of the planes between pyrrole 1 (containing N1) and pyrrole 2 (containing N2) = 31.01°.

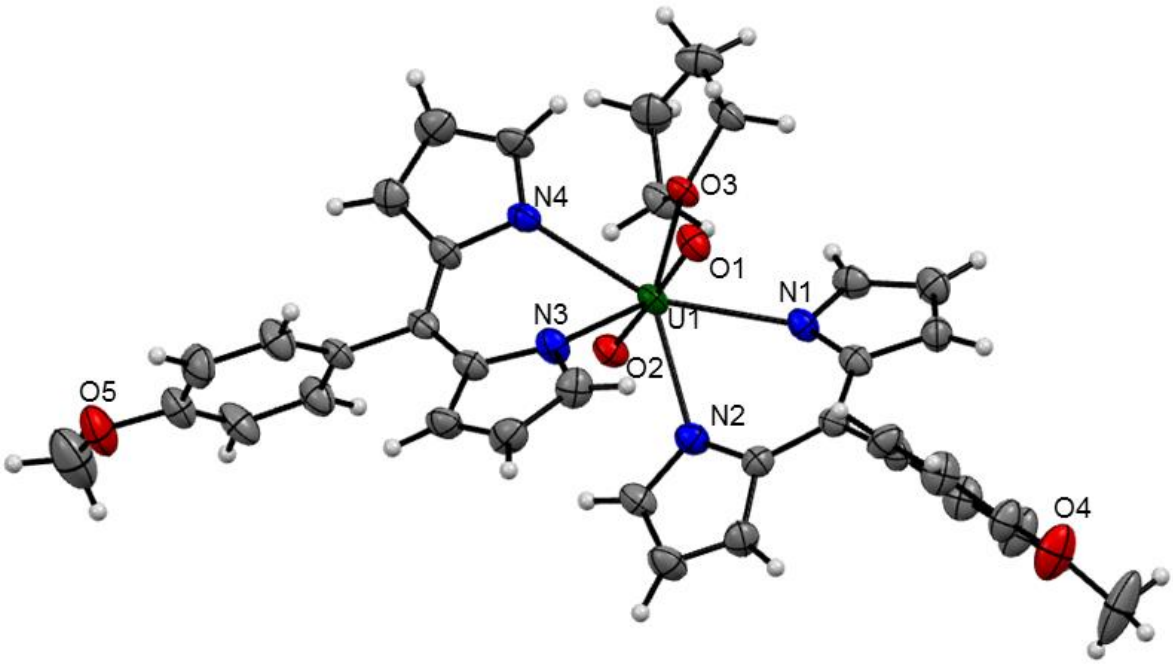

Figure S34 Solid-state molecular structure of **4**^{anis}-THF·THF·C_5H_{12} with 50% probability ellipsoids. Co-crystallized solvent and second molecule of **4**^{anis}-THF omitted for clarity. Selected bond lengths (Å) and bond angles (°): U1-O1 = 1.759(4); U1-O2 = 1.764(4); U1-O3 = 2.463(3); U1-N1 = 2.546(5); U1-N2 = 2.453(5); U1-N3 =2.479(5); U1-N4 = 2.503(5); O1-U1-O2 = 176.8(2); N2-N1-C2 = 164.7(4); N1-N2-C1 = 160.0(4); N4-N3-C3 = 161.7(4); C4-N4-N3 = 163.6(4); N4-U1-O1 = 84.2(2); O3-U1-O1 = 83.9(2); N1-U1-O1 = 98.9(2); N2-U1-O1 = 82.0(2); N3-U1-O1 = 97.6(2); N4-U1-O1 = 84.2(2). Dihedral angle of the planes between pyrrole 4 (containing N4) and pyrrole 3 (containing N3) = 29.58°. Dihedral angle of the planes between pyrrole 1 (containing N1) and pyrrole 2(containing N2) = 29.58°.

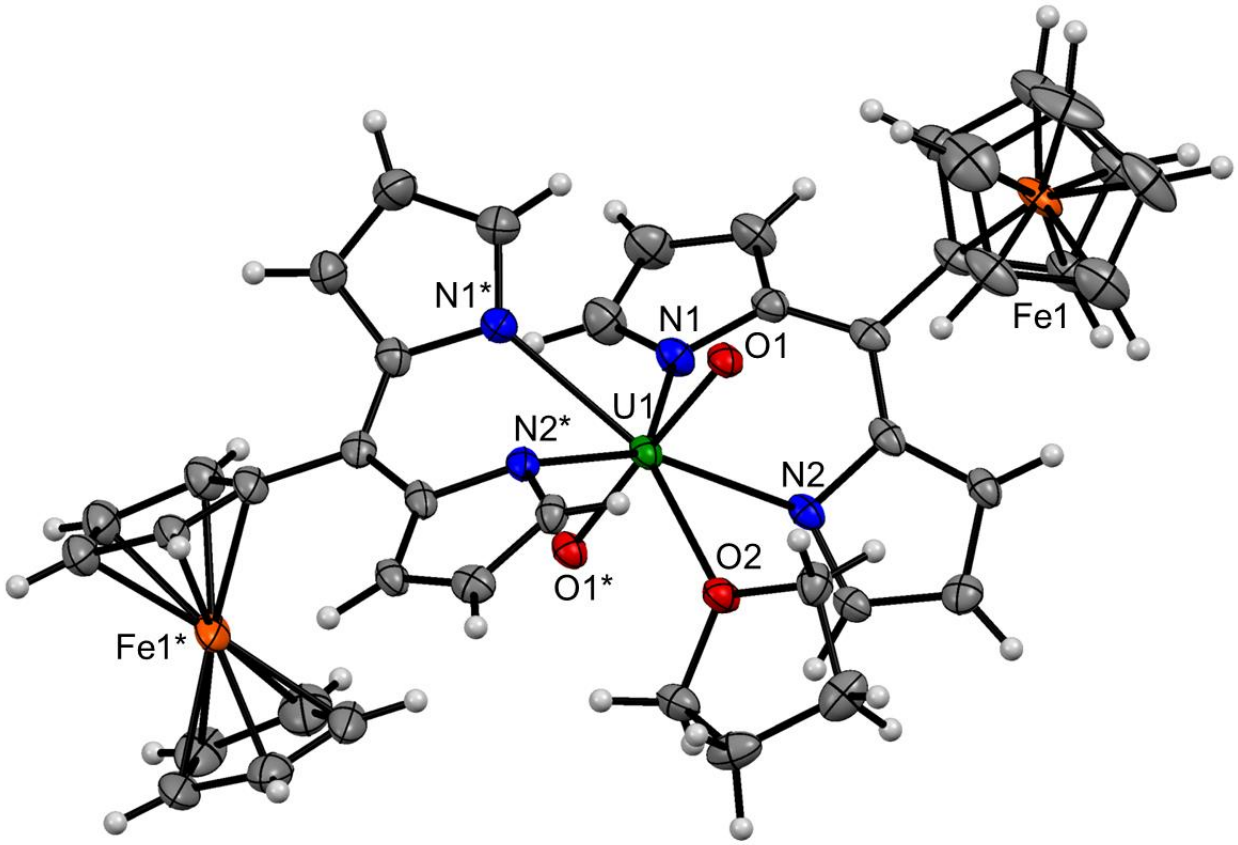

Figure S35. Solid-state molecular structure of $\mathbf{4}^{\mathbf{Fc}}$-THF·C_5H_{12} with 50% probability ellipsoids. Co-crystallized solvent molecule omitted for clarity. Selected bond lengths (Å) and bond angles (°): U1-O1 = 1.773(3); U1-O3 = 2.489(5); U1-N1 = 2.457(4); U1-N2 = 2.482(4); O1-U1-O2 = 177.0; N2-N1-C1 = 150.3(4); N1-N2-C2 = 165.5(4); O3-U1-O1 = 89.1; N1-U1-O1 = 91.3; N2-U1-O1 = 89.1; Dihedral angle of the planes between pyrrole 1 (containing N1) and pyrrole 2 (containing N2) = 37.72°.

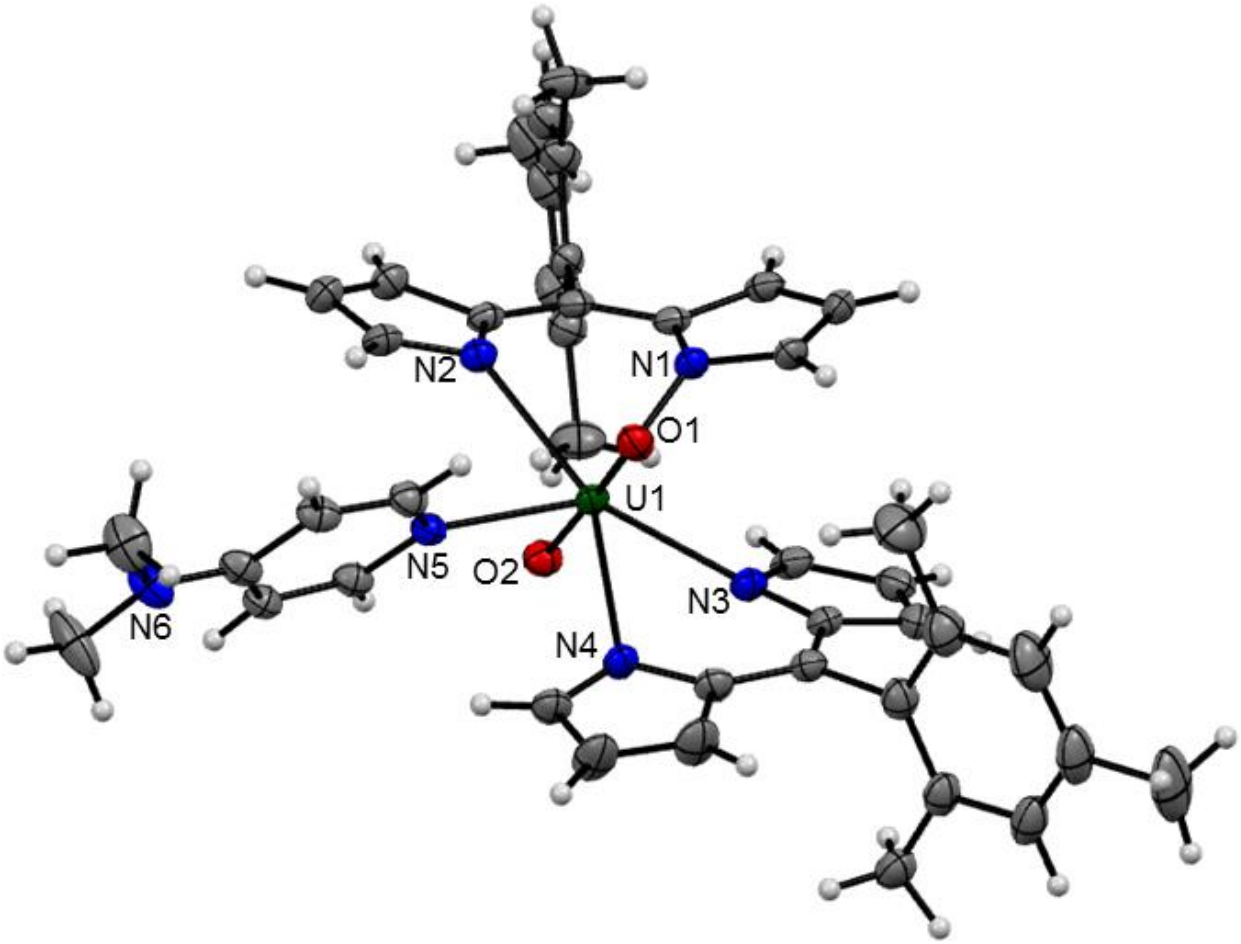

Figure S36. Solid-state molecular structure of **4**^{mes}-DMAP·THF·0.5C_5H_{12} with 50% probability ellipsoids. Co-crystallized solvent omitted for clarity. Selected bond lengths (Å) and bond angles (°): U1-O1 = 1.776(4); U1-O2 = 1.764(4); U1-N5 = 2.489(5); U1-N1 = 2.554(4); U1-N2 = 2.472(5); U1-N3 = 2.556(4); U1-N4 = 2.468(4); O1-U1-O2 = 176.9(2); N2-N1-C1 = 169.2(4); N1-N2-C2 = 164.3(4); N4-N3-C3 = 167.5(4); C4-N4-N3 = 164.8(4); N4-U1-O1 = 100.1(2); N5-U1-O1 = 89.1(2); N1-U1-O1 = 96.4(2); N2-U1-O1 = 82.6(2); N3-U1-O1 = 82.2(2). Dihedral angle of the planes between pyrrole 4 (containing N4) and pyrrole 3 (containing N3) = 22.34°. Dihedral angle of the planes between pyrrole 1 (containing N1) and pyrrole 2(containing N2) = 20.41°.

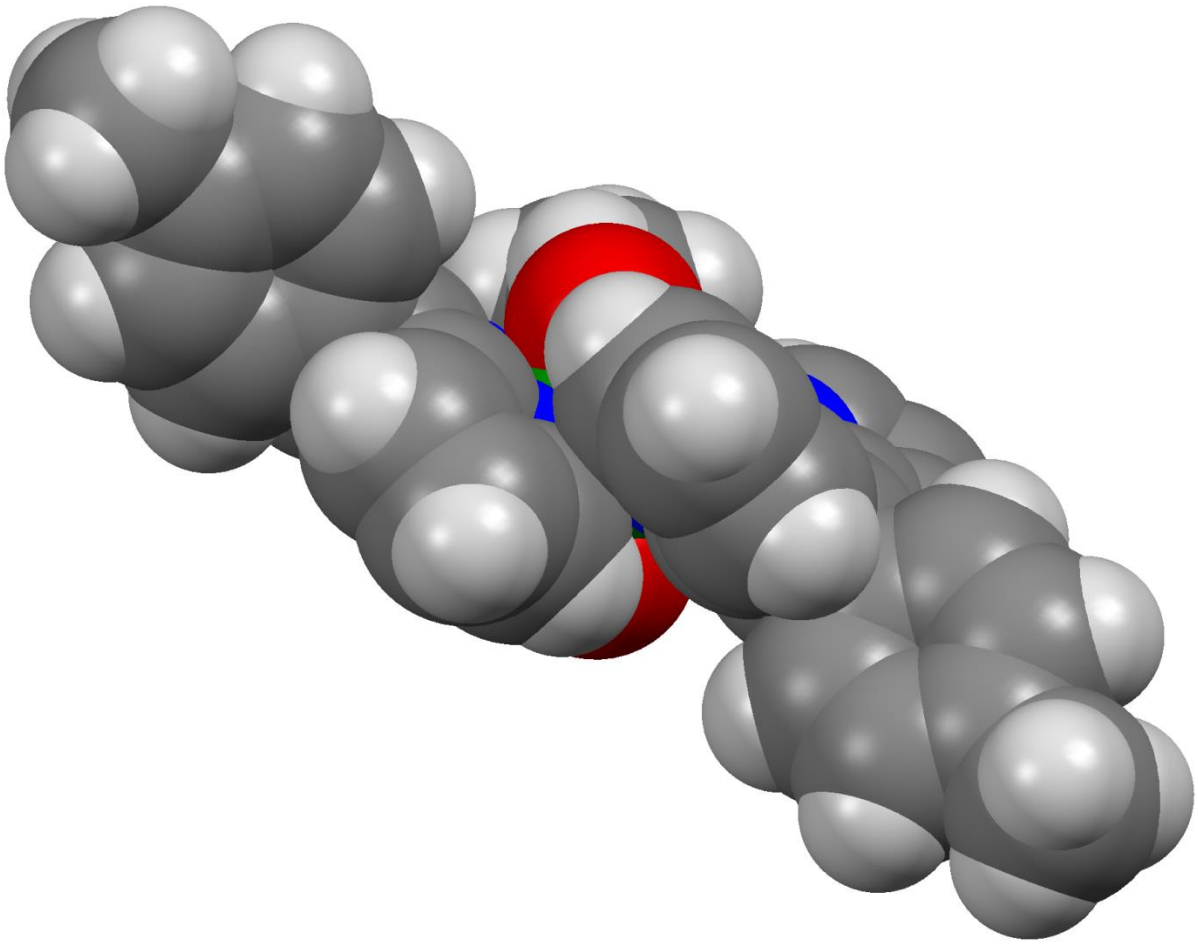

Figure S37. Side view of the solid-state molecular structure of **4**$^{\mathbf{tol}}$-THF·3THF with space filling atoms. Green atom is uranium, red atoms are oxygen, blue atoms are nitrogen, grey atoms are carbon, and hydrogen atoms are white.

Table S1. X-ray crystallographic data for **4**$^{\mathbf{tolyl}}$-THF·3THF, **4**$^{\mathbf{anis}}$-THF·THF·C_5H_{12}, **4**$^{\mathbf{Fc}}$-THF·C_5H_{12}, and **4**$^{\mathbf{mes}}$-DMAP·THF·0.5C_5H_{12}.

	4$^{\mathbf{tolyl}}$-THF·3THF	**4**$^{\mathbf{anis}}$-THF·THF·C_5H_{12}	**4**$^{\mathbf{mes}}$-DMAP·THF ·0.5 C_5H_{12}	**4**$^{\mathbf{Fc}}$-THF·C_5H_{12}
Empirical formula	$U_2C_{72}H_{68}N_4O_6(C_4H_8O)_3$	$U_2C_{72}H_{68}N_4O_8(C_4H_8O)(C_5H_{12})$	$UC_{43}H_{44}N_6O_2(C_4H_8O)(C_5H_{12})_{0.5}$	$UC_{21}H_{19}N_2O_2Fe(C_5H_{12})$
Crystal Habit, color	Block, red-orange	Plate, red-orange	Plate, red	Plate, dark red
Crystal size (mm)	0.18 × 0.10 × 0.05	0.41 × 0.33 × 0.06	0.96 × 0.63 × 0.19	0.72 × 0.15 × 0.01
Crystal system	Triclinic	Triclinic	monoclinic	trigonal
Space group	P-1	P-1	$P2_1/c$	P-3c1
Volume (Å^3)	3618.4(2)	3750.1(3)	4625.7(5)	6141.2(5)
a (Å)	14.4946(5)	14.5004(7)	9.3522(6)	20.5164(8)
b (Å)	15.8228(5)	16.3863(8)	26.9204(16)	20.5164(8)
c (Å)	16.5676(5)	16.7499(9)	18.8537(11)	16.8469(7)
α(°)	98.7660(10) °	99.0510(10)°	90°	90°
β(°)	102.5540(10) °	103.8570(10)°	102.9630(10)°	90°
γ(°)	96.9580(10) °	98.0330(10)°	90°	120°
Z	2	2	4	1
Formula weight (g/mol)	1705.57	1923.66	1116.23	5942.79
Density (calculated) (Mg/m^3)	1.565	1.704	1.603	1.607
Absorption coefficient (mm^{-1})	4.528	4.384	3.563	4.685
F_{000}	1680.0	1892.0	2268.0	2888.0
Total no. reflections	39775	41352	56102	64170
Unique reflections	16322	17045	13066	4714
Final R indices [$I > 2\sigma(I)$]	R_1 = 0.0456, wR_2 = 0.1109	R1 = 0.0404, wR2 = 0.1032	R1 = 0.0538, wR2 = 0.1081	R1 = 0.0330, wR2 = 0.0765
Largest diff. peak and hole (e$^-$Å^{-3})	2.36 and -1.19	2.23 and -0.76	2.65 and -5.48	2.97 and -0.82
GOF	1.045	1.050	1.258	1.142

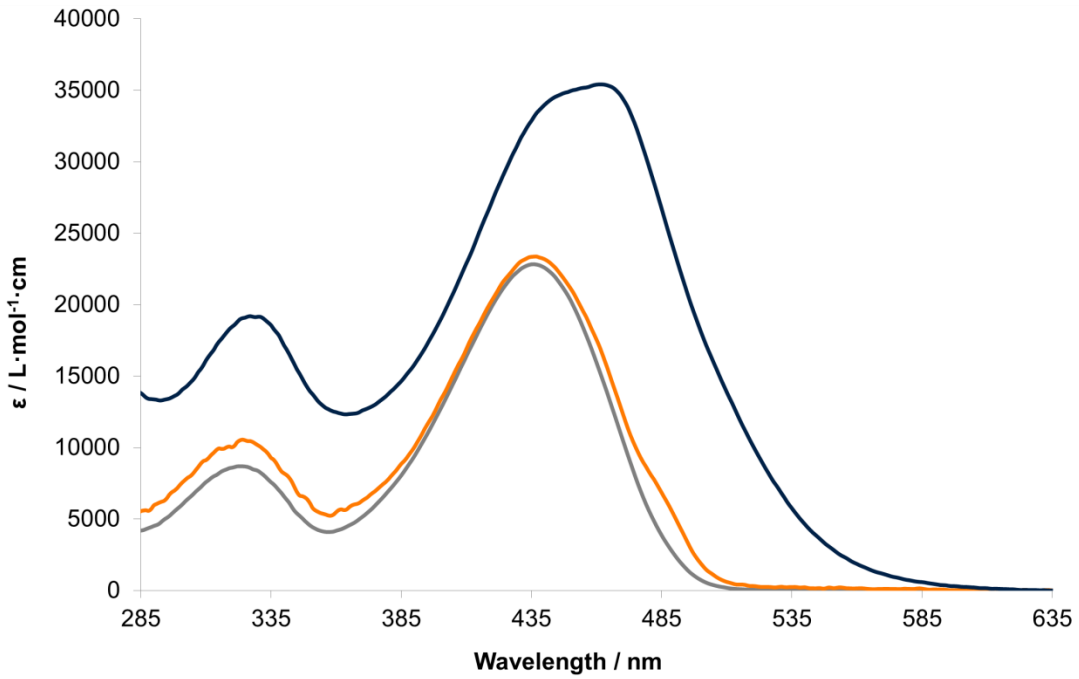

Figure S38. Room temperature UV/vis absorption spectra for **2**^{tol} (benzene, 24.49 μM) (grey), **3**^{tol} (benzene, 10.46 μM) (orange), and **4**^{tol}-DMAP (benzene, 11.8 μM) (black).

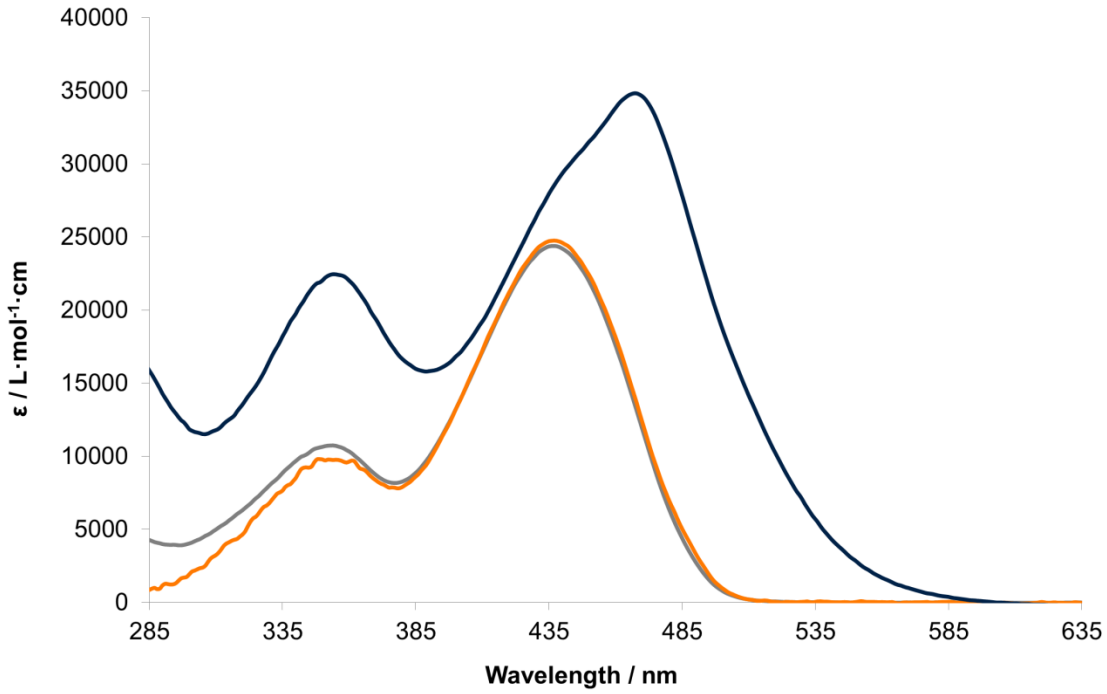

Figure S39. Room temperature UV/vis absorption spectra for **2**^{anis} (benzene, 24.58 μM) (grey), **3**^{anis} (benzene, 9.68 μM) (orange), and **4**^{anis}-DMAP (benzene, 11.76 μM) (black).

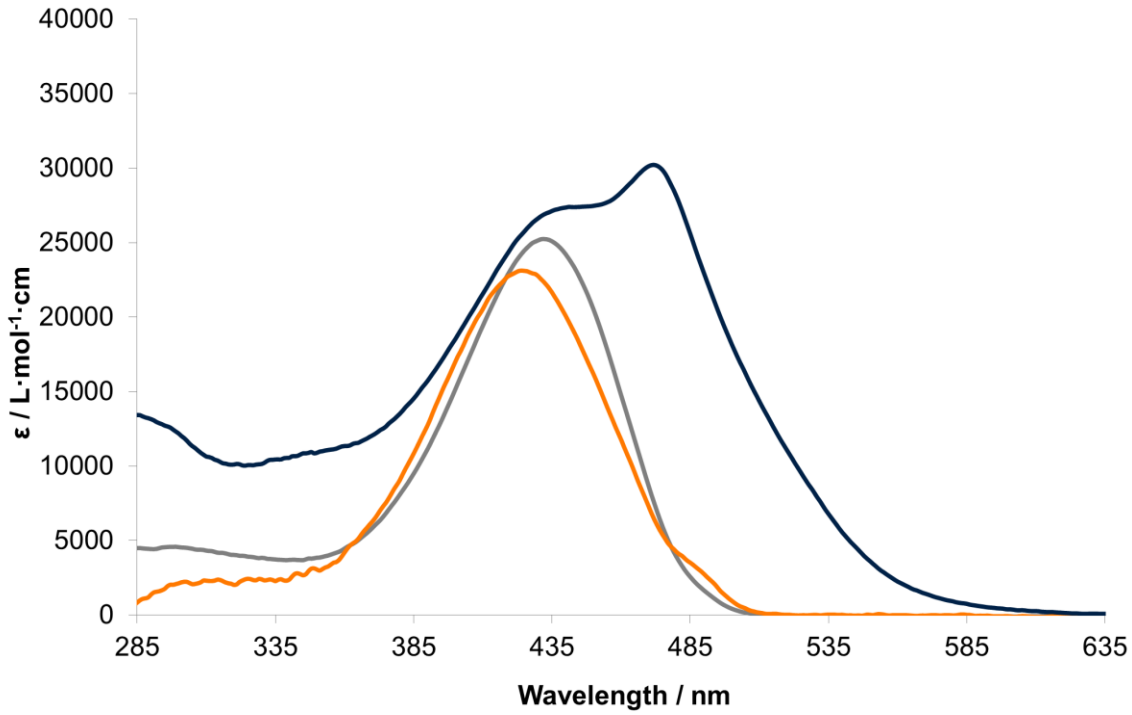

Figure S40. Room temperature UV/vis absorption spectra for **2**^{mes} (benzene, 25.09 μM) (grey), **3**^{mes} (benzene, 9.66 μM) (orange), and **4**^{mes}-DMAP (benzene, 12.9 μM) (black).

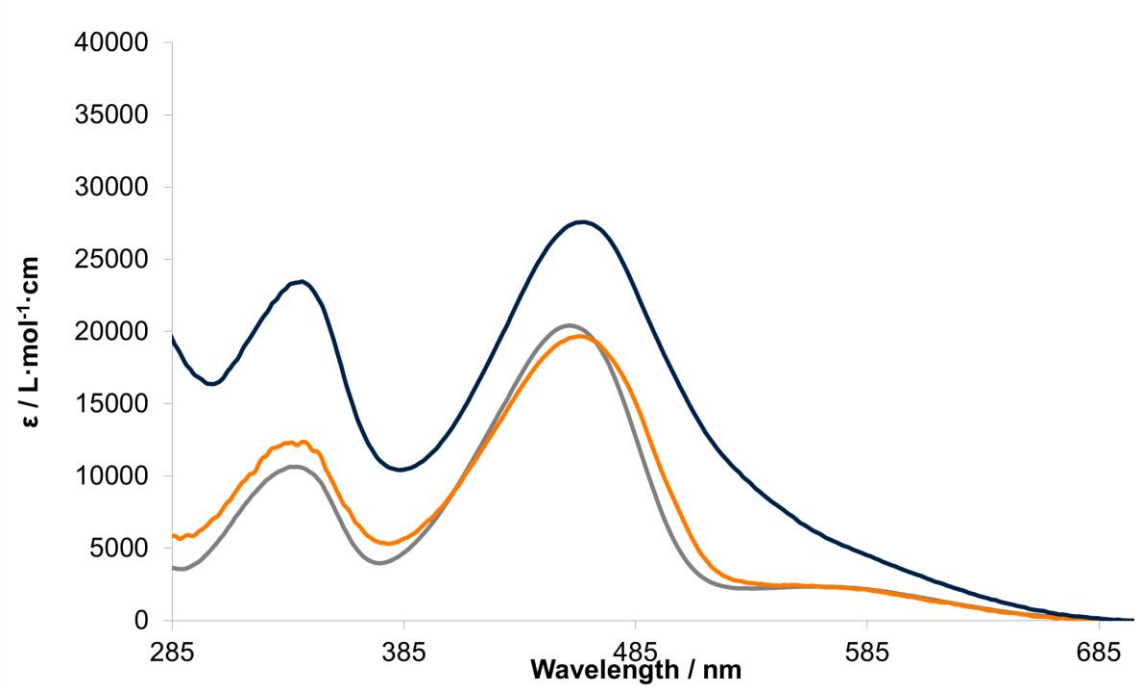

Figure S41. Room temperature UV/vis absorption spectra for $\mathbf{2}^{\mathbf{Fc}}$ (benzene, 27.98 μM) (grey), $\mathbf{3}^{\mathbf{Fc}}$ (benzene, 10.67 μM) (orange), and $\mathbf{4}^{\mathbf{Fc}}$-DMAP (benzene, 10.59 μM) (black).

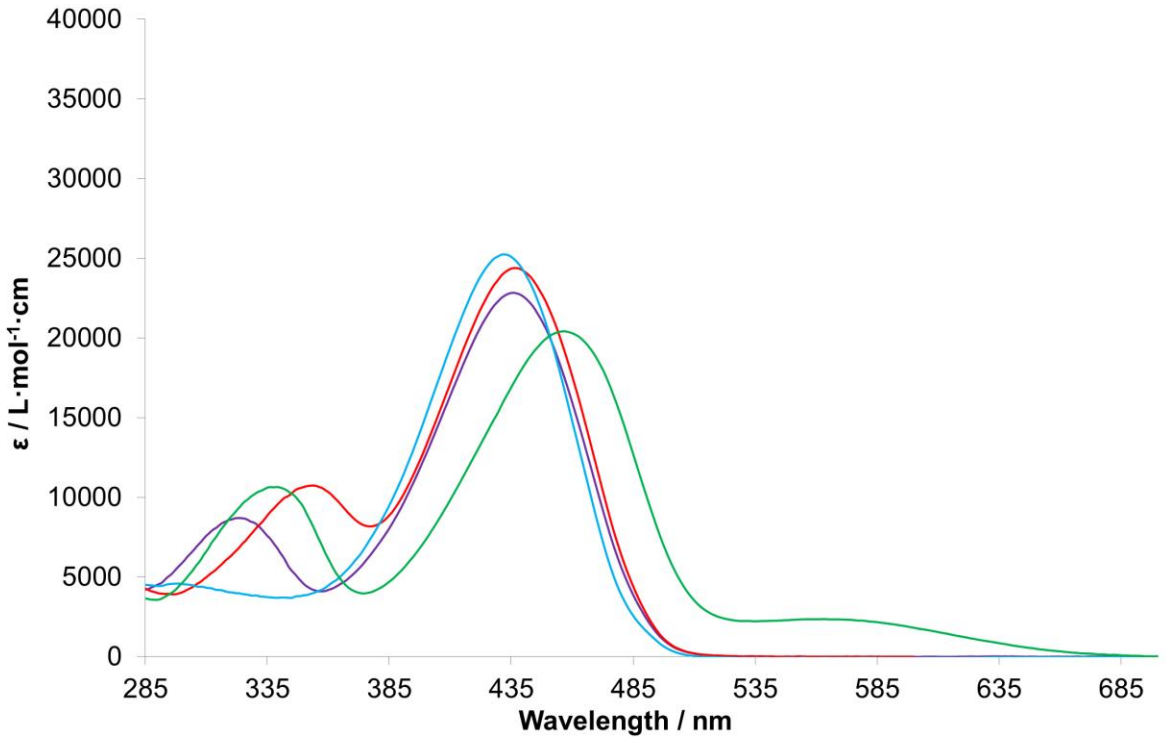

Figure S42. Room temperature UV/vis absorption spectra for protonated dipyrrins $\mathbf{2}^{\mathbf{tol}}$ (purple), $\mathbf{2}^{\mathbf{anis}}$ (red), $\mathbf{2}^{\mathbf{mes}}$ (blue), and $\mathbf{2}^{\mathbf{Fc}}$ (green).

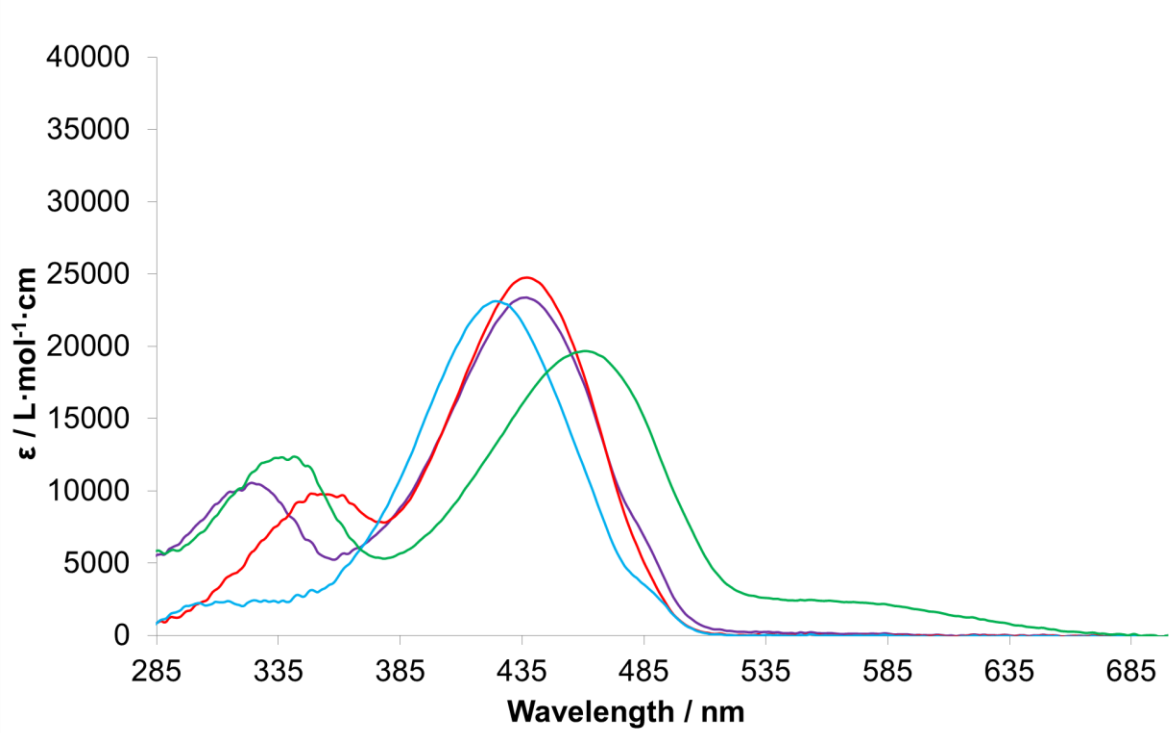

Figure S43. Room temperature UV/vis absorption spectra for sodium dipyrrins $\mathbf{3}^{\mathbf{tol}}$ (purple), $\mathbf{3}^{\mathbf{anis}}$ (red), $\mathbf{3}^{\mathbf{mes}}$ (blue), and $\mathbf{3}^{\mathbf{Fc}}$ (green).

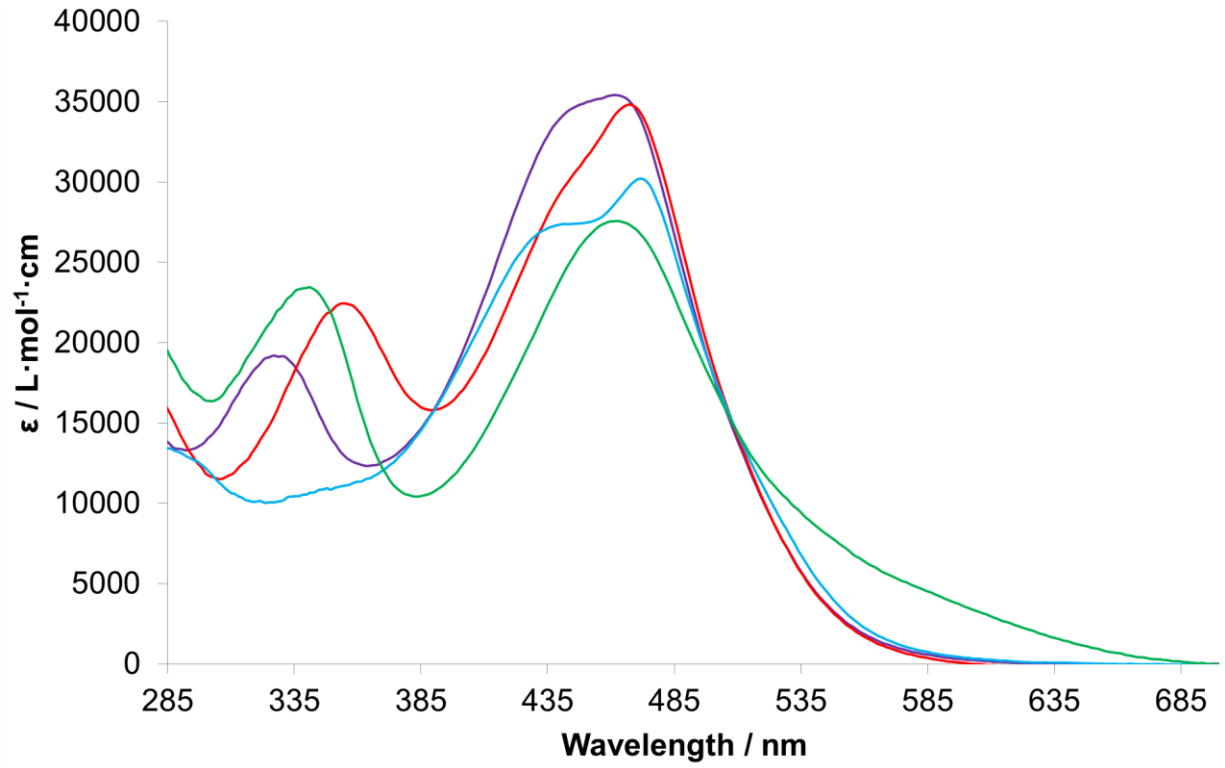

Figure S44. Room temperature UV/vis absorption spectra for uranyl dipyrrins $\mathbf{4}^{\mathbf{tol}}$-DMAP (purple), $\mathbf{4}^{\mathbf{anis}}$-DMAP (red), $\mathbf{4}^{\mathbf{mes}}$-DMAP (blue), and $\mathbf{4}^{\mathbf{Fc}}$-DMAP (green).

Table S2. UV/vis absorption data.

Compound	**Concentration (μM)**	**λ_{max} (nm)**	**ε (L·mol^{-1}·cm)**
2^{tol}	24.49	436	22832
2^{anis}	24.58	437	24385
2^{mes}	25.09	453	18959
2^{Fc}	27.98	456	20412
3^{tol}	10.46	436	23365
3^{anis}	9.68	437	24755
3^{mes}	9.66	432	22375
3^{Fc}	10.67	453	20185
4^{tol}-DMAP	11.8	462	35416
4^{anis}-DMAP	11.76	467	34826
4^{mes}-DMAP	12.9	472	30214
4^{Fc}-DMAP	10.59	462	27578

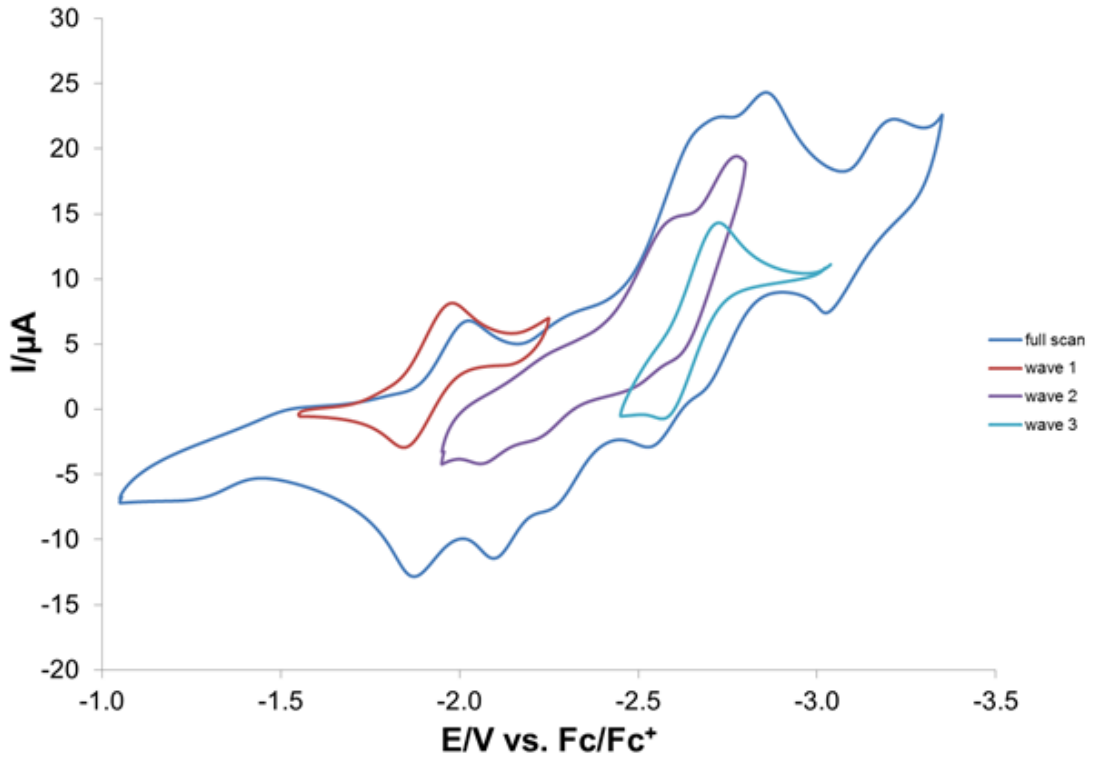

Figure S45. Room temperature cyclic voltammogram of $\mathbf{4}^{\mathbf{tol}}$-DMAP in THF (vs internally referenced Cp_2Fe/Cp_2Fe^+ at $E_{1/2}$ = 0 V). (0.1M $[NBu_4][PF_6]$ as supporting electrolyte). The scan rate is 250 mV/s.

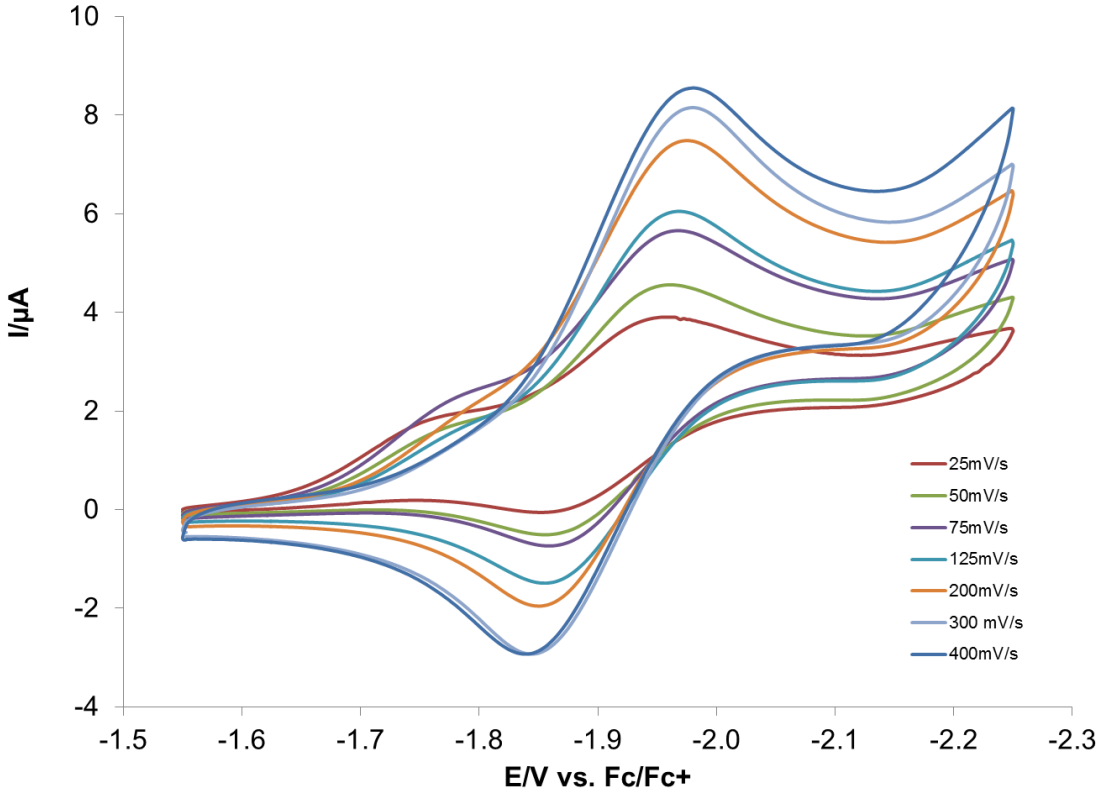

Figure S46. Room temperature cyclic voltammogram of wave 1 of **4**$^{\mathbf{tol}}$-DMAP in THF (vs internally referenced Cp_2Fe/Cp_2Fe^+ at $E_{1/2}$ = 0 V). (0.1M $[NBu_4][PF_6]$ as supporting electrolyte).

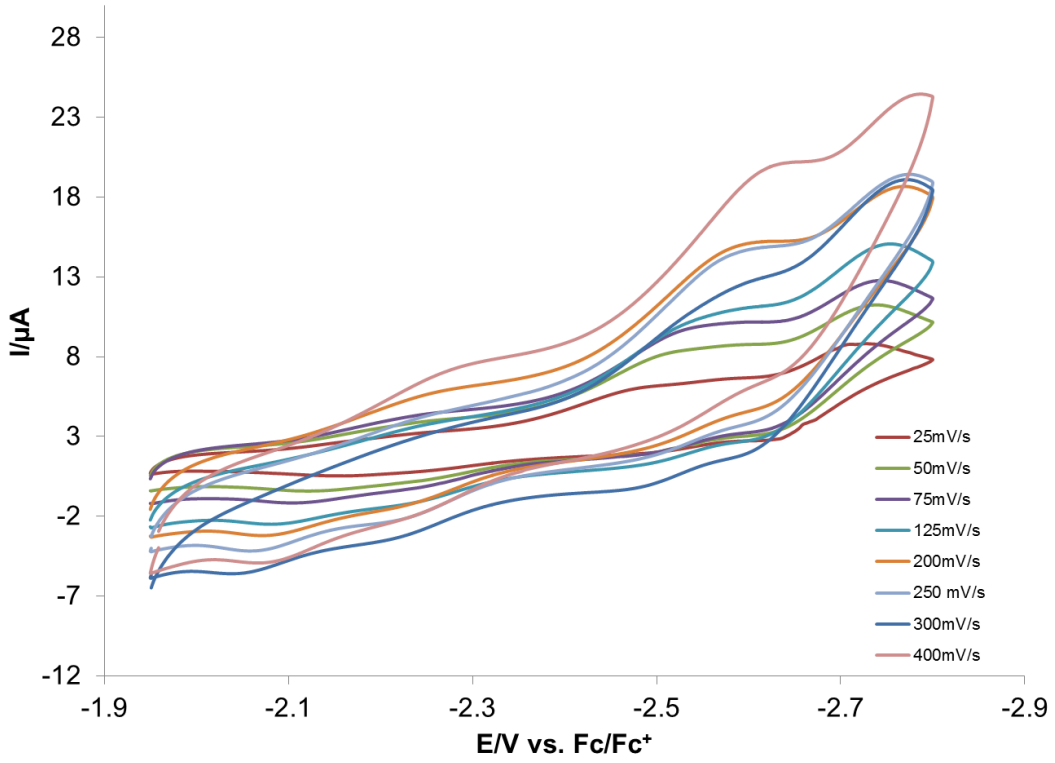

Figure S47. Room temperature cyclic voltammogram of wave 2 of $\mathbf{4^{tol}}$-DMAP in THF (vs internally referenced Cp_2Fe/Cp_2Fe^+ at $E_{1/2}$ = 0 V). (0.1M $[NBu_4][PF_6]$ as supporting electrolyte).

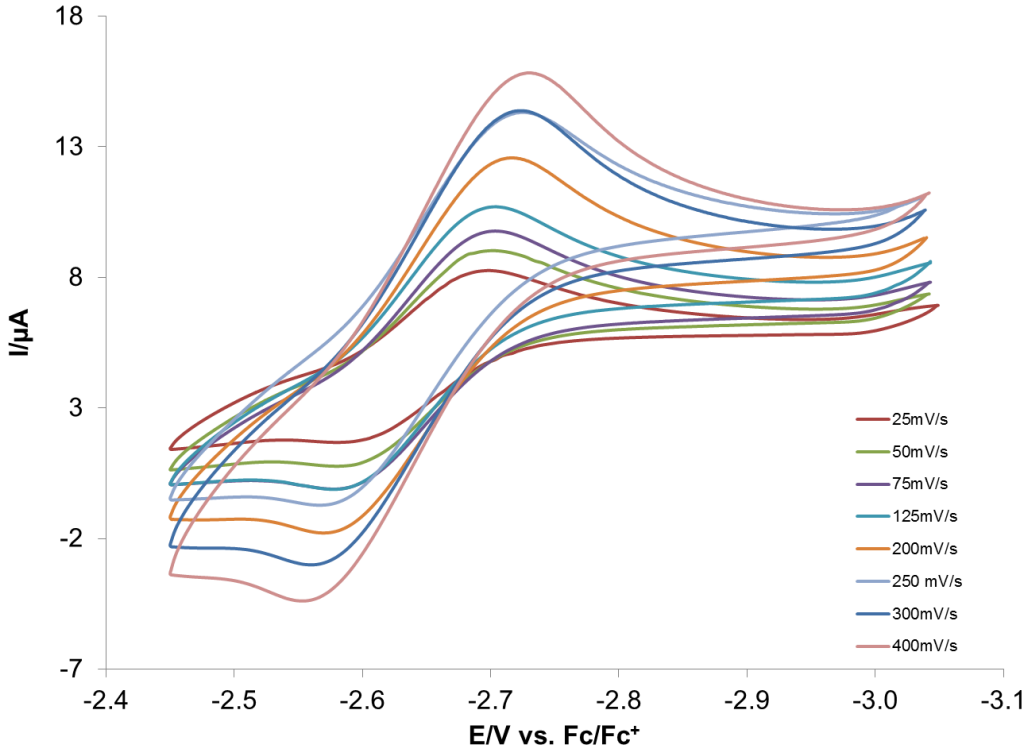

Figure S48. Room temperature cyclic voltammogram of wave 3 of **4**$^{\mathbf{tol}}$-DMAP in THF (vs internally referenced Cp_2Fe/Cp_2Fe^+ at $E_{1/2}$ = 0 V). (0.1M $[NBu_4][PF_6]$ as supporting electrolyte).

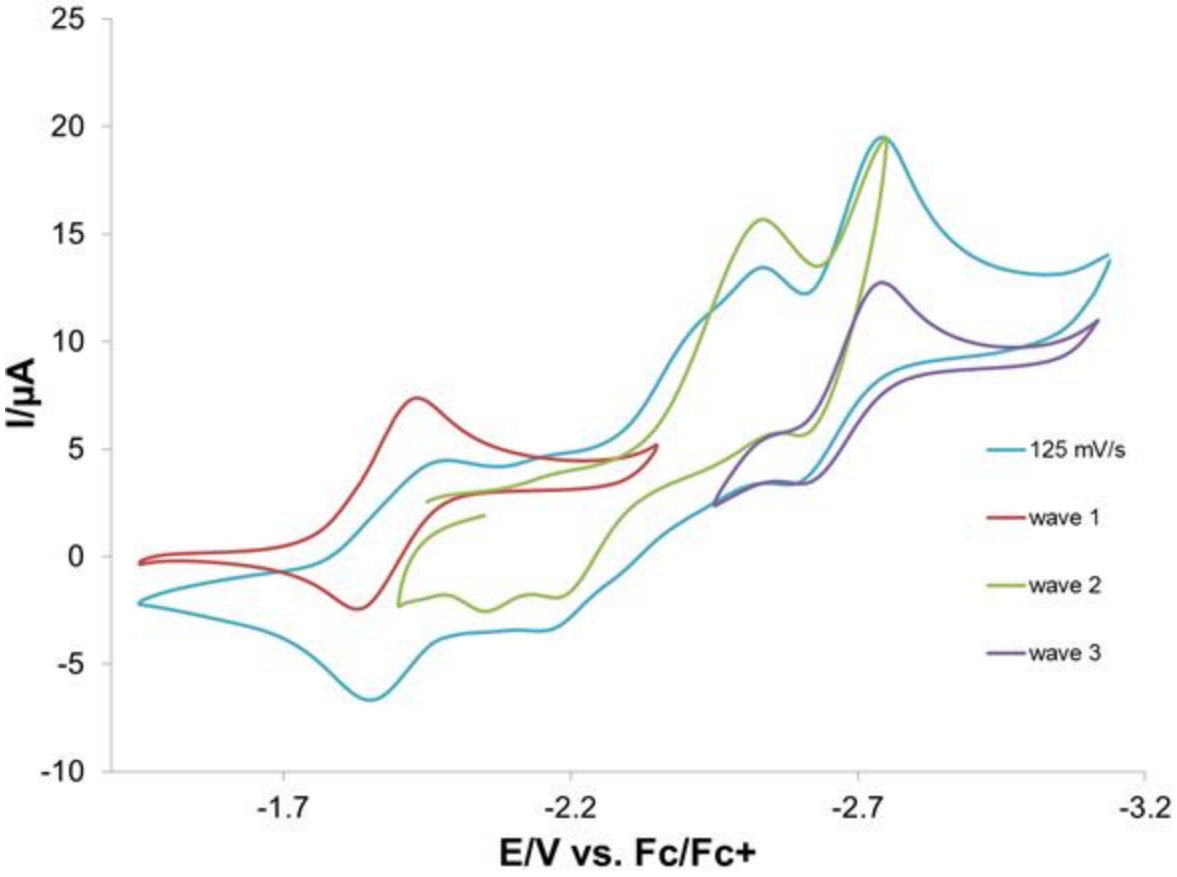

Figure S49. Room temperature cyclic voltammogram of **4**^{anis}-DMAP in THF (vs internally referenced Cp_2Fe/Cp_2Fe^+ at $E_{1/2}$ = 0 V). (0.1M $[NBu_4][PF_6]$ as supporting electrolyte). The scan rate is 125 mV/s.

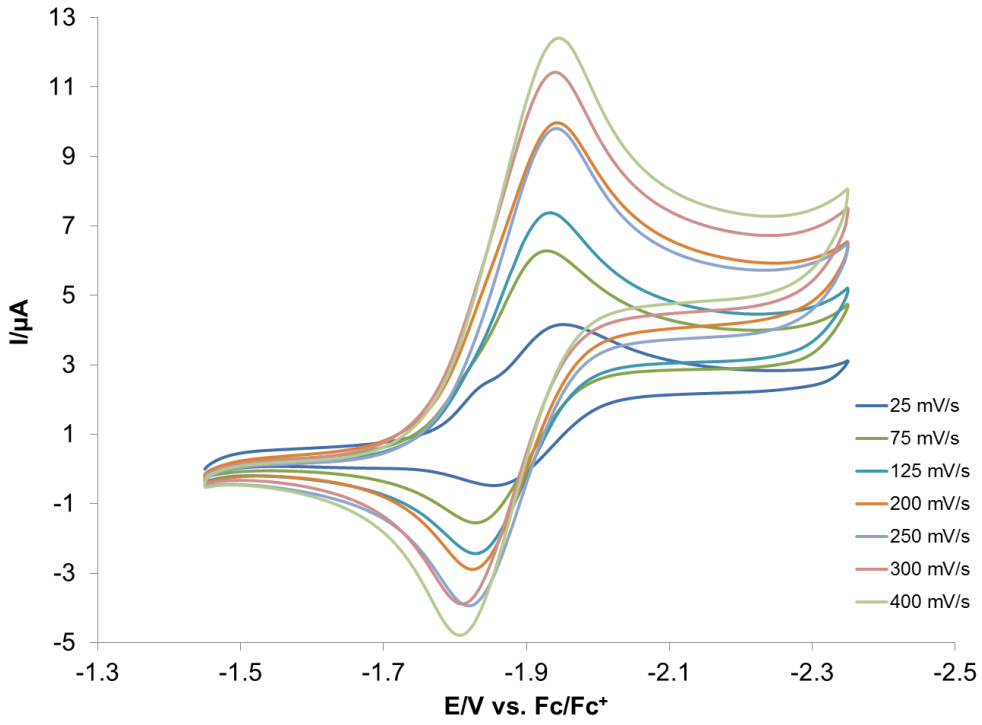

Figure S50. Room temperature cyclic voltammogram of wave 1 of 4^{anis}-DMAP in THF (vs internally referenced Cp_2Fe/Cp_2Fe^+ at $E_{1/2}$ = 0 V). (0.1M $[NBu_4][PF_6]$ as supporting electrolyte).

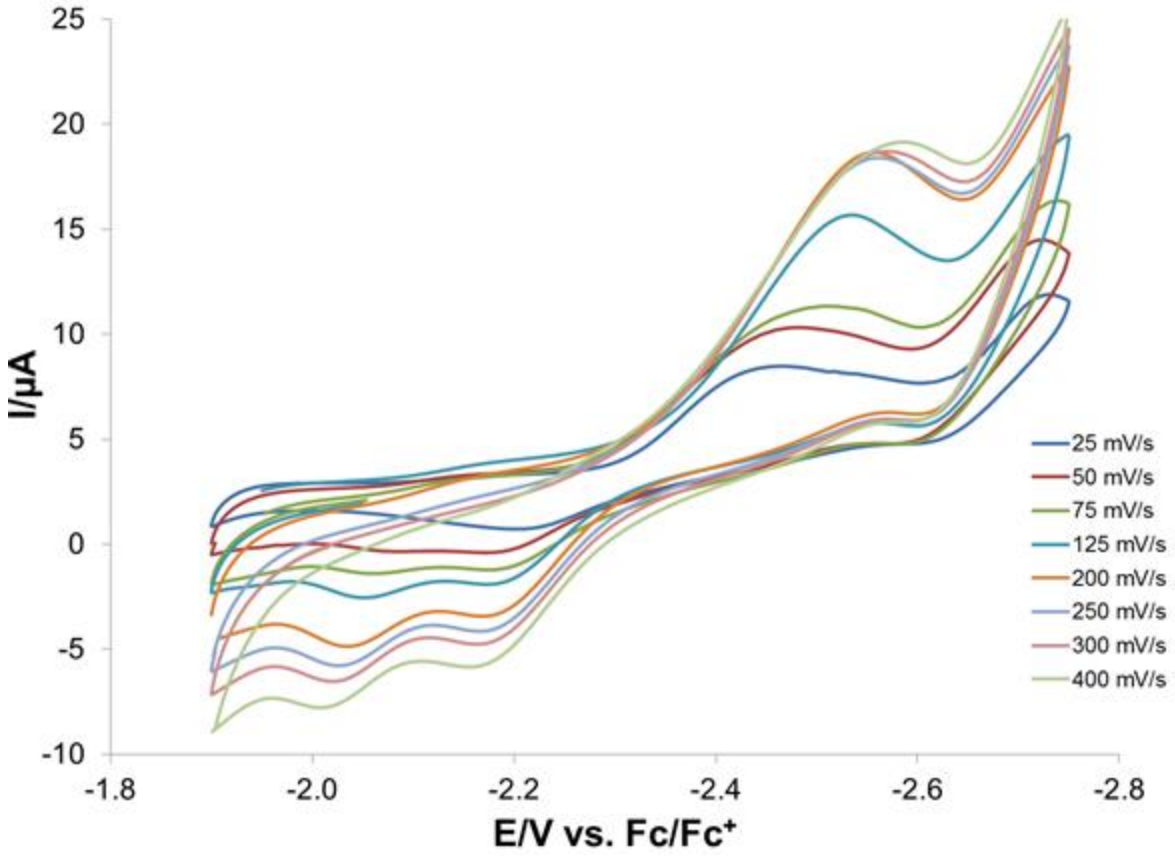

Figure S51. Room temperature cyclic voltammogram of wave 2 of $\mathbf{4}^{\mathbf{anis}}$-DMAP in THF (vs internally referenced Cp_2Fe/Cp_2Fe^+ at $E_{1/2}$ = 0 V). (0.1M $[NBu_4][PF_6]$ as supporting electrolyte).

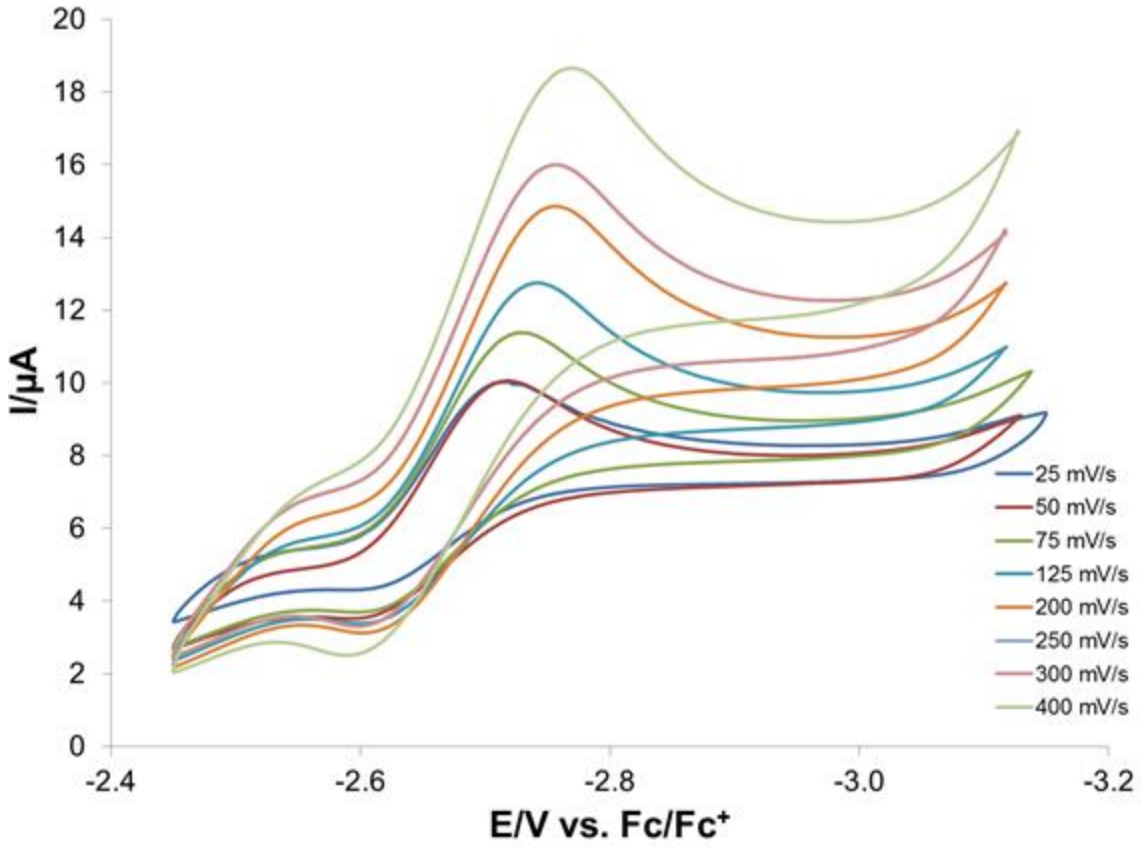

Figure S52. Room temperature cyclic voltammogram of wave 3 of $\mathbf{4}^{\mathbf{anis}}$-DMAP in THF (vs internally referenced Cp_2Fe/Cp_2Fe^+ at $E_{1/2}$ = 0 V). (0.1M $[NBu_4][PF_6]$ as supporting electrolyte).

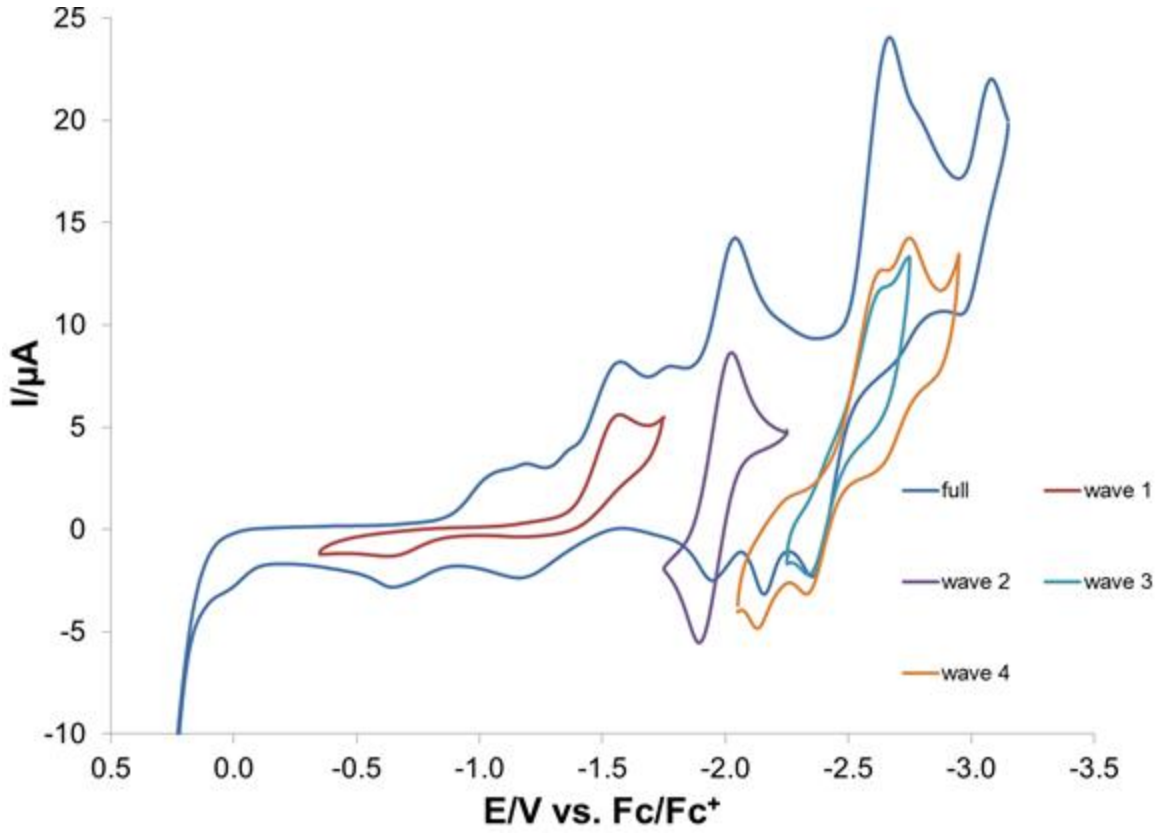

Figure S53. Room temperature cyclic voltammogram of **4**^{mes}-DMAP in THF (vs internally referenced Cp_2Fe/Cp_2Fe^+ at $E_{1/2}$ = 0 V). (0.1M $[NBu_4][PF_6]$ as supporting electrolyte). The scan rate is 125 mV/s.

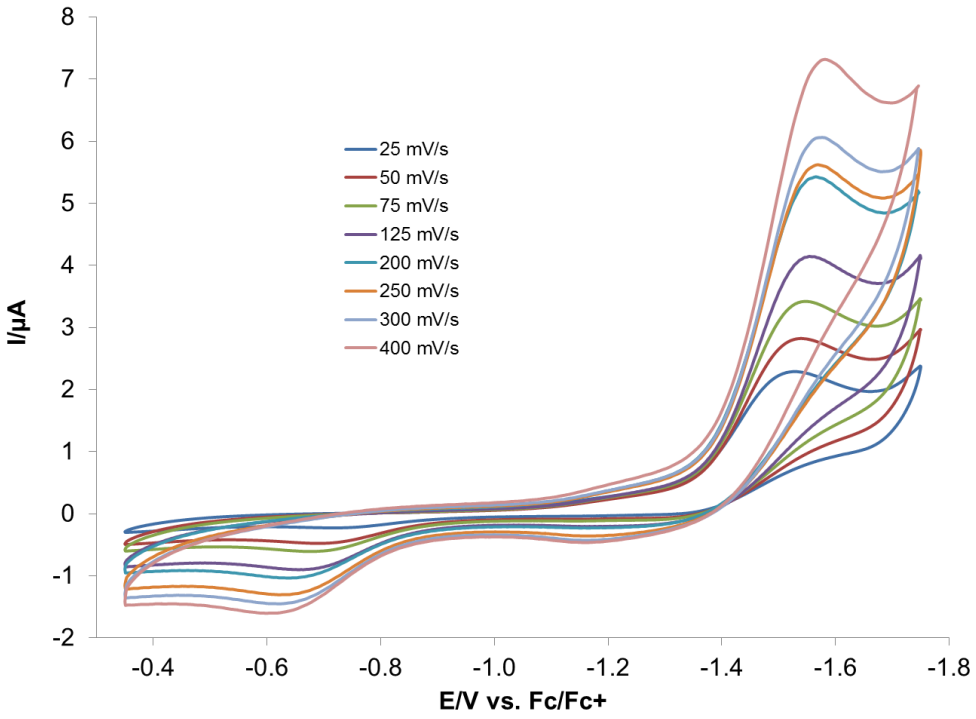

Figure S54. Room temperature cyclic voltammogram of wave 1 of **4**$^{\mathbf{mes}}$-DMAP in THF (vs internally referenced Cp_2Fe/Cp_2Fe^+ at $E_{1/2}$ = 0 V). (0.1M $[NBu_4][PF_6]$ as supporting electrolyte).

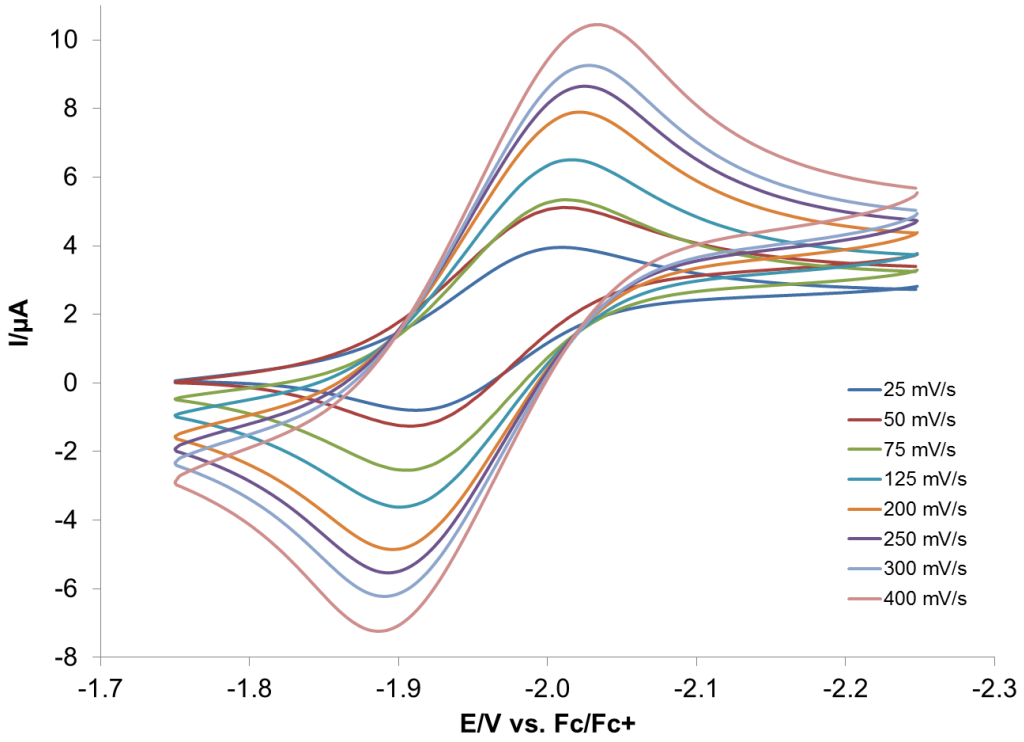

Figure S55. Room temperature cyclic voltammogram of wave 2 of **4**$^{\mathbf{mes}}$-DMAP in THF (vs internally referenced Cp_2Fe/Cp_2Fe^+ at $E_{1/2}$ = 0 V). (0.1M $[NBu_4][PF_6]$ as supporting electrolyte).

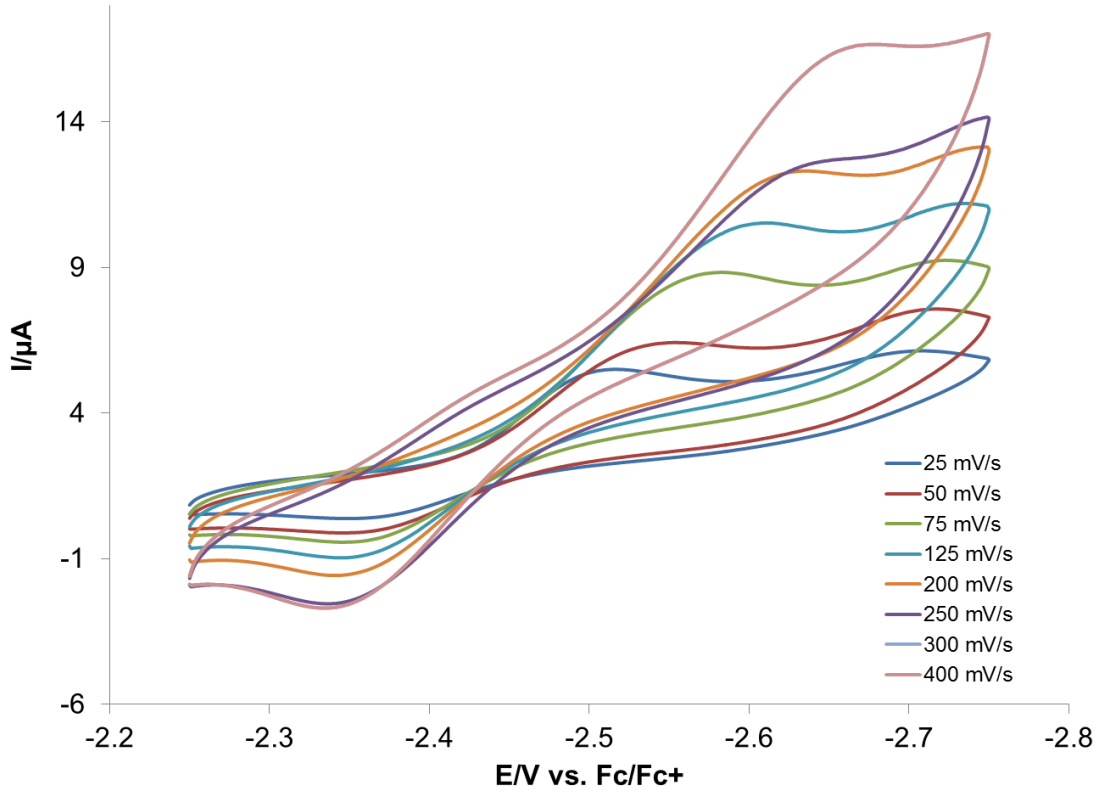

Figure S56. Room temperature cyclic voltammogram of wave 3 of **4**^{mes}-DMAP in THF (vs internally referenced Cp_2Fe/Cp_2Fe^+ at $E_{1/2}$ = 0 V). (0.1M $[NBu_4][PF_6]$ as supporting electrolyte).

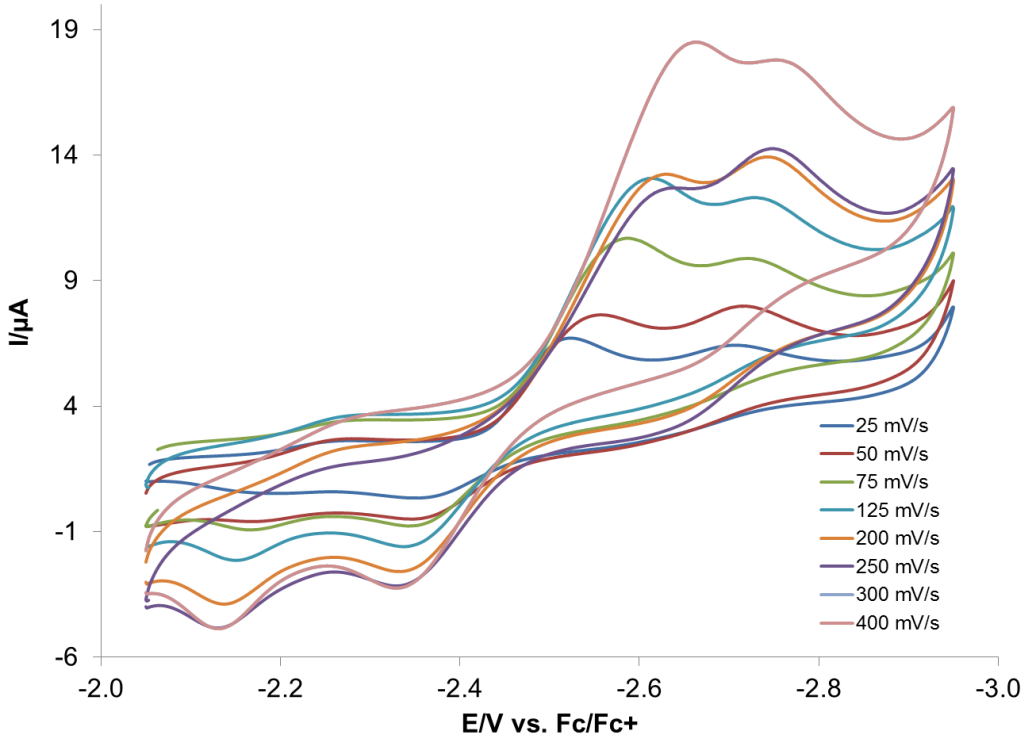

Figure S57. Room temperature cyclic voltammogram of wave 4 of **4**^{mes}-DMAP in THF (vs internally referenced Cp_2Fe/Cp_2Fe^+ at $E_{1/2}$ = 0 V). (0.1M $[NBu_4][PF_6]$ as supporting electrolyte).

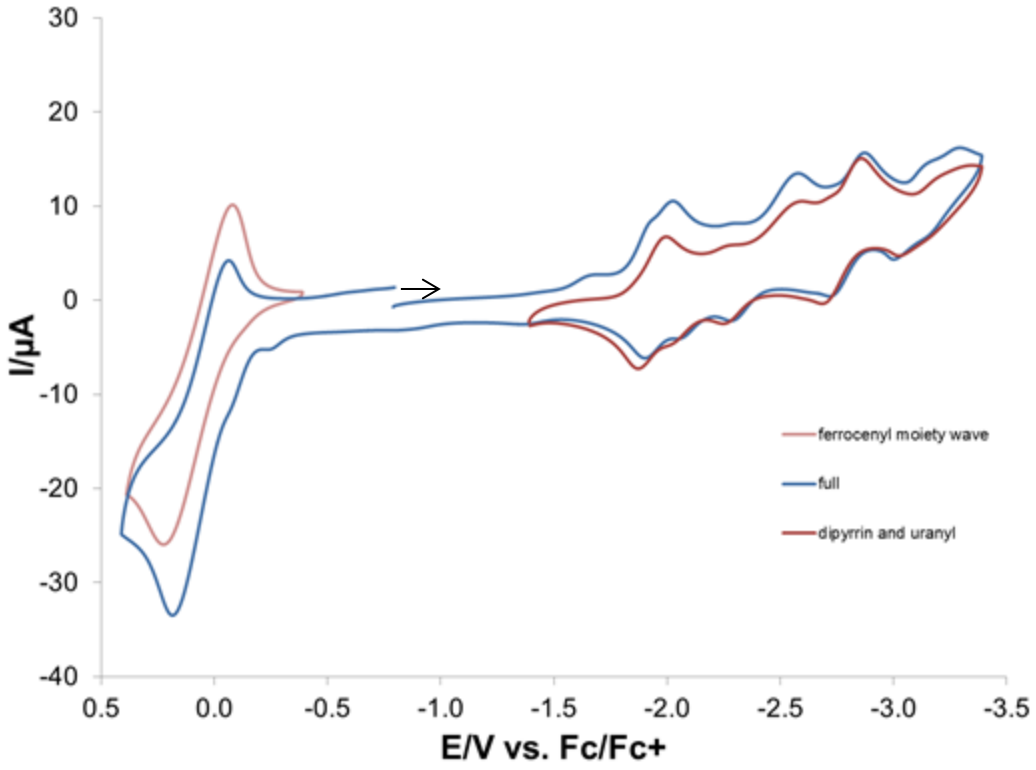

Figure S58. Room temperature cyclic voltammogram of $\mathbf{4}^{\mathbf{Fc}}$-DMAP in THF at 125 mV (vs internally referenced Cp_2Fe/Cp_2Fe^+ at $E_{1/2}$=0 V). (0.1M $[NBu_4][PF_6]$ as supporting electrolyte). The scan rate is 125 mV/s.

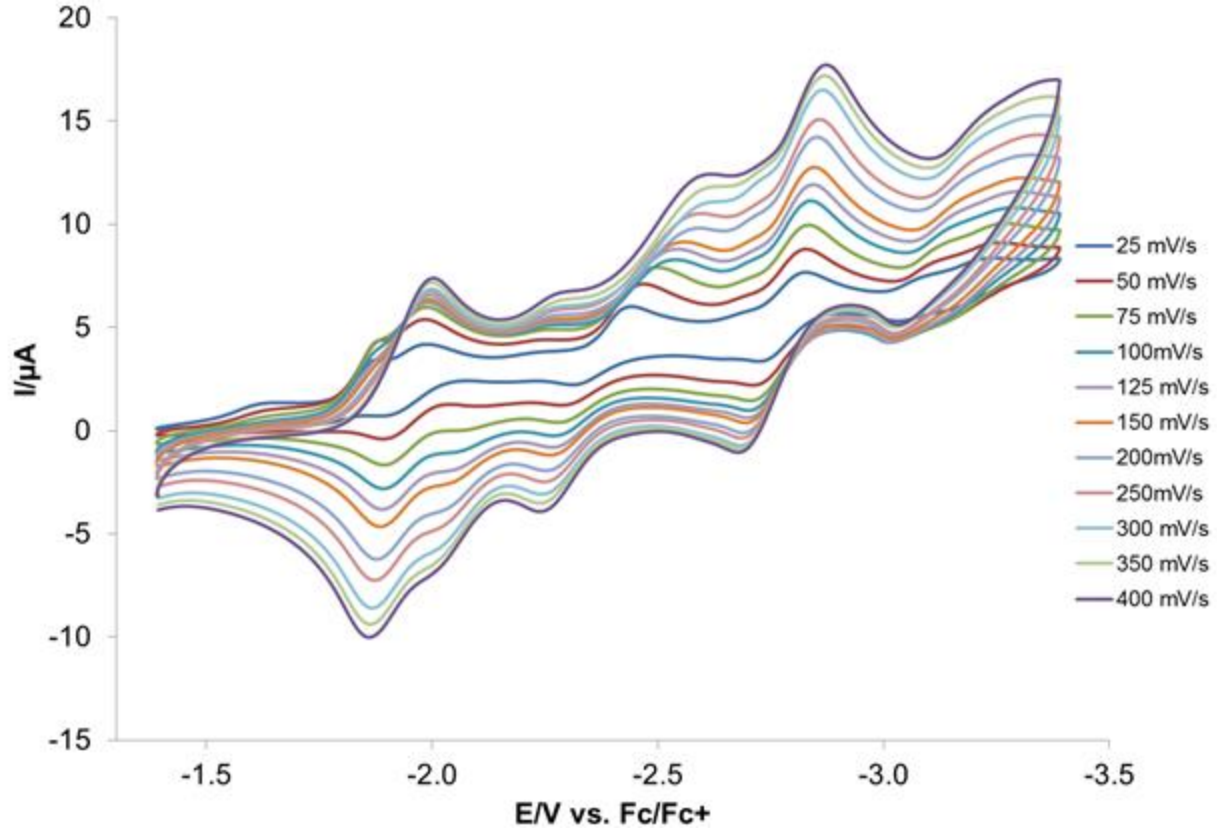

Figure S59. Room temperature cyclic voltammogram of $\mathbf{4}^{\mathbf{Fc}}$-DMAP in THF (vs internally referenced Cp_2Fe/Cp_2Fe^+ at $E_{1/2}$=0 V). (0.1M $[NBu_4][PF_6]$ as supporting electrolyte).

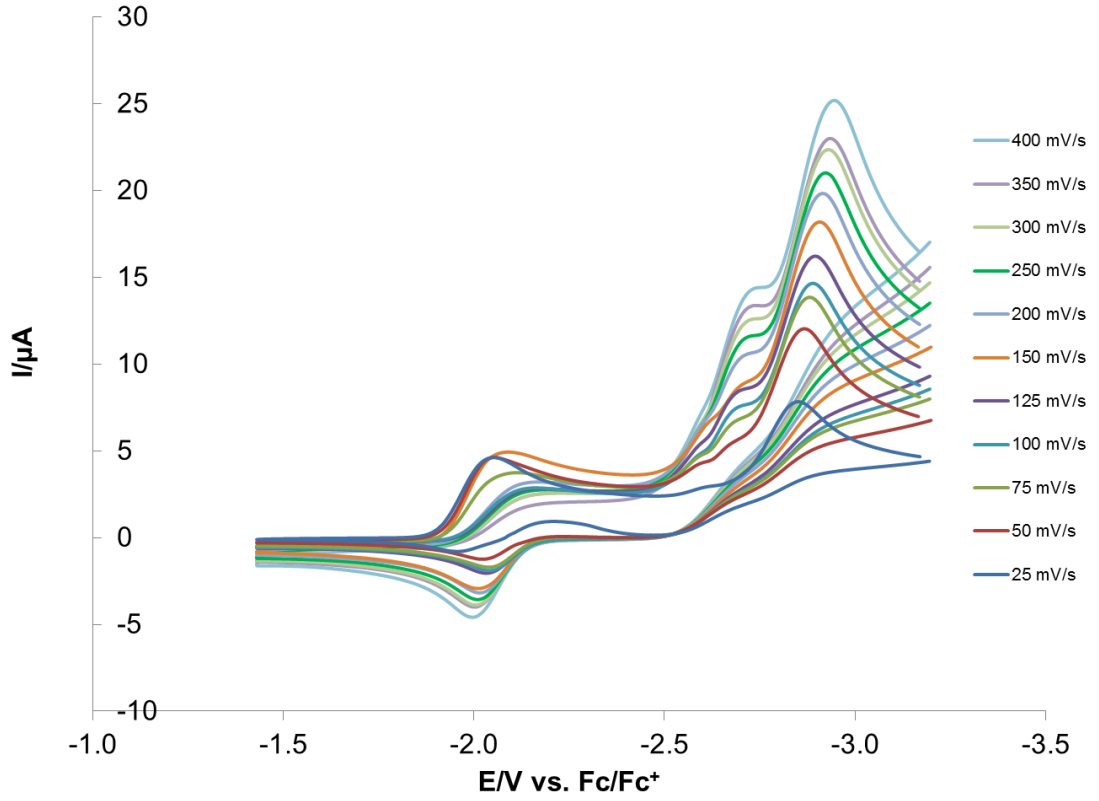

Figure S60. Room temperature cyclic voltammogram of **2**$^{\mathbf{anis}}$ in THF (vs internally referenced Cp_2Fe/Cp_2Fe^+ at $E_{1/2}$=0 V). (0.1M $[NBu_4][PF_6]$ as supporting electrolyte).

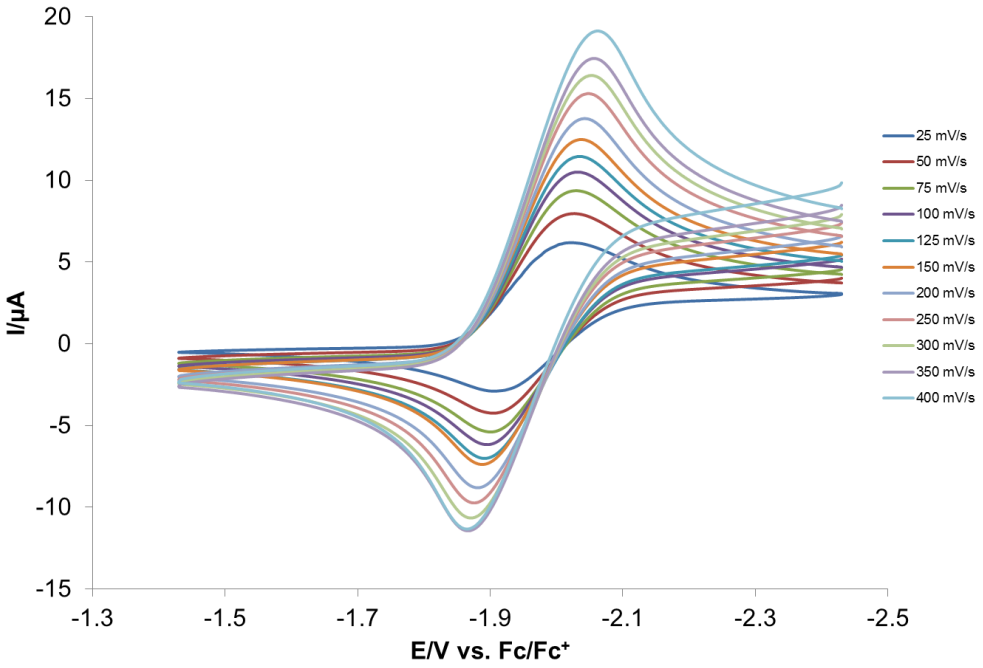

Figure S61. Room temperature cyclic voltammogram of wave 1 of $\mathbf{2}^{\mathbf{anis}}$ in THF (vs internally referenced Cp_2Fe/Cp_2Fe^+ at $E_{1/2}$=0 V). (0.1M $[NBu_4][PF_6]$ as supporting electrolyte).

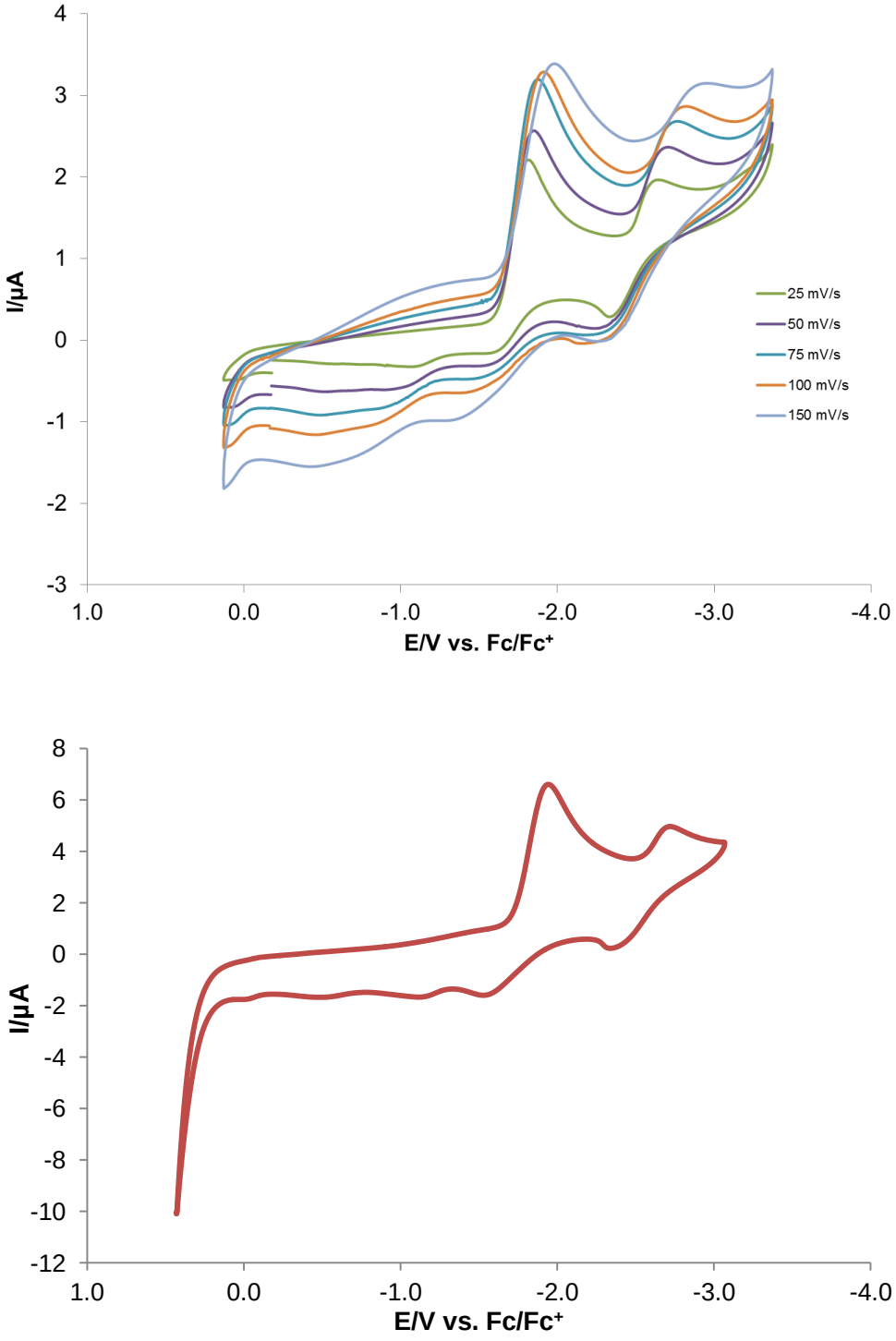

Figure S62. Room temperature cyclic voltammograms of $UO_2(N(Si(CH_3)_3)_2)_2(THF)_2$ in THF (vs internally referenced Cp_2Fe/Cp_2Fe^+ at $E_{1/2}$ = 0 V). Bottom voltammogram at a scan rate of 250 mV/s.

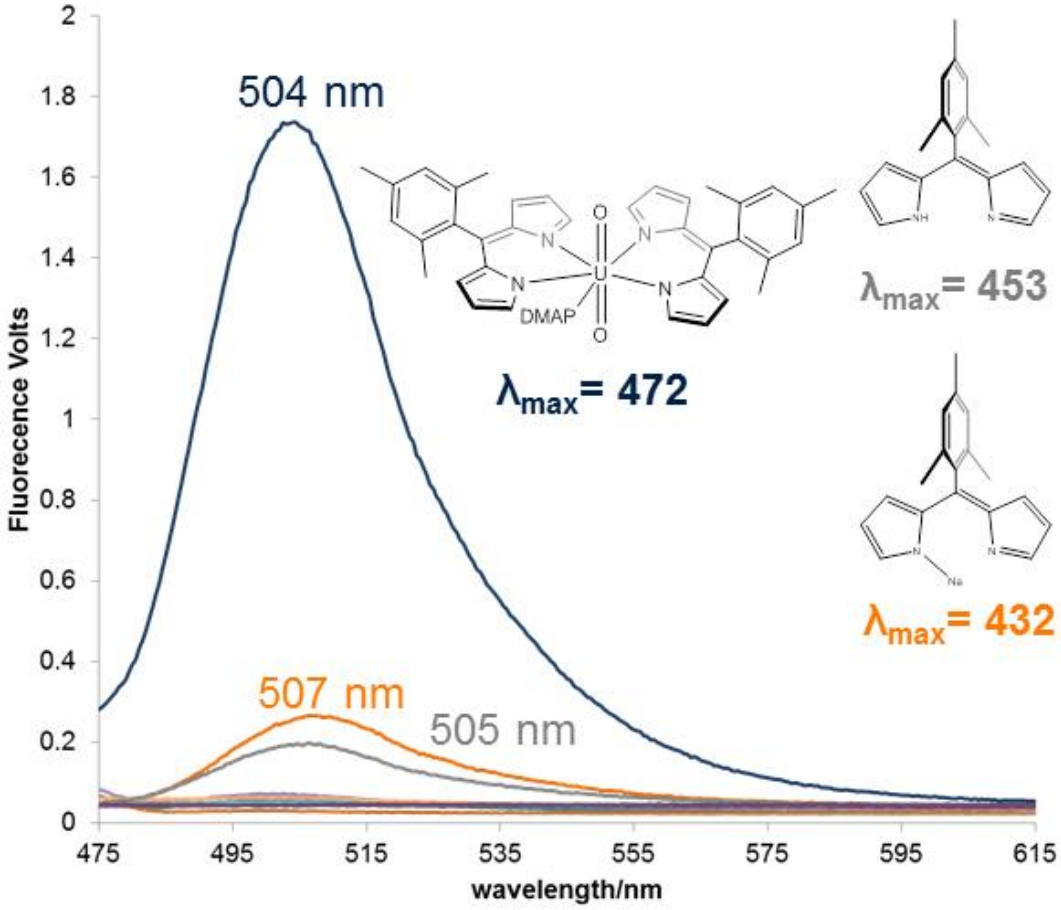

Figure S63. Fluorescence spectra of dipyrrins (**2**), sodium dipyrrins (**3**), and uranyl bis(dipyrrins) (**4**) in benzene (10 μM) with excitation wavelengths set to their respective absorption maxima determined in the same solvent and concentrations.

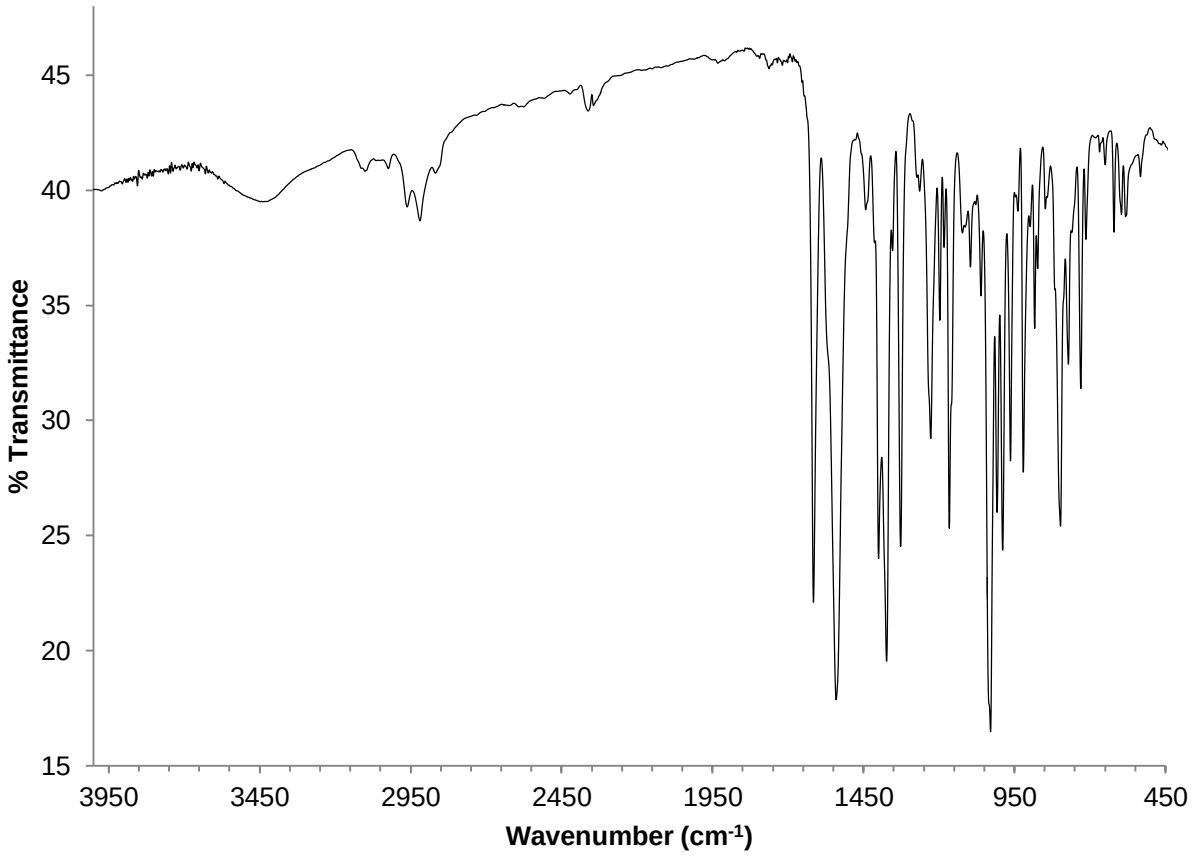

Figure S64. IR spectrum (KBr pellet) of **4^{tol}**-DMAP.

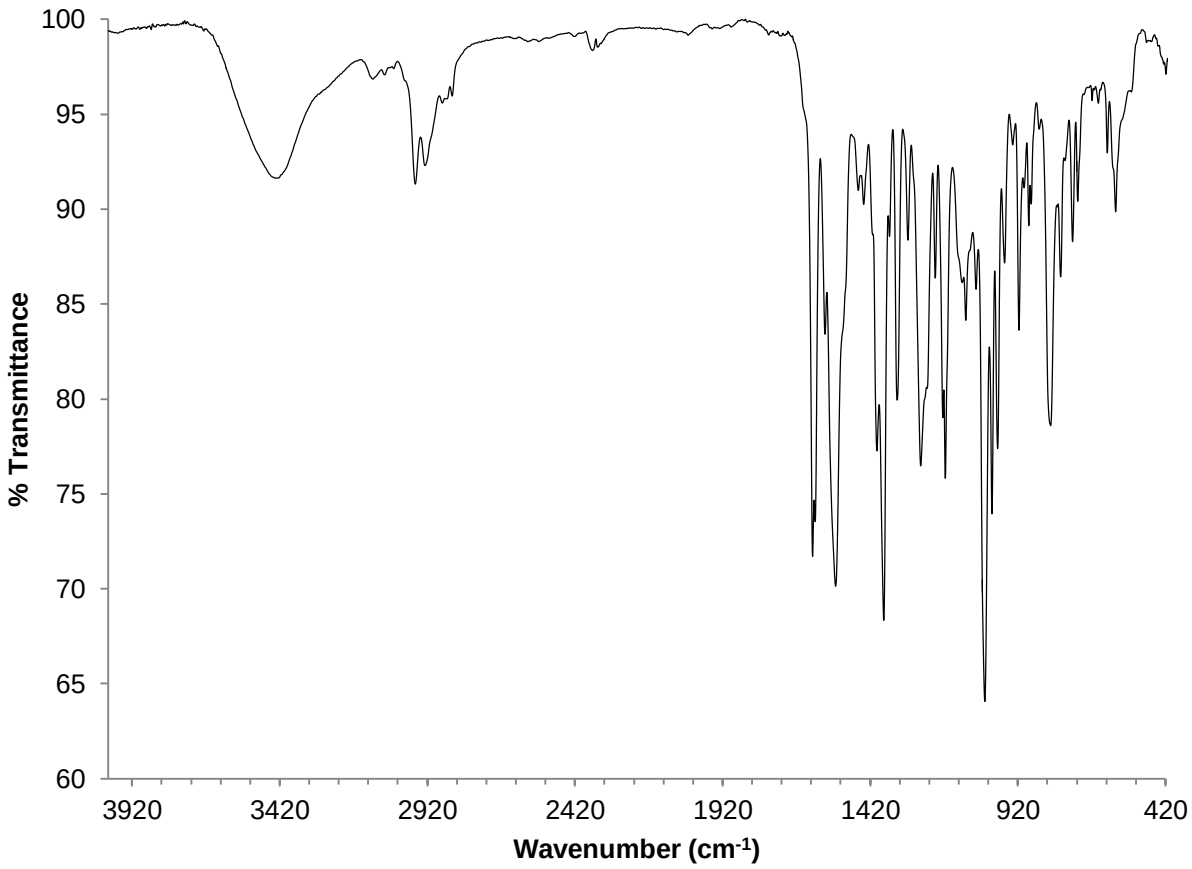

Figure S65. IR spectrum (KBr pellet) of **4**^{anis}-DMAP.

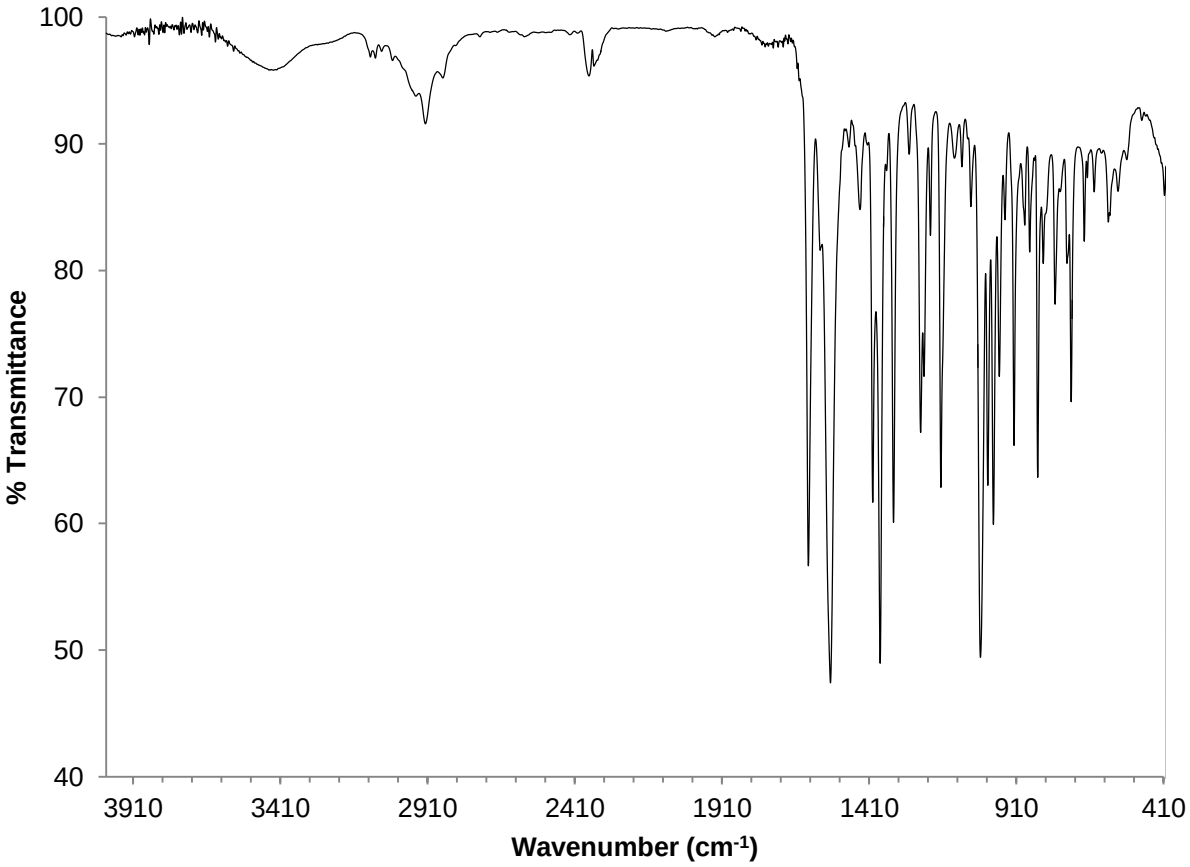

Figure S66. IR spectrum (KBr pellet) of **4**^{mes}-DMAP.

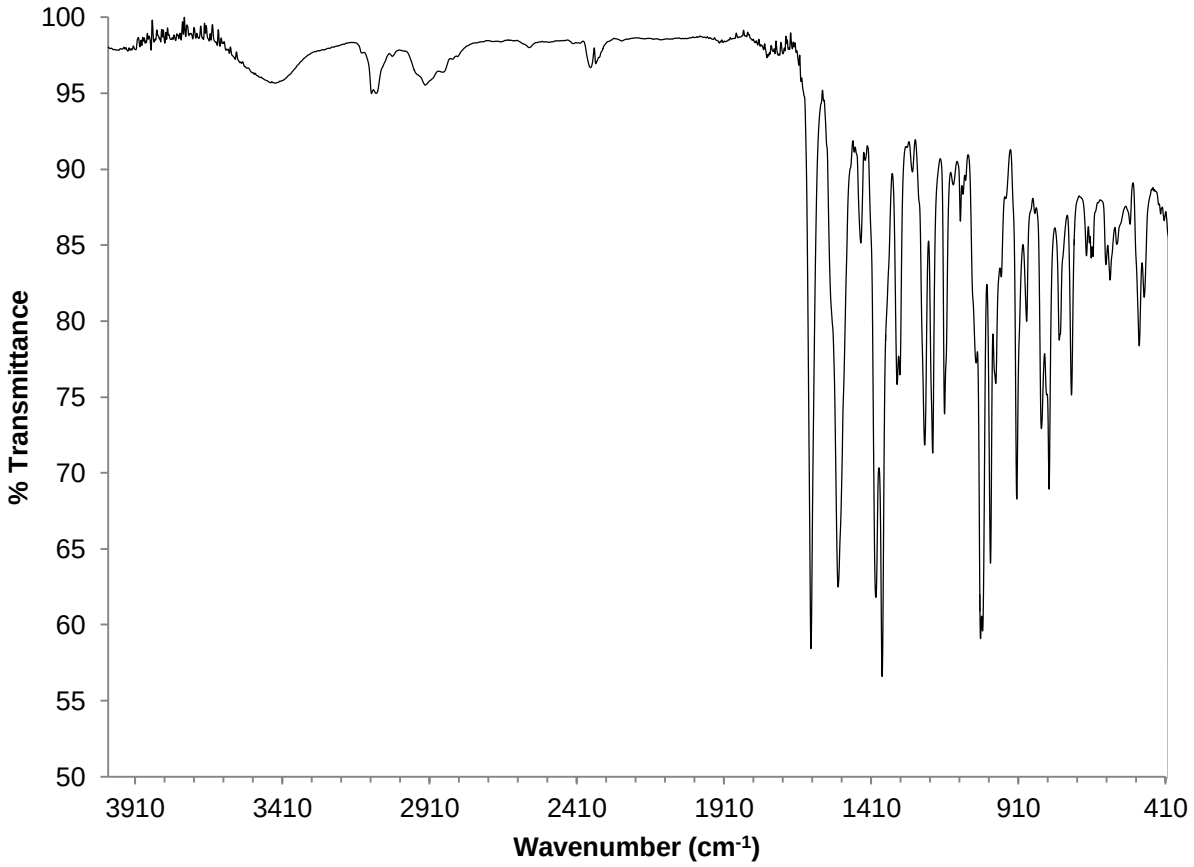

Figure S67. IR spectrum (KBr pellet) of $\mathbf{4}^{\mathbf{Fc}}$-DMAP.

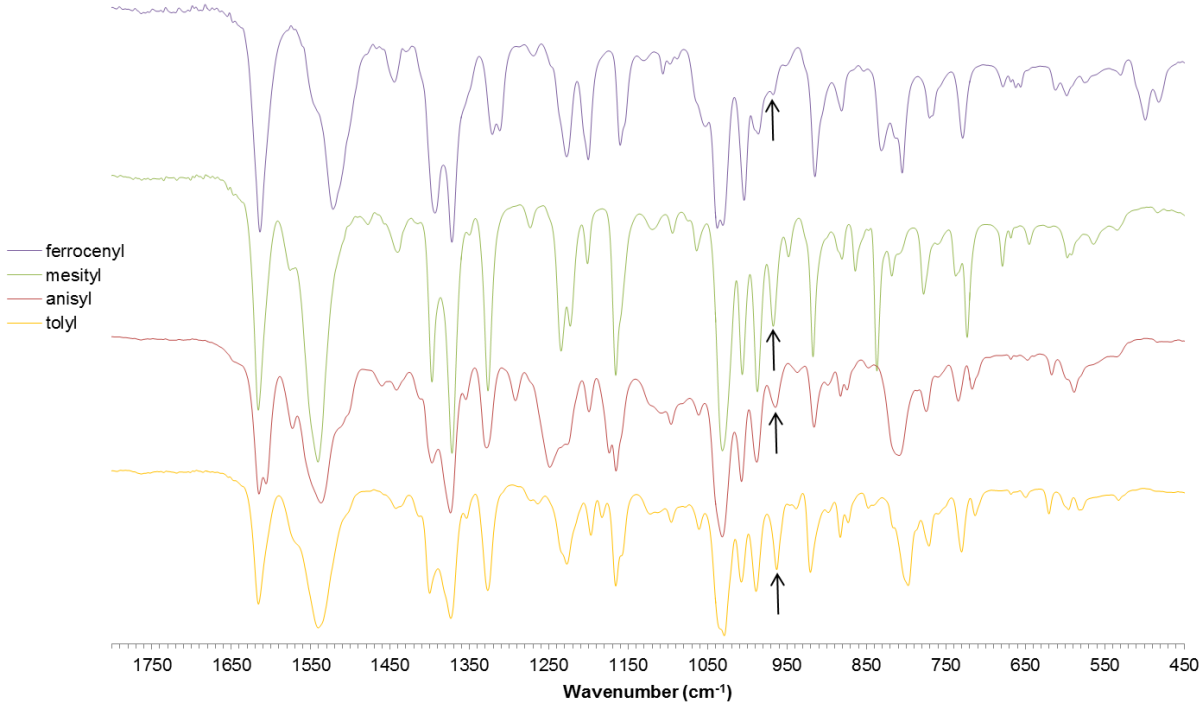

Figure S68. IR spectra (KBr pellet) of uranyl bis(dipyrrin) complexes. The arrows indicate the asymmetric ν_3 U-O stretch of uranyl at 963 cm^{-1}.